DEVELOPMENT OF A LASER INDUCED FLUORESCENCE SYSTEM FOR MEASURING OIL FILM THICKNESS IN TWO DIMENSIONS IN A RECIPROCATING ENGINE

by

PIERRE M. MULGRAVE
B.S. Aerospace Engineering, Polytechnic University
(1995)

SUBMITTED TO THE DEPARTMENT OF MECHANICAL ENGINEERING
IN PARTIAL FULFILLMENT OF THE REQUIRMENTS FOR THE DEGREE OF

MASTER OF SCIENCE IN MECHANICAL ENGINEERING

at the

MASSACHUSETTS INSTITUTE OF TECHNOLOGY

June, 1997

Signature of Author Pierre M. Mulgrave
Department of Mechanical Engineering
2 May, 1997

Certified by
Douglas P. Hart
Assistant Professor, Department of Mechanical Engineering
Thesis Supervisor

Certified by
Dr. Victor Wong
Lecturer, Department of Mechanical Engineering
Thesis Supervisor

Accepted by
Ain A. Sonin, Chairman
Departmental Committee on Graduate Studies
Department of Mechanical Engineering

ABSTRACT

PART I

Simultaneous Laser Induced Fluorescence (LIF) and Sulfur dioxide (SO_2) testing was performed on the Chrysler 2.2L Spark Ignition engine. The objective of the experiment was to investigate how oil film thickness on both the lands and rings of the piston changed with engine speed and to relate this with a change in oil consumption as derived from the SO_2 data. The laser accessed the cylinder liner of the no. 4 cylinder through a quartz window. Real-time SO_2 based oil consumption diagnostic equipment was adapted to the Chrysler Engine. The exhaust from the no. 4 cylinder was sampled just downstream of the exhaust port. The piston rings were unpinned rings in this experiment.

Analysis of the LIF data revealed that lubricant is present on the crown land during firing conditions and that second land oil film thickness data indicates an oil transition from the region just above the second ring to the region immediately below the compression ring. Analysis of the SO_2 data revealed considerable variability in oil consumption values for the three engine speeds considered.

PART II

A two dimensional oil film thickness (2D-OFT) measuring system is being developed for use with a Kubota single cylinder, production diesel engine. The engine setup has been designed to facilitate acquisition of 2D-OFT data, via a prismatic window in the cylinder liner, and a water tight optical path provided by a collar and a supporting manifold plate.

Several dyes have been investigated and detailed research and testing have been performed to realize the optimum fluorescent dye compatible with excitation sources currently available and high temperature environments. The information derived from this project will aid in clarifying various oil consumption models which now exist and will establish a greater understanding of oil consumption and oil transport phenomena in internal combustion engines.

Pierre M. Mulgrave - Experimental Engineer

Thesis Advisors - Professor Douglas P. Hart

Dr. Victor Wong

May 2, 1997

(This Page Left Intentionally Blank)

ACKNOWLEDGEMENTS

I would like to thank the faculty at the MIT Sloan Automtoive Laboratory, who made my two years as a graduate student a truly challenging experience. In particular I would like to thank Dr. David Hoult who was always patient in explaining the research process, Dr. Victor Wong who was always open to my many ideas and helped me by giving me the freedom to explore and learn like a true experimentalist, Professor John Heywood who kept me on track and taught me a great deal about internal combustion engines and my advisor, Professor Douglas Hart, without whom this project would never have been possible.

I would also like to specially thank Brian Corkum and Pete Manard, who both gave unselfishly of their time in assisting me tackle the many engine and machining problems in the lab, including the setup of the Chrysler and Kubota engines and related diagnostic equipment.

Throughout my two years, my fellow graduate students have helped me become a more rounded person. I would like to thank my former office mates from the fishbowl, Sam Young Han, Haissam Haidar, Robert Meyer, Kelly Baker, Norman Peralta, Mike Shelby and Younggy Shin, who all gave of their time in assisting me whenever I needed help. A special thank you to my office mates from "the office with the view", including Denis Artzner, Jorge Maurino, and Benoist Theordeau. To the other graduate students who have help make the Sloan Automotive a pleasant place to work, I would like to thank Tian Tian and Bouka Noordzij, Steve Casey, Wolf Bauer, Chris, Dave, Wole, Marcus Stewart, Helen, Luis Pallacious, Brad Vanderweege, Mark Kiesel, John Fox, Peter Hinze, Kuo Chiang Cheng, Josmar Pagluisio, Bertrand and Alan Shihadeh who was always ready to listen to my ideas about life and research, thank you. Most naturally Sloan Automotive would not be complete without Nancy Cook, a truly genuine person who added a special touch to the lab. Thank you Nancy!

I would like to thank Gerry Wentworth and Fred from the Laboratory for Manufacturing and Productivity, Libby Shaw and Jean from The Center for Material Science, Professor Fonstad from the department of Material Science who gave me access to his chemical etching laboratory, Bill Kutz of Gould Precision Optics, Marty Gould of Zen Machine Shop, whose expert craftsmanship has never failed to surprise me.

Finally in this last paragraph of 'thank you's' I reserve a special thank you to a lady who has risen to great prominence in my life, my fiancee Victoria, for her understanding, kindness, support and above all her love and devotion through all my ups and downs.

This work has been supported by the MIT research Consortium on Lubrication in Internal Combustion Engines, whose members are; Peugeot, Renault, Caterpillar, Dana Corporation, Shell Oil Company, Pennzoil and Ford Motor Company.

Pierre M. Mulgrave

February 28, 1997

(This Page Left Intentionally Blank)

TABLE OF CONTENTS

LIST OF TABLES

LIST OF FIGURES

LIST OF FIGURES (continued)

NOMENCLATURE

Abbreviations:

LIF	Laser Induced Fluorescence
2D-LIF	Two Dimensional Laser Induced Fluorescence
OFT	Oil Film Thickness
RPM	Revolutions per minute
CCD	Charge Coupled Device
BDC	Bottom Dead Center
TDC	Top Dead Center
UV	Ultra Violet
S.I.	Spark Ignition
PMT	Photomultiplier Tube
EDM	Electro-Discharge Machining
MFT	Modulation Function Transfer
SO_2	Sulfur Dioxide
NO_2	Nitrogen Dioxide
NO	Nitric Oxide
O_3	Ozone
L	Liter
W	Watts
M	Molar
mol/l	Moles per liter
LPM	Liter per minute
lb	pounds
ft-lb	foot pounds
C	Fluorescent dye concentration
psi	Pounds per square inch
g	grams
f	frequency
CA	Crank Angle
ATC	After Top Center
BTC	Before Top Center
OC	Oil Control
INT	Intake
COMP	Compression
EXP	Expansion
EXH	Exhaust
PLIFINT	Microsoft Macro for manipulating pressure, LIF data starting at intake
PLIFCOMP	Microsoft Macro for manipulating pressure, LIF data starting at compression
PLIFEXP	Microsoft Macro for manipulating pressure, LIF data starting at expansion
PLIFEXH	Microsoft Macro for manipulating pressure, LIF data starting at exhaust

Prefixes:

m	milli ($x10^{-3}$)
n	nano ($x10^{-9}$)
μ	micro ($x10^{-6}$)

(This Page Intentionally Left Blank)

Chapter 1

Motivation

1.1 Introduction

The problem of understanding lubricant flow in the piston ring pack of internal combustion engines continues to be an area of major concern. The primary goal of this project was to develop a means for measuring oil film thickness in two dimensions such that a thorough understanding of lubricant behavior in the piston ring pack under all operating conditions could be achieved. To facilitate this study it is desirable to accurately measure the oil film thickness between the piston rings, lands and the cylinder liner. A study of the flow of lubricant within the piston ring pack is therefore justified. The research in this area will therefore advance the state of the art in piston ring, groove and land design. The result will be higher engine operating efficiency, characterized by lower fuel and oil consumption. Piston ring pack design is also indirectly tied to air pollution through oil consumption. Oil lost via transport through the ring pack represents 80-90% of the total oil consumed by the typical production engine[1]. The Environmental Protection Agency (EPA) has made significant progress to date in reducing ambient SO_2 emissions. In accordance with the Clean Air Act (CAA), the EPA has reviewed and revised the air quality criteria upon which the existing National Ambient Air Quality Standards (NAAQS) for sulfur oxides are based. The national composite average of SO_2 emissions decreased 18% between 1986 and 1995[2]. This trend is expected to continue as emission regulations become more stringent.

Automotive Piston Ring Requirements

In both gasoline and diesel engines it is absolutely essential to provide and maintain a circumferential gas seal between the reciprocating surfaces of the piston and the cylinder bore. It is however not generally feasible for the piston itself to provide adequate sealing with the bore due to a variety of reasons stemming from bore distortion resulting from differential temperature and expansion characteristics. It is therefore necessary to resort to the use of split rings fitted with grooves in the piston that by virtue of their design and material characteristics, maintain a sealing pressure with the cylinder bore. The piston rings themselves perform two major functions. The primary function is in sealing against the cylinder pressure and the secondary

function is the metering of lubricating oil in order to minimize friction and maintain the primary function over time. These dual functions typically require the use of at least two or three rings in gasoline engines and more in diesel engines which are characterized by higher engine operating temperatures and pressures.

Piston rings are also required to provide low friction losses and wear rates, tolerance to marginal lubrication environments, long-term stability, consistency of performance and satisfactory heat transfer properties. Cost and life must be compatible with the total economics of the system whether the emphasis is on lowest first cost, as it tends to be in gasoline engines, or on long maintenance free life as it tends to be in modern diesel engines.

To some extent, the requirements of ring lubrication and minimum oil consumption appear to be incompatible and it therefore becomes important to understand the phenomena if any optimum result is to be achieved. Piston ring lubrication is clearly characterized by rapid and extreme variations in speed and load. At the midstroke location, piston speed is maximum and hydrodynamic lubrication is dominant. Throughout the cycle an oil film is generated by wedge action depending on ring velocity and ring profile relative to the bore. In the recent years, a number of techniques have been established for measuring not only the pressure and temperature at various points on the piston but the dynamic lubricant film thickness as well. The process of correlating this data with observations of engine behavior is now well under way and will eventually lead to a more systematic and quantified approach to component design[3].

1.3 Project Objectives

Part I

The objectives of this part of the research are:

1. Obtain simultaneous LIF and SO_2 data for the Chrysler 2.2L S.I. engine for various engine operating conditions.
2. Observe trends in oil film thickness with oil consumption for this engine.

Part II

The objectives of Part II of this project are:

1. To optimize a single cylinder diesel engine for the purposes of obtaining LIF data in two dimensions. This involved designing, installing and testing an optical interface system.
2. Develop a procedure for matching fluorescent dyes with optical pump sources through a

thorough understanding of fluorescent dye chemistry.

3. Develop an effective calibration device
4. Implement an optical data acquisition system, consisting of an optical pumping source, optical equipment, and CCD array imaging for data collection and analysis.
5. Observe oil film thickness variation under each ring in the piston ring pack with engine operating conditions.
6. Observe ring rotation and oil film thickness changes on piston lands under dynamic cases of variable engine load and speed.

PART I

Simultaneous Laser Induced Fluorescence (LIF) and Sulfur Dioxide (SO_2) testing performed on the Chrysler 2.2L S.I. Engine.

This section includes a detailed description of the following:

Chapter 2 Experimental Apparatus.

Chapter 3 Experimental Procedure and Data Processing.

Chapter 4 Data Analysis and System Recommendations.

(This Page Intentionally Left Blank)

Chapter 2

Experimental Apparatus

2.1 Engine Description

The test engine used in this experiment was a production Chrysler 2.2L spark ignition, in-line four cylinder engine. This particular engine is commercially available in the 1989 Dodge Daytona. The pistons are manufactured from cast aluminum and have valve cuts to provide valve clearance and may be dished to provide various compression ratios. The pistons are lubricated from directed holes in the connecting rod assembly. The cylinder block is cast iron. The cylinder head is cast aluminum with in-line valves arranged with alternating exhaust and intake. An integral oil gallery within the cylinder head supplies oil to hydraulic lash adjusters, camshaft and valve mechanisms. The engine lubrication system is of the full flow filtration, pressure fed type. The oil pump is mounted within the crankcase and driven by an auxiliary shaft. Pressurized oil is then routed through the main oil gallery, running the length of the cylinder block. Camshaft and valve mechanisms are lubricated from a full length cylinder head oil gallery supplied from the crankcase main oil gallery. The engine bore is 87.5 mm and the stroke is 92 mm. The fuel used in these experiments had an extremely low sulfur content and was fractionally distilled for the lowest possible sulfur content. The lubricating oil was SAE 20W50. A detailed description of this engine is given in Table A1 of Appendix A. Several modifications were made on the Chrysler engine and are outlined below:

1. A sealed optical passage was installed through the no. 4 cylinder wall. This optical passage must (a) hold the focusing probe normal to the liner surface, (b) prevent coolant leaking between the probe face and the fused silica window and (c) allow for adjustment of the probe so that the laser light can be focused onto the inner liner surface. The window is located at coordinates $z = 40mm$ and $\theta = 90°$ on the anti-thrust side, referenced respectively from the fire deck (TDC) of the engine and from the forward wrist-pin axis. See figures 2.1 and 2.2. This position was selected since it provided an acceptable tradeoff between mechanical interference as far as access and installation were concerned and an appropriate location for observing the entire ring pack and a portion of the skirt on the film trace. The skirt section is important since machine marks on the piston skirt allow for calibration of oil film thickness data. This optical passage interfaced directly with a polished fused silica window (Dynasil 4000). This was the

same window employed by Shaw[4]. See figure 2.3. The diameter of the fused silica window is 0.48cm. This window is bonded to the liner using a high-temperature hydrocarbon-resistant silicone adhesive (Dow Corning 730). This window was then honed flush with the cylinder liner surface.

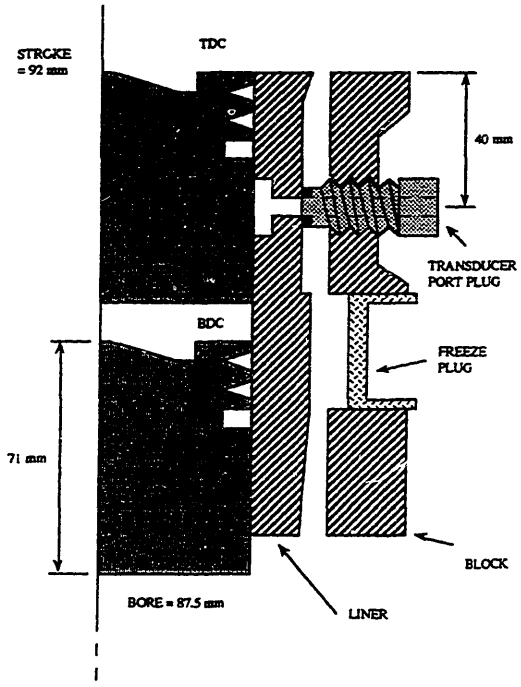

Figure 2.1 Partial Section of Cylinder no. 4 showing the Optical Access Port and Window Location

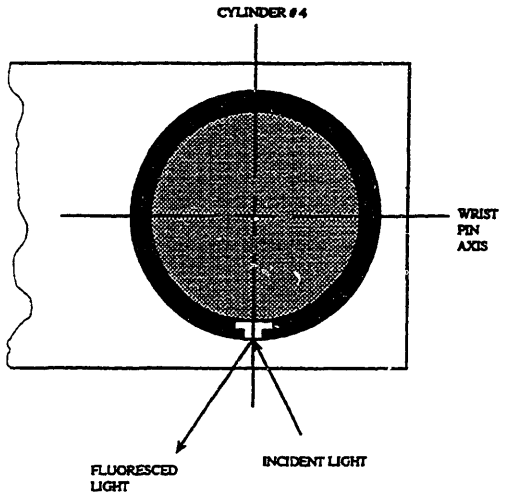

Figure 2.2 Plan View of the Cylinder no. 4 showing the Window Location

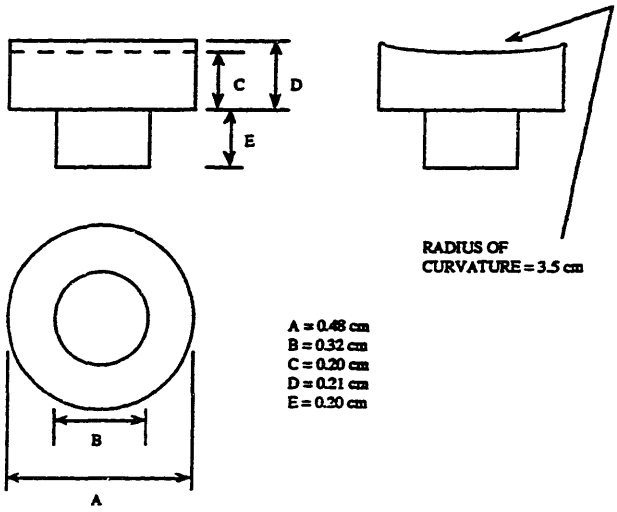

Figure 2.3 Fused Silica Window Specifications

2. The cylinder head of the engine was modified to accept piezo-electric pressure transducers for cylinder pressure monitoring. The pressure transducers were calibrated for use with a Kistler 5001 amplifier. Inherent error of the transducers was less than 2%.
A model SA pressure transducer, with range 0-25 psia, was installed in the intake manifold to measure intake vacuum pressure.

3. Various engine temperatures were monitored with the aid of chromel-alumel K-type thermocouples. Temperatures monitored included inlet coolant temperature, outlet coolant temperature, inlet oil temperature, outlet oil (sump) temperature, inlet fuel temperature, intake air temperature, exhaust gas temperature and second cylinder coolant temperature. The second cylinder coolant thermocouple was installed in order to monitor the engine coolant temperature at its hottest region i.e., the region close to the spark plug. The liner thermocouple was specially mounted in the no. 4 cylinder liner in the same horizontal plane as the fused silica window, i.e., 40mm below TDC. This thermocouple was glued in place with a high temperature, thermally conductive epoxy adhesive (OMEGABOND 200). See figure 2.4. The thermocouple is located as close as possible to the window so that inferences about the liner oil temperature can be made but far enough away from the window so that the flow field around the window is not disturbed appreciably.

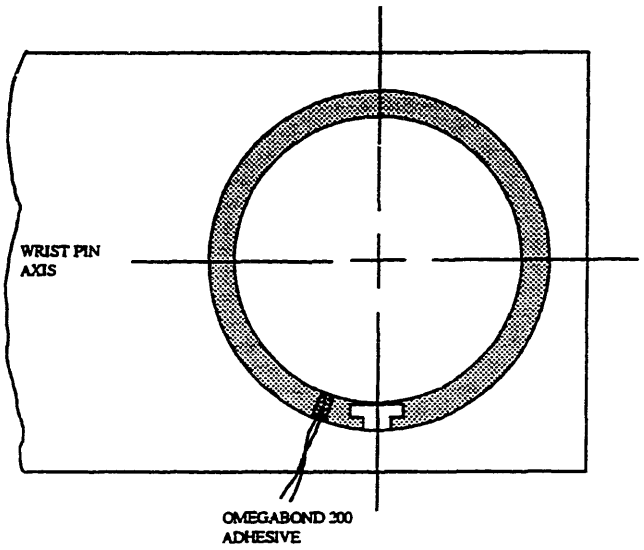

Figure 2.4 Plan View of Liner Thermocouple Location in Cylinder no. 4.

4. The exhaust system was modified to allow separate exhaust sampling of cylinder no. 4. This is especially important as far as simultaneous acquisition of LIF and SO_2 data from one cylinder is concerned. The no. 4 cylinder exhaust line was insulated to reduce heat loss, thus preventing condensation in the line prior to subsequent analysis.

2.2 Laser Induced Fluorescence (LIF) System

2.2.1 Brief History

The LIF system at MIT has evolved over more than a decade into a the compact, portable, easily installed and highly effective system it is today. By incorporating fiber optic technology, the data acquisition system has improved spatial resolution due to smaller beam diameter and signal to noise (S/N) ratio. The LIF system is used to measure dynamic oil film thickness on the lands of the piston, under the piston rings, piston skirt and free liner surface. Early studies of lubricant behavior between a reciprocating piston and the cylinder wall employed either reluctance or capacitance methods[5,6]. A technique for measuring oil film thickness on rotating cylinders based on natural absorption and emission response of some oils to ultraviolet light was developed by Smart[7] and Ford[7].

Ting[8] studied the lubricant behavior in a motored engine fitted with a transparent lexan cylinder sleeve, but did not calibrate the system. A means of calibrating the system response was then developed by Hoult[9] and Rifai[9]. Since then, system optimization was successfully

reflected in the work of several research engineers and faculty at MIT[10-15]. Tamai[16] and Noordzij[17] contributed to final system optimization and documentation.

2.2.2 Description of Laser Induced Fluorescence Apparatus

A schematic of the LIF system is shown below in figure 2.5. The laser source for the apparatus is a 14mW Liconix 4214NB He-Cd laser operating in the blue at 442 nm. The laser output power to the engine is approximately 3 to 4 mW.

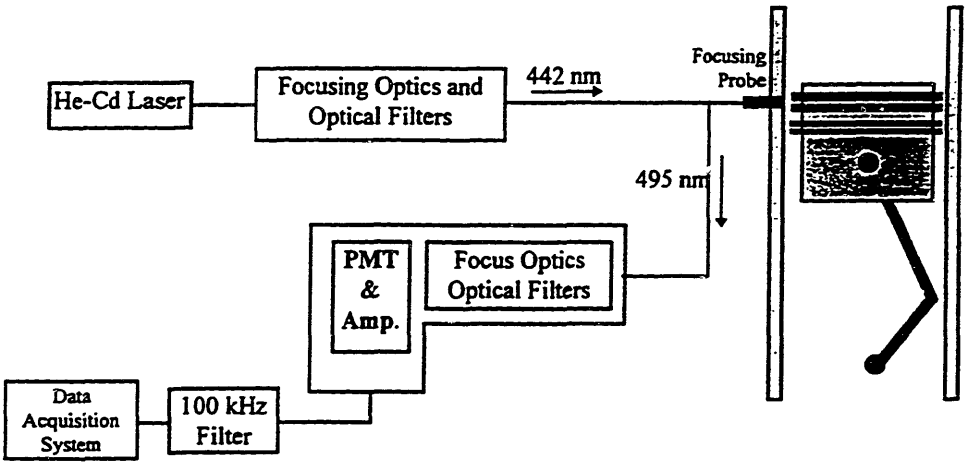

Figure 2.5 Schematic of the Laser Induced Fluorescence System.

The laser beam is first filtered through a 442 nm filter which eliminates any wavelengths outside the narrow band width of the filter. In this application the diameter of the optical fiber is 50μm, while the diameter of the laser beam is 1 mm. Therefore the beam is then focused by an eccentric coupler, (see Appendix B), in such a way that the beam incident on the fiber is within the acceptance angle of the fiber optic cable. The acceptance angle for the fiber optic cables used was 28°. The light is then totally internally reflected along the length of the fiber optic cable where it emerges and is again focused via a focusing probe mounted in the engine block. Focusing optics at the engine interface are required to decrease beam diameter to a small spot and thus allow the light to travel through the thickness of the liner and reach the oil[18]. Beam diameter at the liner oil interface is on the order of 50 microns. The engine oil is mixed with Coumarin 523 obtained from Exciton Inc. This dye is excited at an excitation wavelength of 442 nm and fluoresces at a positive Stokes shifted wavelength of 495 nm.

This peak fluorescence wavelength of 495 nm is then optically conducted via coaxial optical fibers to a narrow band pass filter tuned for 495 nm transmission. The light is then focused onto the photosensitive area of a photomultiplier tube which converts the fluorescence

signal into a weak electrical current. This electrical current is then filtered by a 100kHz low pass noise filter and digitized by an analog to digital (A/D) converter card mounted on the PC board. A PMT voltage of 650V was found to be adequate for the data sets collected. Favorable adjustment of the PMT voltage is critical in obtaining the strongest possible LIF signal. A high voltage setting results in a high LIF signal amplification. There are two reasons for setting an upper bound on the PMT voltage. The first is the exponential increase in average noise level for voltages above 700V. An excessive PMT voltage setting results in the LIF signal on the oscilloscope exceeding 10V, resulting in signal saturation. Tamai[16] has plotted representative curves of average noise levels versus voltage for the PMT used in this experiment. The curves have been reproduced in Appendix C.

2.2.3 Influence of Oil Film Thickness and Temperature on Fluorescence Intensity

The fluorescence intensity is in general linearly proportional to oil film thickness for the range 0 to 80μm[10]. Lee[19] found linearity in the range 0 to 125μm. For these experiments, the laser focusing probe was adjusted so that the LIF signal on the oscilloscope, representative of the flooded areas on and around the oil control groove and skirt, was maximized. Fluorescence efficiency decreases with increasing oil temperature. Therefore the PMT voltage must be adjusted at steady state operating conditions to compensate for the decay in fluorescence efficiency.

2.2.4 Recent LIF System Modifications

Bouka[17] made several changes to the LIF system in an attempt to enhance performance. The first change involved upgrading the eccentric coupler from the General Fiber Optic model 85-22 to a model 8612-12501. The built-in focusing lens of the latter model increased the amount of laser light accepted by the fiber optic cable. The bifurcated fiber cables were replaced with higher efficiency cables with enhanced light carrying capability. See table D1 of Appendix D, for a list of the major LIF System components. Further modification involved replacing the high purity UV grade fused silica lenses in the focusing probe assembly with appropriately ground glass lenses, which were cost effective and did not compromise system integrity or efficiency. The internal dimensions of the probe housing assembly were modified to accommodate the new glass lenses and is shown below in figure 2.6.

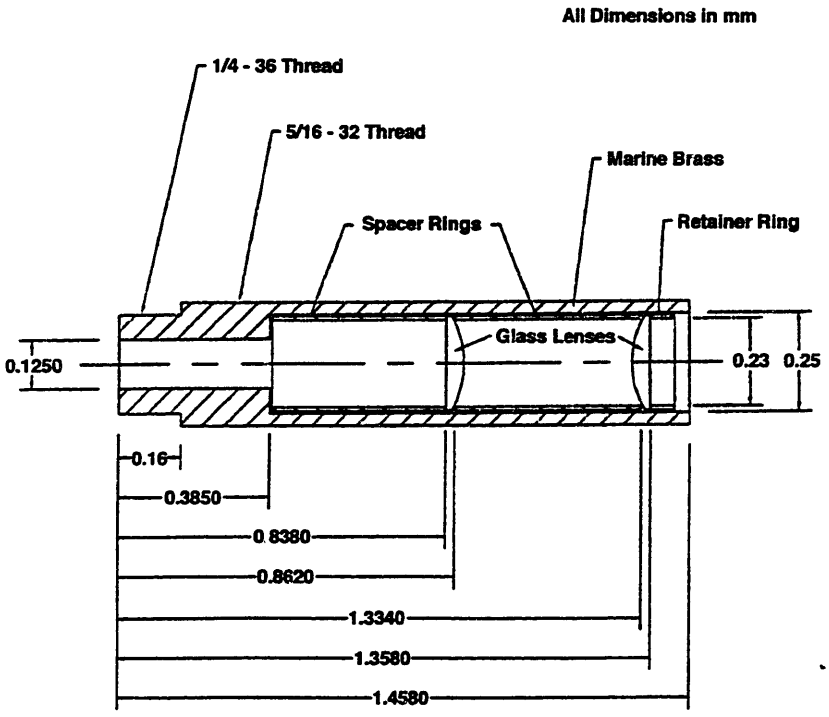

Figure 2.6 LIF Probe Housing.

The LIF probe above screws into a specially designed transducer plug shown below in figure 2.7. This transducer plug seals the probe housing from circulating coolant in the engine block. Proper sealing is accomplished by sufficiently compressing a viton O-ring against the surface of the cylinder liner in the region surrounding the optical window.

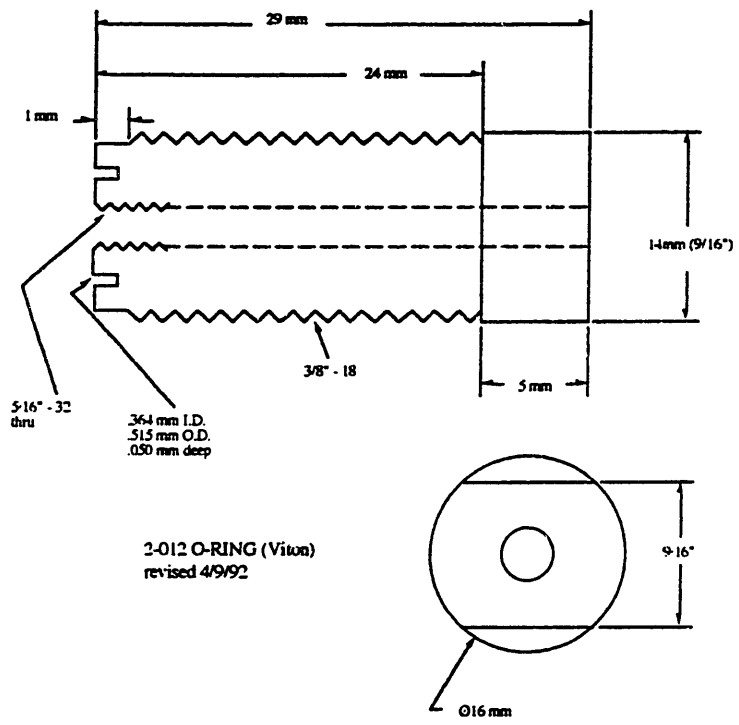

Figure 2.7 Transducer Port Plug.

2.2.5 LIF Data Acquisition System

A Personal Computer based data acquisition system was used to collect LIF data for this experiment. A Kiethley Metrabyte DAS-58 board was installed in an IBM clone. The data acquisition system is externally clocked by a BEI optical shaft encoder at a rate of 2000 pulses per revolution. This pulse rate yields approximately 10 points per millimeter across the compression ring, resulting in a horizontal resolution of 0.1 mm. The oil film character can hence be easily observed. The DAS-58 also incorporates a digital trigger, which was connected to the 5V pulse per revolution channel from the encoder. This 5V pulse was aligned with the start of the intake and expansion strokes. This alignment was performed with the engine motored at wide open throttle. The 5V pulse per revolution was then aligned with cylinder pressure peak produced, therefore referencing the Top Dead Center (TDC) position of the piston. Alignment was achieved by rotating the shaft encoder during engine motoring, such that the 5V blip on the oscilloscope screen coincided with the peak of the cylinder pressure trace. Two active channels for pressure data and LIF data acquisition were utilized. Therefore the 2000 pulses per revolution of the shaft encoder were split been the two active channels.

For consistent data analysis it is necessary to start the data acquisition system at the same stroke for all testing, which has generally been the intake stroke for LIF sampling. Eleven cycles of LIF and pressure data were taken and then analyzed. The data sets were imported into Microsoft Excel where they were first checked and truncated if necessary to the start of the intake stroke.

2.3 Oil Consumption Measurement

2.3.1 Previous Work

Many oil consumption studies have been performed at M.I.T. The most recent studies were carried out by Jackson[20] and Miller[21], in which the SO_2 tracer system was used in characterizing real time oil consumption in a Cussons Hydra single cylinder research diesel engine. Artzner[22] utilized the SO_2 tracer system in investigating oil consumption mechanisms in the Chrysler 2.2L S.I. engine and Schofield[23] utilized the same system in measuring oil consumption rates in a Richardo Hydra single cylinder direct injection diesel engine. He found a variability in oil consumption at one particular speed and load similar to that found by Hartman below. Earlier oil consumption studies employed the use of radio-tracer techniques, by Lusted[24] and Hartman[25]. Lusted studied the oil consumption behavior in a production four cylinder spark ignition engine and found a variability of greater than 20% at one specific speed and load. Hartman performed similar oil consumption measurements on a single cylinder Kubota diesel engine and his results showed a large unexplained variability at one speed and load. At this point in time this phenomena has not been fully described. Schofield has however hypothesized that this large variability may be due to ring dynamics within the cylinder.

2.3.2 Sources of Oil Consumption

There are four primary paths for oil consumption in internal combustion engines as outlined by Hill[26]. They are as follows:

1. Piston-ring-liner system
2. Overhead valve seals
3. Crankcase ventilation system
4. Oil pan, crankcase, turbocharger, and other component gasket seals.

This study focuses on overall oil consumption and is hence not limited to any particular source. Crankcase ventilation is not coupled with the intake manifold and there is no turbocharger present. In such a case oil consumption can be attributed to the piston-ring-liner system and overhead valve seals. If the valve train is isolated or a zero sulfur oil is utilized then any valve oil consumption would not contribute to any SO_2 in the exhaust and hence would not be measured by the system. However this was not done since only the overall oil consumption is being measured.

2.3.3 SO_2 Diagnostic System

A pyrofluorescence sulfur dioxide testing diagnostic system developed by Cummins Engine Company was utilized in the engine emission analysis. The operating principle is based on tracing the sulfur in the oil through the combustion process into the exhaust gas. To ensure that the $SO_2(g)$ in the exhaust originated from the oil, a highly refined zero sulfur fuel is used. A diagram of the system setup is shown below in figure 2.8.

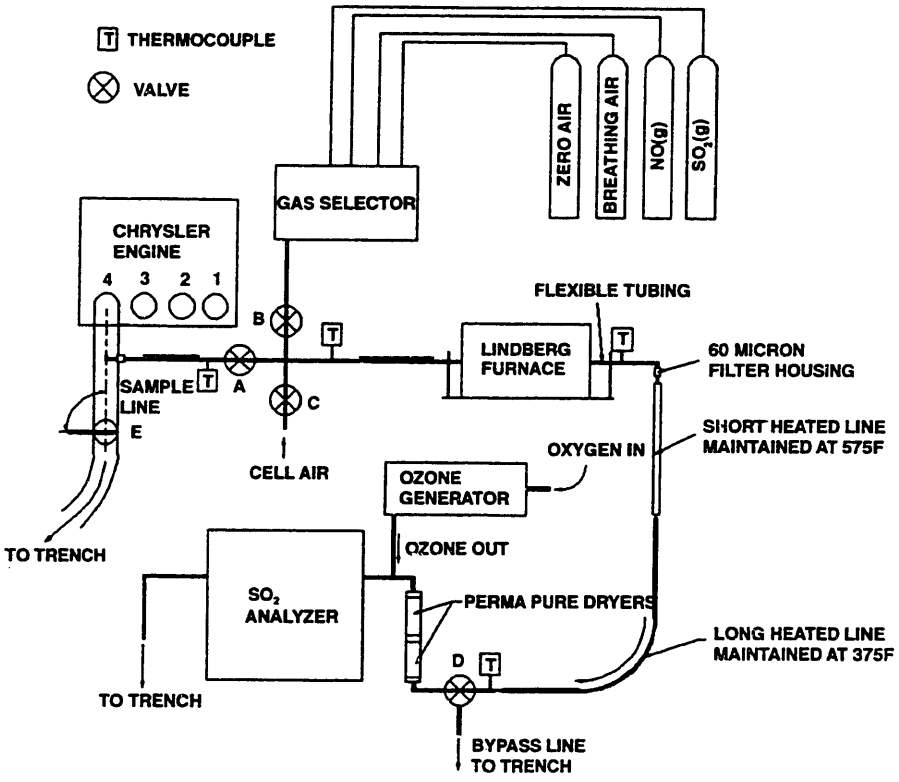

Figure 2.8 SO_2 System Setup for the Chrysler 2.2L Engine

It should be noted that only the exhaust of the no. 4 cylinder was monitored, such that a possible correlation between the LIF data taken from that engine cylinder could be made. The exhaust gas sample is drawn from the isolated exhaust line of the no. 4 cylinder via a 14 inch stainless steel sample line, ¼ inch in diameter. At the engine end, the sample line was clamped via a swage lock fitting, into a small elbow with the open end oriented upstream and located along the center line of the no. 4 cylinder exhaust line. This elbow served to direct the exhaust sample at a sufficient flow rate through the sample line without having to substantially increase the back pressure at the exhaust port. The elbow could be rotated to achieve the maximum sample flow rate. Every attempt was made to limit the length of the sample line by mounting the furnace as close as possible to the engine, thereby reducing the possibility of any oil becoming resident in the line. The sample line was wrapped with heating tape and maintained at a temperature T_1 of 960°F. The no. 4 exhaust line was insulated between the top of the manifold and the sample line junction, to retain as much heat energy as possible in the line.

The sample line transfers exhaust gas through a solenoid valve (A) which allows for isolation of the exhaust gases from the system during calibration. Solenoid valves (B) and (C) regulate the flow of calibration gases and cell air through the system respectively. Cell air is sampled to determine the background reference amount of airborne SO_2. This can then be subtracted from the final SO_2 readings obtained. The solenoid cluster lines including the line leading to the furnace, were wrapped with heating tape and maintained at 950°F, via a variac type temperature controller.

Immediately following the solenoid valves was the Lindberg Hinged 55000 series furnace, set to heat the sample gas to 1000°C, through a 2 inch bore quartz furnace tube. This quartz tube was housed between two semi-cylindrical heating modules. Each module is a composite unit of high temperature ceramic fiber insulation and a LGO embedded alloy heating element. The furnace tube diameter was increased from 1 to 2 inches. This resulted in the gas residence time increasing by a factor of 4. Gas residence time is important since this ensures that any sulfur in the sample is completely oxidized. The furnace tube was also packed with chipped quartz fragments which increased the surface area in contact with the gas. There is a limit to which the furnace tube can be packed, without adversely affecting the pressure drop across it. The furnace tube was linked at each end via soft graphite farrel-type swage locks. Extreme care was exercised in tightening these swage locks to prevent fracture of the glass ends.

After the furnace the sample gas flows through a flexible corrugated type tubing. This tubing absorbed any shock or bending moments transmitted to the furnace tube, thereby preventing fracture. The corrugated tubing was placed after the furnace to prevent accumulation of non oxidized exhaust components upstream of the furnace, which could dislodge and result in the analyzer registering spikes in SO_2 concentration. This flexible tube was also wrapped in heating tape and maintained at 200°F. All heated line temperatures are maintained by variac type heaters preset to appropriate temperatures above the condensation point of the SAE 20W50 oil used i.e. 900°F. The sample gas is then filtered through a 60μm filter before entering a short and a long heated line maintained at 525°F and 375°F respectively.

The sample gas is then dried by a pair of Perma Pure membrane type dryers connected immediately prior to the analyzer. These dryers remove 3-12% of water in the exhaust directly from the vapor phase. A chemically modified form of tetrafluoroethylene called Nafion, selectively absorbs water vapor from the sample gas. A diagram illustrating the Perma Pure Dryer Design is indicated in figure 2.9 below.

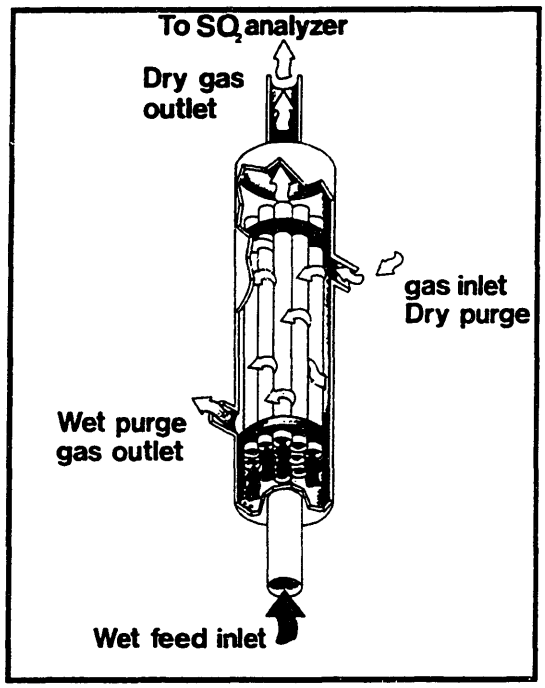

Figure 2.9 Perma Pure Dryer Design.

As shown, Nafion dryers consist of one or more strands of Nafion tubing surrounded by an external shell and fittings to supply a continuous flow of dry purge gas over the exterior of the tubing. As gases pass through the Nafion tubing, water vapor is selectively absorbed into

and moves through the tubing walls, driven by the water vapor pressure gradient and evaporates into the surrounding purge gas. The entire process is self regenerating. Since water is removed from the sample stream in the vapor phase, there is no loss of water soluble gases. In other words the sample is not exposed to condensate that can dissolve the analyte in this case $SO_2(g)$. The purge gas was supplied by one of the breathing air bottles. When the sample exits the dryer, its temperature is at ambient and its water content is non-condensing.

When monitoring SO_2 levels of 10ppm or less, SO_2 losses into the condensate are significant, and as little as 0.6% of water in the sample can cause substantial interference. Therefore thorough sample drying is essential.

The dried sample is then mixed with ozone $O_3(g)$ to oxidize any NO(g) in the sample exhaust to $NO_2(g)$. Ozone was generated by an Ozone generator which was set at a flow rate of 10 cc/min. The sample is finally analyzed by a pulsed fluorescent ambient SO_2 detector. The detectors linear DC voltage output is then recorded by a 486/66 MHz computer with an Analog to Digital card inserted on the mother board. This data acquisition system was capable of monitoring a maximum of 6 channels. Only one active channel was used in acquiring real-time SO_2 concentration within the exhaust gas. The signal was converted using Global Lab software and was then imported into an Excel Spreadsheet for conversion to the appropriate oil consumption values.

The system was operated in the configuration outlined above for all test runs. The system requires that back pressure be applied to the exhaust line to get a suitable flow rate to the analyzer. System back pressure and hence bypass flow can be adjusted in three ways:

1. Rotating the elbow within the no. 4 cylinder exhaust line.
2. Adjusting the setting of valve (E) downstream of the sample elbow of the no. 4 cylinder exhaust line.
3. Adjusting valve (D)

See figure 2.8.

The bypass acts like a 'vent' for the analyzer, thereby preventing the gas pressure in the analyzer from exceeding 1 atm. The bypass line was periodically monitored for flow using a 'floating ball' flow meter installed in the system. A bypass flow rate of 0.6 L/min was maintained throughout the calibration and testing. Any reading at the bypass meter would be sufficient to ensure that the analyzer was getting a pure sample. Jackson[20] and Miller[21] found that a change from 1.5 L/min to 0.5 L/min bypass flow changed the SO_2 concentration of a known span gas by 10%. They also found that transient type unsteady behavior occurred at the higher bypass flow

rates. Transient phenomena was absent at lower flow rates. It was for this reason in conjunction with the negative effects incurred by increasing engine exhaust back pressure that a lower flow rate was selected.

2.4 System Precautions

The following system precautions should be adhered to when operating the SO_2 diagnostic equipment.

a) The Ozonator should never be turned on before ensuring that there is an appropriate amount of *deionized* water in the chiller reservoir.

b) To prevent instrument damage, an appropriate supply of oxygen must be checked before turning on the Ozonator.

c) No gas bottle should be used till completely empty. This ensures that deposits at bottom of the bottle are not ingested in the system.

d) Breathing air should be allowed to purge the system overnight. Recommended purge flow rate is 1.5 L/min. The purge air prevents any condensation in the system.

e) The pressure in the SO_2 analyzer should never be allowed to exceed 1 atmosphere.

f) The same bypass flows must be maintained at all times, that is during calibration and testing. Changing engine speed and/or load will affect the exhaust flow rate, thus the bypass flow rate. Therefore the bypass flow rate must be adjusted by one of the 3 methods outlined in section 2.3.3 above.

g) Heated line temperatures will change with a change in system flow rate. Steady state conditions must then be achieved before resetting the temperature controllers. System flow rate is influenced by engine speed and load.

h) All system filters should be checked for proper orientation and cleanliness and changed if required.

Chapter 3

Experimental Procedure and Data Processing

Experimental Procedure

3.1 Engine/Dynamometer Operating Procedures

The Chrysler Engine and dynamometer were operated according to the test procedures outlined in Appendix E. The safety procedures used were in accordance with applicable Sloan Automotive Laboratory Safety instructions. The fluorescent dye used was Coumarin 523, manufactured by Exciton Inc. The appropriate dye concentration was achieved by mixing 0.15g of Coumarin 523 in 75 milliliters of dichloromethane (CH_2Cl_2), an intermediate solvent. Lee[19] recommends heating the dye solvent mixture up to a maximum temperature of 80°C before mixing with oil. This ensures thorough dissolution. A mechanical stirrer is then used in mixing the dye/solvent mixture with 2 liters of SAE 20W50 motor oil. The engine was then motored at 1500 RPM until the oil pressure rose to 70 psi, to break the oil in. The dye was selected because of it's relatively high quantum efficiency allowing the use of a lower dye concentration. This resulted in only a minimal effect on the lubricant additive package and the rheology of the oil. The reader is here referred to the detailed dye chemistry outlined in Chapter 7 of this report. Lee has found that the intensity of the fluorescence was linear with film thickness for films less than 125μm.

Before any data was collected, the fuel was shut off and the throttle set to the wide open position. The engine was then motored at 1500 RPM for approximately one hour to allow temperatures to stabilize.

3.2 LIF System Operating Procedure

The LIF system was first tuned by adjusting the eccentric coupler. The laser beam was focused by rotating the LIF probe in the transducer port until the sharpest possible signal was achieved on the monitoring oscilloscope. The probe was then locked into position via a lock nut. The laser power was then checked after the one hour warm period. A power level range of 12-13 mW was found to be satisfactory. The high voltage on the PMT was then adjusted so that the peak of the LIF signal fell within a 8 to 9 volt range. The data acquisition board only reads

up to 10 volts as previously mentioned in Chapter 2. A PMT voltage of 650V was found to be acceptable. With the laser adjusted and the pressure charge amplifier warmed up, the engine was prepared for firing. The procedure outlined in Appendix E was followed. The engine was then fired at 2000 RPM and allowed to stabilize at this speed and a mid load setting of 20in-Hg (67.5 KPa) for 45 minutes. The SO_2 system was then prepared for operation.

3.3 SO_2 System Operating Procedure and System Calibration

The SO_2 diagnostic system was first purged with 'Zero Air' which is compressed air with sulfur compounds filtered out. This occurs once the system has reached its steady operating condition, i.e. for the first test speed and load. All heated line temperatures, engine speed and load were monitored for stability. After zeroing the SO_2 analyzer with the zero air, a known concentration of SO_2 was then introduced into the system from an SO_2(g) calibration bottle. This span gas was then allowed to flow through the system for approximately six minutes. The span setting on the front of the SO_2 detector was then set so that the readout exactly matched the concentration of the span gas. If required, the photo-multiplier setting within the detector housing could be adjusted, if the span knob was insufficient in aligning the system with the known concentration of SO_2 in the system. During this time, the dedicated SO_2 data acquisition system was preset to receive first the calibration data.

The system was then purged with zero air for a minimum of six (6) minutes or until the detector settled on zero (±0.005ppm). Following this, the system was checked for NO response sensitivity. Nitric Oxide gas (NO) at 5000ppm was then introduced into the system and allowed to flow for approximately six minutes. The detector output was monitored for a spike. Once the detector began spiking, Ozone (O_3) was introduced into the system. The detector was then allowed to zero again with the NO disconnected. Span gas was then reintroduced into the system and monitored by the computer. This was done to check that the SO_2 trace attained its original level. The span gas was then disconnected and the system purged with zero air. The detector was again checked for zero output (±0.005ppm). The reader is here referred to figure 3.1 overleaf. Once the system was purged, the exhaust gas solenoid valve was opened and the calibration gas valve was closed. See figure 2.8. This permitted the engine exhaust gases to enter the system. The exhaust back pressure valve, valve (E) in figure 2.8 was regulated in conjunction with valve (D) to ensure proper bypass flow. In this case it was set to 0.6 L/min. The system was then allowed to settle out for approximately 45 minutes to an hour. Once the system settled at the appropriate test condition, data was taken.

LIF, Cylinder Pressure and SO_2 concentration data was then taken at 2000, 2500 and 3000 RPM respectively at Mid load. The SO_2 diagnostic heated line temperatures were

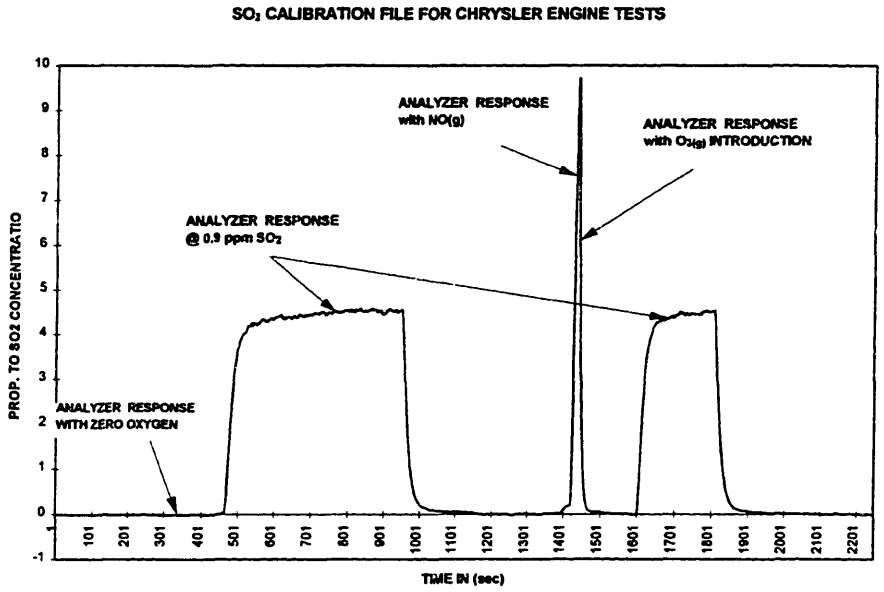

Figure 3.1 SO_2 Analyzer Calibration Output File

consistently maintained for all engine speeds. Bypass flow was maintained at 0.6 L/min. Manual monitoring occurred for all other parameters of the engine, LIF and SO_2 diagnostic system. The SO_2 data was collected over three (3) minute intervals under engine and system steady state conditions. The LIF and pressure data were collected during these three (3) minute intervals. At the completion of testing, the engine solenoid valve was closed and the 'calibration gases' valve was opened, see figure 2.8. This allowed zero air to flow through and hence thoroughly purge the system. Once the detector again reached zero, span gas was again introduced into the system and the detector was again calibrated to check for any drift which may have occurred. Every change in engine speed resulted in system wide changes in heated line temperatures and engine oil temperature. Temperatures typically took up to 50 minutes to stabilize. Therefore temperatures had to be carefully, and patiently monitored to maintain consistency. The engine operating and SO_2 diagnostic system temperatures are listed in table F1 of Appendix F along with engine load, speed, intake manifold pressure, bypass flow rate and fuel flow rate.

Data Processing

3.4 LIF Data Processing

The steps in processing a raw LIF data set consist of converting digital bits to volts, crank angle to distance from the top of the piston and finally the PMT voltage output to oil film thickness in microns through the calibration process. The raw LIF and pressure data in volts were saved in ASCII format (comma delimited, DOS file) i.e. L2000M2.DAT. Here L implies 'Laser data', followed by the four digit number representing the speed at which the data was taken. The 'M' means the mid load condition and the number '2' means the second series of data taken. The first data series was merely a test of system performance and is not considered here. This initial '.DAT' file was then copied to another file designated GENERIC.DAT and read by the appropriate macro i.e. PLIFINT or PLIFEXP for TDC triggered data at the start of intake or expansion stroke respectively or PLIFCOMP or PLIFEXH for BDC triggered data at the start of the compression and exhaust strokes respectively. The macros were written such that the first 45 lines of non-data information were always ignored. The raw data was then read from the beginning of the intake stroke only. Therefore for TDC triggered data at the start of intake, the raw data was read from the first line onwards. For TDC triggered data at the start of expansion, the first 2000 lines of raw data were ignored. For BDC triggered data at the start of compression the first 3000 lines of raw data were ignored and for BDC triggered data at the beginning of exhaust, the first 1000 lines of the raw data file were ignored. A raw LIF trace for a full engine cycle is shown below in figure 3.2.

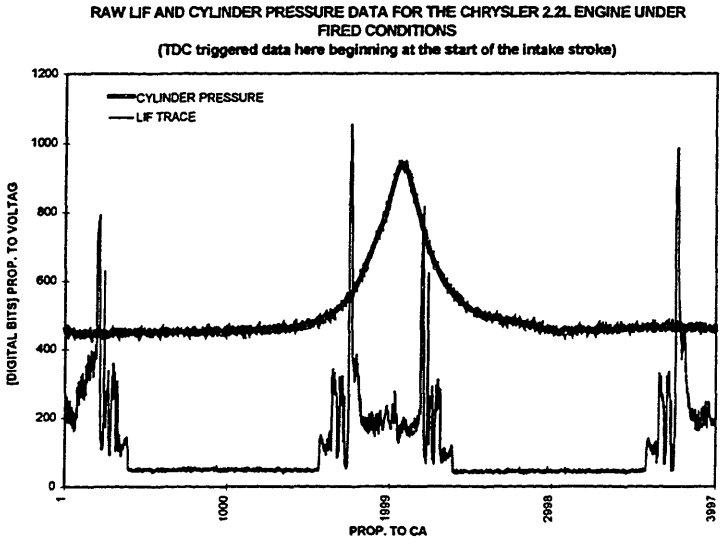

Figure 3.2 Raw LIF and Cylinder Pressure Data from Cylinder no. 4

From the data it can be seen that the LIF trace begins at the start of the intake stroke. As the piston moves downward in the intake stroke, the skirt region passes by the window first, indicated by the jagged profile of the LIF trace, which rapidly increases in amplitude as the fully flooded oil control ring region passes by. There is then an attendant drop in oil film thickness and hence LIF trace profile as the third land, second ring, second land, compression ring and finally the crown land pass by. A free oil film is then left on the inner surface of the liner indicated by the constant horizontal line of the LIF trace. The piston then passes by the window during the compression stroke with the above major features being indicated in the reverse order. The expansion and exhaust stroke LIF trace profiles are similar to the intake and compression stroke profiles.

As mentioned previously the shaft encoder produces 2000 points per revolution, resulting in the LIF data being recorded in 0.18 increments. Since distance from the top of the piston is a convenient way to express oil film thickness data for various speeds and loads, the increments of rotation in crank angle degrees was converted into a linear unit. The distance from the top of the piston is given by the following equation:

$$DP = WL - (a + l) + a\cos\theta + (l^2 - a^2 \sin^2 \theta)^{1/2} \qquad (3.1)$$

where: DP = distance from the top of the piston

WL = window location from TDC, in this case 40mm

a = crank radius

l = connecting rod length

θ = crank angle

The data was then arranged cycle by cycle, 4000 data points per cycle in 20 alternating columns of cycle pressure and cycle LIF respectively. The data was then averaged and fed into another spreadsheet called OFTANALYS.xls (Oil Film Thickness analysis). Here the data for the intake, compression, expansion and exhaust strokes is appropriately shifted to take into account piston tilt and piston ring axial movement in the piston ring groove. The output is then stored in files with name format SK(speed)M2.xls, i.e. SK2000M2.xls.

3.4.1 LIF Data Calibration

Next the data is calibrated by examining the oil film thickness data for the compression stroke in the region of the piston skirt, 2.65cm to 3.5cm from the top of the piston. It is assumed here that the machine grooves on the skirt are fully flooded during the compression stroke. Application of the upper skirt machine marks in calibrating LIF oil film data proves to be a reliable method as described by Deutsch[27]. An important consideration is that the uppermost tool marks on the skirt suffer little or no wear, due to the barrel shaped profile of the skirt. Tamai[16] also suggests using the upper oil control rail as an alternative means of calibrating the LIF data. The major advantages and disadvantages of each method are clearly outlined by Tamai. Figure 3.3 below shows the piston skirt machine marks used in calibrating the LIF data.

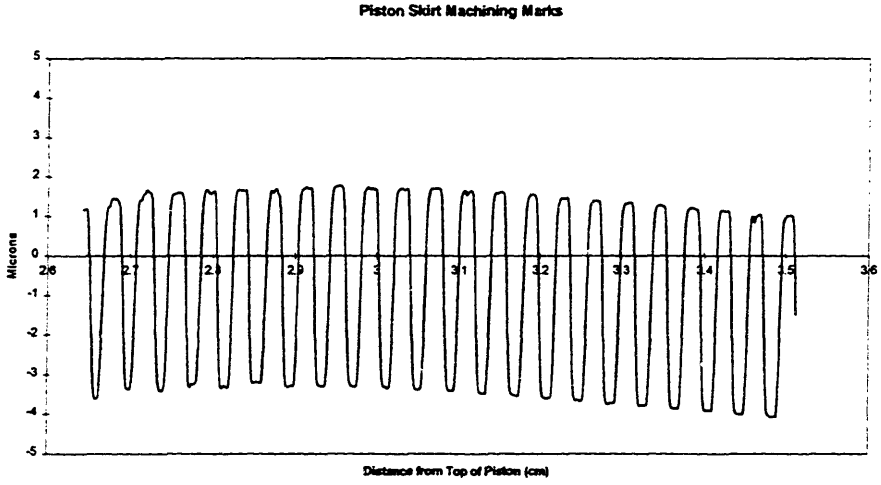

Figure 3.3 Piston Skirt Machining Marks for the Chrysler 2.2L Engine

To calibrate the LIF signal by utilizing the piston skirt machine marks, a single trace was employed. There were usually several cycles where the repeatability of flooded machine marks allowed for accurate calibration. In general when at least three flooded consecutive machine marks were observed the calibration constant was determined within a spreadsheet called L(speed)M2.xls. A sample calibration overlay is shown below in figure 3.4.

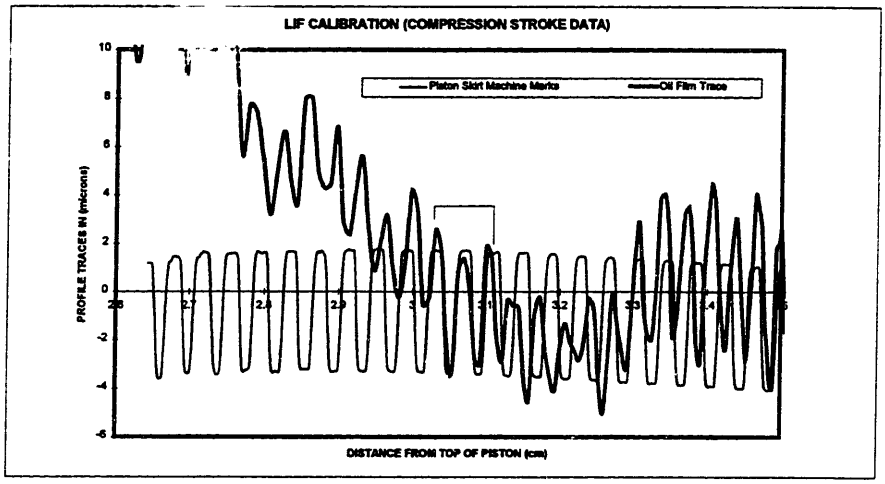

Figure 3.4 Piston Skirt Machine Mark Calibration Method

After the calibration coefficient is determined from a single cycle trace profile, it was then applied to the averaged LIF data file.

(This Page Intentionally Left Blank)

Chapter 4

Data Analysis and System Recommendations

4.1 Simultaneous SO_2 and LIF Data Analysis

The oil film thickness data for each of the three speeds was plotted on the same graph for each of the four engine strokes considered. The following conclusions where drawn from the analysis of the simultaneous data.

a) As previously found the crown land for the Chrysler piston runs wet, at all engine operating conditions considered. The average oil film thickness on the crown land was approximately 15 microns for the intake, compression and exhaust strokes decreasing to 10 microns for the expansion stroke. The reader is here referred to figures G1 through G4 in Appendix G.

b) There was a higher average oil film thickness on the crown land at 2000RPM for all strokes (see figures G1 to G4). However there is no direct link to higher average oil film thickness on the crown land and oil consumption at that speed. This is clearly indicated in figure G5 in Appendix G. The lowest oil consumption occurred at 2000RPM and at the mid load condition.

c) There is an important second land transient phenomena clearly apparent at each stroke as engine speed is increased from 2000RPM through 2500RPM to 3000RPM. There is a pronounced migration of oil from above the scraper ring where the film thickness is greatest at 2000RPM to a zone immediately below the compression ring where the film thickness is greatest at 3000RPM. The lubricant film thickness can be said to undergo a transition at the speed 2500RPM as indicated by the transition traces for each stroke at that speed.

d) If the ring gap of the compression ring were to become aligned with this transition zone, and the second land pressure were higher than the crown land pressure, then a jet of lubricant could be sprayed into the combustion chamber, which would explain the higher oil consumption observed at higher engine speed (see figure G5). Care must however be exercised in generalizing one-dimensional oil film thickness data with what may be occurring azimuthally around the piston.

e) The average oil film thickness between the liner and compression and scraper rings respectively was on the order of 10 microns for the intake and compression strokes. For the expansion and exhaust strokes, film thickness between the liner and compression and

scraper rings respectively was approximately 6 microns. This could be attributed to higher instantaneous liner temperature resulting in reduced lubricant viscosity and hence thinner oil films for the expansion and exhaust strokes.

f) Temperature must be a significant factor in engine oil consumption. As discussed in a) above, thicker films were observed on the crown land at lower engine speeds with lower oil consumption. This shows that thicker films on the crown land is not the only criteria for higher engine oil consumption. A mechanism must be involved where higher instantaneous liner temperatures result in vaporization of oil films off the free liner surface and crown land. This would explain the higher oil consumption observed at higher engine speeds, where engine operating temperatures are higher.

4.2 Conclusions

A comparison was made between the SO_2 data obtained and that obtained by Versteegh[28] and Artzner[22]. A chart of oil consumption per cylinder in milligrams (mg) per cycle versus engine speed for the Chrysler engine fired at mid load is shown in figure G6 of Appendix G. The trend in oil consumption is exactly opposite to that obtained by Versteegh's tritium method. The scatter on Artzner's data is such that no real trend can be determined. Comparative oil film thickness data for the top land of the Chrysler piston during the compression stroke is provided in table G1 of Appendix G. The trends in average oil film thickness are different, with Versteegh's data showing an increase in oil film thickness at 2500RPM followed by a decrease at 3000RPM. The Chrysler piston was equipped with a C1 type ring pack with unpinned rings and a modified second ring gap, six times standard. The details of the C1 ring pack are listed in table G2 of Appendix G.

From the data it can be seen that there is a high degree of variability in oil consumption values for the speeds considered. More important however is the possibility that the speed range may not be large enough to observe any real trend in oil consumption. Furuhama[29,30] and Hyuga[29] have found that there is a consistent increase in oil consumption with increasing engine speed for the engine speed range considered above for a variety of spark ignition test engines used. Further data is required to confirm the trends in oil consumption observed.

4.3 System Recommendations

The following system recommendations are suggested for better operating efficiency.

a) The first major improvement that can be made is the complete elimination of the long and short heated lines in the system. This has been done by Kiesel[31] on the Kubota single cylinder diesel engine with better observed performance.

b) The possibility of reducing the number of joints in the system must be investigated. Joints can accumulate deposits which can then become dislodged in the system at a later time, thereby potentially affecting the analyzer output.

c) A method should be found to eliminate the furnace thereby making the system more portable. A possible solution to this problem would involve wrapping a sample tube around the exhaust pipe itself in the form of a short helix. The sample tube is then in turn wrapped with heating tape. The conductive as well as the radiative heating of the exhaust manifold is therefore fully utilized.

d) A better method of collecting exhaust samples is required. Kiesel suggests utilizing a specially designed sampling probe which would be inserted into the exhaust manifold. This sampling probe would be designed such that clogging with particulates of diesel exhaust would not occur. The same probe could be applied to spark ignition engines.

e) The possible reaction of exhaust gas components with sample line material must be investigated. The ideal system would consist of nonreactive high-temperature material, with a smooth internal surface finish and gradual changes in curvature. There should be no right angles in the flow. Quartz tubing would work very well, but a means must be found to shield the system tubing from engine vibration and shock.

f) A reliable method must be found to verify SO_2 concentration in all calibration gasses.

g) A means of metering the correct amount of ozone to destroy the NO(g) produced by the engine must be investigated further. Kiesel suggests that 10 times the amount of ozone necessary to destroy the maximum amount of NO(g) produced by the engine should be used. This might be considered wasteful but nevertheless essential if one is to ensure that there is no NO(g) reaching the SO_2 detector. An alternative solution might involve the utilization of a catalytic converter that selectively removes NO(g) from the exhaust. The pressure drop across this should be low enough so as not to restrict the flow.

h) A system that relies on another type of SO_2 detection could be used, i.e. an infrared detector, which is not sensitive to NO(g). This would solve another problem inherent in the

current SO_2 system which utilizes ultra-violet light to fluoresce the SO_2 sample. The ozone added to the exhaust gas sample to eliminate NO(g) also absorbs UV light in the detector resulting in a decrease in the signal output of the detector proportional to the percentage of residual ozone remaining. A system change will overcome this problem.

i) The MIT SO_2 detector has a published time to respond to an SO_2 concentration step change of 3 to 4 minutes before 95% of the new value is reached. The sampling system with the long and short heated lines included can add another 20 to 30 seconds before the signal starts to rise. This long response time makes the system insensitive to oil consumption caused by short term transients which may occur in the engine. These transient effects are especially critical for gasoline engines which are influenced by rapid intake pressure changes. An effective means must therefore be found to shorten the system flow path.

j) System response time is also affected by exhaust back pressure used in driving the sample flow through the system. It is recommended that a pump be used to minimize the response time.

Application of the above system recommendations will aid in the development of a reliable system which will facilitate evaluation of rapid time scale transient phenomena. In addition advanced exhaust emission analysis will yield valuable oil consumption information in conjunction with new Two Dimensional Laser diagnostic methods being developed.

PART II

Development of a Two Dimensional Laser Induced Fluorescence (LIF) System for the Kubota Single Cylinder Indirect Injection Diesel Engine.

This section includes a detailed description of the following:

Chapter 5 Kubota Engine Modification and Supporting Component Design.

Chapter 6 Experimental Setup.

Chapter 7 Fundamental Dye Chemistry.

Chapter 8 System Calibration

(This Page intentionally Left Blank)

Chapter 5

Kubota Engine Modification and Supporting Component Design.

5.1 The Kubota Engine

The engine utilized in this research is a single-cylinder indirect injection diesel engine model EA300 NB1. This engine is built up from a die cast aluminum block and an alloyed cast iron cylinder head. The bore and stroke of this engine are 75mm by 70mm respectively[32]. These engines are typically used as remote power generators for a variety of industrial and commercial applications. This engine was selected for Two Dimensional Laser Induced Fluorescence (2D-LIF) research for the following reasons:

a) Significant One Dimensional Laser Induced Fluorescent (1D-LIF) studies were performed on the Kubota EA 300 NB1 model in the past. It is therefore logical that the same engine should be used as a test bed for further study and correlation with the past history of oil film thickness data already obtained.

b) Sulfur Dioxide (SO_2) Diagnostic equipment is currently being optimized in parallel on another Kubota EA 300NB1engine. It is intended to obtain simultaneous SO_2 and 2D-LIF data for this engine.

c) The Kubota diesel engine is small, portable and inexpensive.

d) The Kubota engine utilizes removable cylinder liners permitting comparatively easy installation of quartz or fused silica optical windows.

e) Finally the Kubota diesel engine lends itself to easy modification because of the modular layout of the major components including the radiator and fuel tank.

Engine specifications, and operating characteristics are listed in table H1 of Appendix H.

5.2 Kubota Piston and Ring Pack.

5.2.1 Piston

The piston is made from high-silicone aluminum alloy and consists of three machined piston ring grooves for a compression, scraper and oil control ring respectively. The piston head is flat-formed. The crown land of the piston has 11 machined circumferential grooves. These machined grooves aid in effectively dissipating heat and preventing piston scuffing. The second

land, third land and skirt are smooth. The piston skirt is barrel-shaped and is non-existent in the region of the wrist pin axis[12].

5.2.2 Piston Rings

The top ring is a half-keystone with a 7° angle on the top surface to prevent gas leakage. The surface of the ring is plated with hard chromium for better wear resistance.
The second ring i.e. the oil scraper ring has a tapered outer face and an undercut on the outer periphery which effectively prevents the rise of oil along the cylinder liner. The third ring is the oil control ring. The oil control ring is a two piece design featuring symmetric dual rails with chamfered contact faces. Radial tension is maintained by a circumferentially coiled spring located on the inner diameter of the oil control ring. The area between the two rails contains eight slots which are spaced at regular intervals and facilitates oil transport through escape holes in the piston. The oil control rings are plated with hard chrome to enhance wear resistance. See figure 5.1 below.

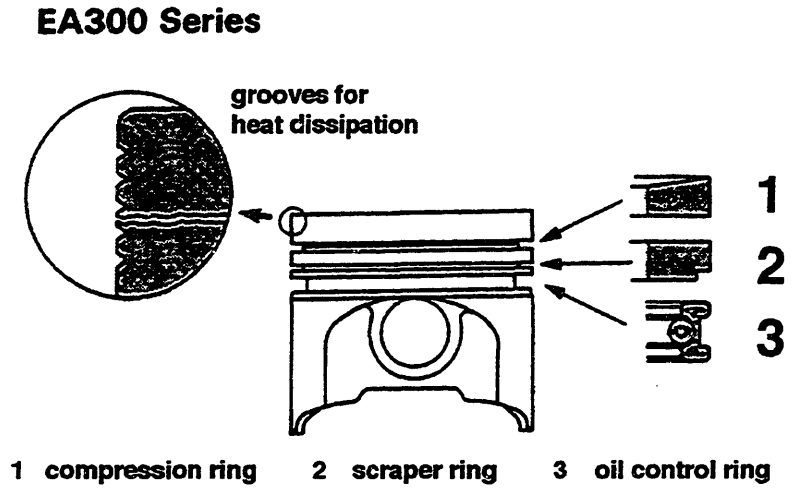

Fig. 5.1 Drawing of the Kubota Piston and Ring Cross Sections.

5.3 Engine Block and Cylinder Liner

The engine block of the EA 300NB1 is made from die-cast aluminum. The block is provided with oil galleries which aid in lubricating the crankshaft, main bearing case and rocker arm bracket. The cylinder liner is made from a special cast iron possessing excellent wear

resistance. The cylinder liner can be press fitted into the engine block by applying hand tools and is cooled by a coolant mixture of antifreeze and water. See figure 5.2. Heat release is facilitated by natural convection of the coolant mixture upwards and through the radiator which in turn liberates heat via forced convective air flow provided by a crankshaft driven fan. Two O-rings located at the lower part of the cylinder liner periphery prevent water leakage. Gas leakage is prevented by compressing a cylinder-head gasket against the protruding portion of the cylinder liner and cylinder head.

EA 300 SERIES

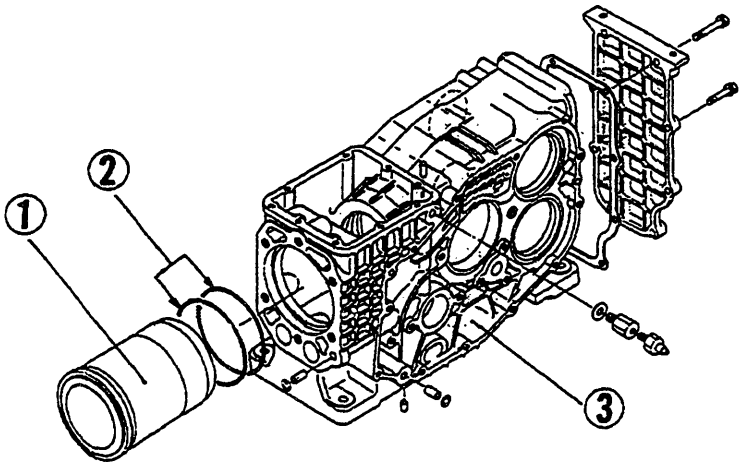

1 CYLINDER LINER 2 O-RINGS 3 ENGINE BLOCK

Fig. 5.2 Drawing of the Kubota Engine Block and Cylinder Liner.

5.4 Kubota Engine Block and Accessibility

A detailed cross sectional drawing of the Kubota engine is shown below in figure 5.3. From this drawing it can be seen that the cylinder liner is only accessible from the *minor* and not the *major* thrust side of the engine. Also important is the restricted area as depicted in detail in figure I1 of Appendix I.

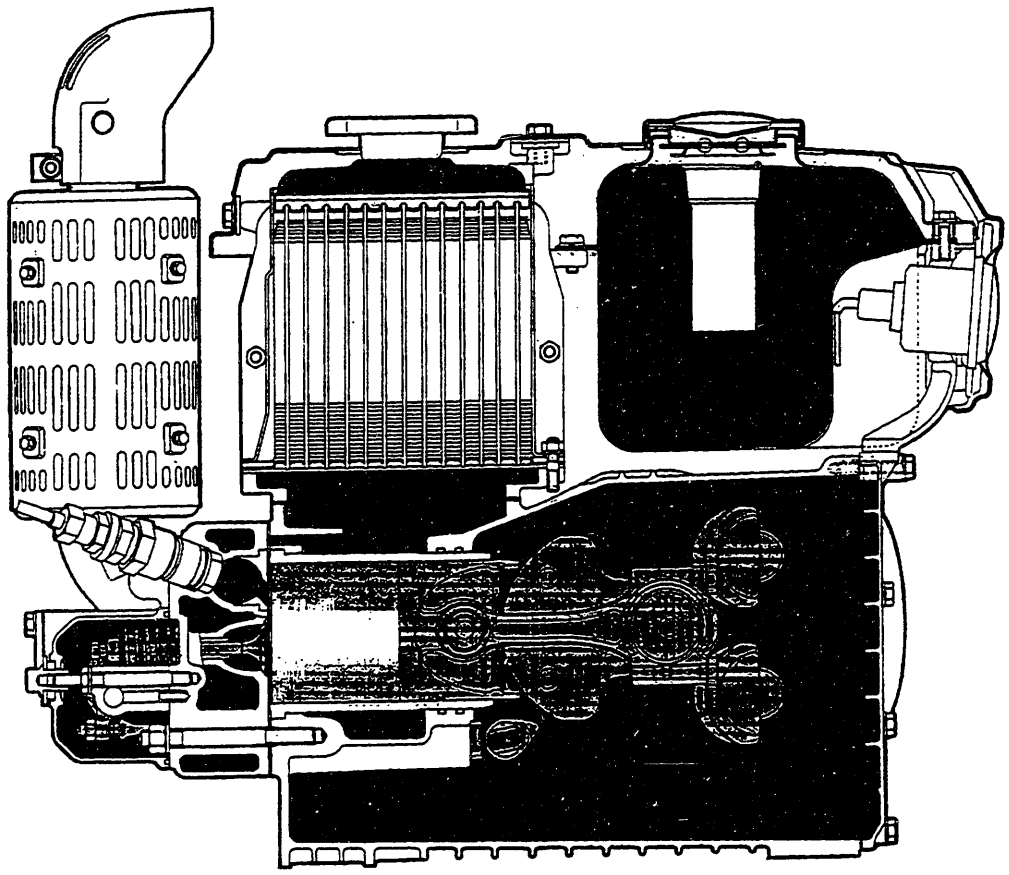

Fig. 5.3 Cross Section of the Kubota Single Cylinder Diesel Engine.

The restricted area available for optical access is constrained for the following reasons:

a) The uppermost cylinder-head stud-housing, protrudes directly over the cylinder liner by .7 inches.

b) There are two O-rings sealing the lower end of the cylinder liner thus making intrusive optical access unavoidable in the event that the entire piston stroke is to be observed.

c) The cylinder liner is barrel-shaped and tapers towards the base of the liner. This introduces window-sealing problems as there is less material to support an optical window in this region. Refer to the detailed drawing in figure I1 of Appendix I .

From figure I1, it can be seen that for non-intrusive optimization, maximum linear accessibility is 1.82 inches. A rebuilt Kubota engine was established as a stand-alone unit such that the optical diagnostic and data acquisition systems could be optimized. Direct access to the minor thrust side of the cylinder liner was accomplished by making modular changes in the Kubota equipment layout.

5.5 Kubota Engine Modifications

The following modular modifications were made:

a) The radiator was removed from it's location immediately above the cylinder liner and was bolted to a support mount on the engine block. This component relocation meant that the crankshaft driven fan had to be replaced with an externally powered blower for forced convective cooling.

b) The fuel tank was removed from it's original location on top of the engine block and mounted on a support bracket just behind and above the crankcase backing plate.

Relocation of the above components provided the necessary access for the diagnostic equipment. Interface components for sealing the coolant chamber and providing an optical pathway to the cylinder were then required.

5.6 Interface Component Design

A manifold plate and an optical collar were designed to seal the coolant chamber and provide optical access to the cylinder liner.

5.6.1 Manifold Plate

The manifold plate with external dimensions matching the base interface dimensions of the radiator housing was designed and manufactured. This manifold plate was machined from 6061 aluminum alloy. Nine (9) clearance holes were drilled to accept M7 securing bolts. A through hole for the optical access collar was machined to the toleranced dimensions as indicated in figure I2, showing the engineering drawing of the manifold plate, see Appendix I. The manifold plate was then surface finished on opposite faces and on the optical collar clearance hole.

5.6.2 Optical Access Collar

An optical access collar was designed and manufactured using a wire electro-discharge machining (EDM) process. This collar consists of a hollow neck 2.754 inches long, which terminates with a slotted groove at one end. This slotted end groove houses an O-ring which seals the interface between the end of the collar and the flat machined on the cylinder liner. End sealing against the coolant was accomplished by applying sufficient pressure to this face sealing O-ring. Two threaded fasteners held the collar in place relative to the manifold plate, via clearance holes and threaded holes in the former and latter. By adjusting the torque on these fasteners the O-ring compression was controlled. Helicoils were inserted in the threaded holes of the manifold plate to enhance strength and increase maximum tightening torque. Care was taken to supply enough compression to provide an effective seal and not change the bore distortion of the cylinder liner. The pathway between the collar and the manifold plate was sealed via a radial type O-ring housed within a circumferential slot machined in the optical access collar. The dimensions of each O-ring seat were selected by reference to the appropriate O-ring tables and determination of the necessary percent O-ring compression required. Engineering drawings of the optical access collar are shown in figures I3 and I4 respectively of Appendix I. Photographs of the optical access collar are shown in figures I5, I6 and I7 of Appendix I.

5.7 Optical Window Material Selection

5.7.1 Typical Materials

The optical window required for these experiments had to meet the following criteria:

a) The window has to resist the maximum cylinder pressure.

b) The window should allow for transmission of wavelengths within the visible spectrum i.e. 400 - 700 nm.

c) The window should be durable and scratch resistant.

d) The window should perform well under thermal load cycles and sustain high thermal shock, with maximum operating temperature in excess of 400°F .

Sapphire, quartz and fused silica are the major optical materials available that perform well under engine operating conditions.

5.7.2 Sapphire Windows

Sapphire was initially eliminated due to it's high cost but has superior qualities worthy of mention. Sapphire in many ways makes for a superior window material. Because of its extreme surface hardness, sapphire can only be scratched by few substances (such as diamond or boron nitride) other than itself. Chemically inert and insoluble in almost everything except at highly elevated temperatures, sapphire can be cleaned with impunity. For example, even hydrogen fluoride fails to attack sapphire at temperatures below 300°C. Sapphire exhibits high internal transmittance from 150nm in the vacuum ultraviolet to 6000nm in the middle infrared. External transmittance is shown in figure J1 of Appendix J. Because of its high strength (Young's modulus is roughly five times higher than fused silica and most glasses), sapphire windows can safely be made much thinner than windows of common dielectrics. This is very important especially in the case of thin walled cylinder liners. Because of the exceptionally high thermal conductivity of sapphire, thin windows can be effectively cooled by forced air or other methods[33].

5.7.3 Fused Silica Windows

Synthetic fused silica (amorphous silicon dioxide) is formed by chemical combination of silicon and oxygen. It is not to be confused with fused quartz which is made by crushing and melting natural crystals. Synthetic fused silica is far purer than fused quartz. This increased purity assures higher ultraviolet transmission and freedom from striae and inclusions. See figure J2 of Appendix J for a semilogarithmic comparison of the internal transmittances of UV grade synthetic fused silica and BK7 glass[33]. Fused silica was selected instead of quartz because of the following advantages:

1. Greater UV and IR transmission.
2. Low coefficient of thermal expansion, providing stability and resistance to thermal shock over large temperature excursions.
3. Wider thermal operating range.
4. Much higher resistance to radiation darkening from UV.
5. Increased hardness and resistance to scratching.

The reader is here referred to table J1 of Appendix J for a comparison of the optical properties of various transmitting media.

5.8 Optical Window Design

Several window designs were considered and are shown below in figure 5.4.

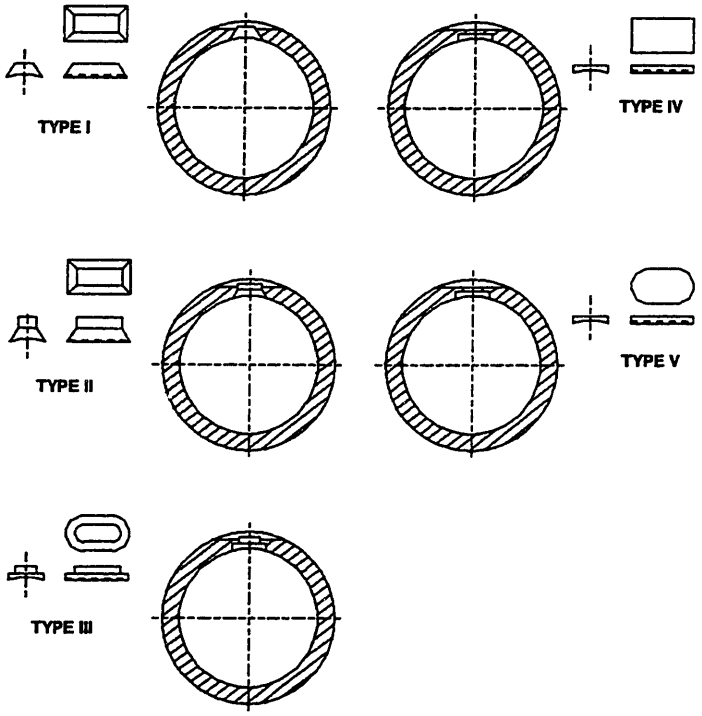

Fig. 5.4 Various Optical Window Designs Considered for the Kubota Diesel Engine.

All rectangular planform designs would retain oil at their transverse edges, which would increase the oil film thickness in those regions thereby affecting the OFT data collected. This was especially a problem anticipated for the type IV window design. The type IV window design had the major cost advantage compared to all windows in that it was the easiest and cheapest to manufacture, but was eliminated based on possible oil retention at the transverse edge and high stress considerations due to compromises between minimum cylinder wall thickness and minimum window thickness. Windows with semicircular end profiles had an advantage in that the semicircular oil retention was less dramatic because of better edge contour conformity with the walls of the cylinder liner. These windows were however very difficult to manufacture and concentricity tolerances were costly to maintain. Therefore type III and V designs were eliminated. Type II was eliminated as this was merely a complicated version of type I and necessitated an expensive shaping tool be made for manufacturing the part. It was therefore decided to accept the type I design as this provided a low stress design, was tried and proven by Toyota and required a rather simple trapezoidal matching slot be machined in the cylinder

liner. Also the sloping faces of this design allowed the transverse edge to be shifted well out of the optical data acquisition zone thereby reducing window edge effects on the data collected.

With all the window designs considered, it was important to realize the tradeoff between the cost of machining the window geometry from fused silica stock and machining a matching groove in the cylinder liner. It was for this reason why only simple geometric shapes were selected. See figure I8 of Appendix I, for the engineering details of the type I window design. The window dimensions were influenced by **a)** the restricted zone which allowed for non-intrusive optical access and **b)** the minimum wall thickness of which the optical access port could be made, since no contact should occur between the window and the internal edges of the optical access port after assembly, see figure I11 of Appendix I. It should be noted that the available standard O-ring cross sectional diameters influenced the minimum wall thickness of the optical access port and hence indirectly influenced the window planform dimensions.

5.9 Cylinder-Liner Window-Slot Location and Geometry.

Based on the restricted area within the engine block, the cylinder liner slot location was selected to provide for non-intrusive initial access. See figure I9 of Appendix I, for details of the slot location. It should be noted also that the external characteristics of the cylinder liner i.e. the liner external surface contour influenced the window slot location. It can be seen that the slot is located in a zone characterized by the minimum change in surface contour, that is the zone of the cylinder liner that is essentially cylindrical. The reader is here referred to figures I10 and I11 of Appendix I for the interface details of the collar and the window. Figures I12 and I13 of Appendix I are photographs showing the window located in the slot machined in the liner.

5.10 O-ring selection and groove design

5.10.1 Material

In any particular application, the compound of which the O-ring is made is usually based on the polymer having the optimum combination of characteristics matching the requirements of the application. For the Kubota engine application, silicone based O-rings were found to be optimum for the following reasons:

1. A minimal compressive force was required in deforming the rings thereby effecting a seal without deforming the cylinder liner, in the case of the face seal type O-ring.
2. Silicone based O-rings were found to be chemically compatible with the service fluid, in this

case the engine coolant.

3. Silicone O-rings performed well over the Kubota engine operating temperature range.
4. Silicone O-rings exhibited sufficient elongation.

The reader is here referred to table K1 of Appendix K.

5.10.2 Cavity Design

A rectangular cross-section groove is recommended for most applications[34]. Both the face and radial seal grooves have rectangular cross-sections. The planforms of the radial and face seal grooves are both rectangular. The corners were radiused for the best possible O-ring contour fit. The outside and inside face seal groove corners were .302 inches and .150 inches respectively. The sides of the groove slope outward from the bottom, up to ten degrees. The internal groove corner radius for the radial seal was .261 inches as shown in the auxillary view of figure I4 of Appendix I. The sides and bottom of the groove were finished to 50 micro inches rms. All internal corners were broken to .030 inches. External corners were broken to .005 inches. Cross-sectional squeeze of the O-rings when installed was no less than .005 inches. The maximum O-ring stretch was not allowed to exceed 5% at installation.

5.10.3 Assembly Precautions

All sharp edges on the optical access port were removed via a deburring process and subsequent polishing. Vacuum grease was smeared over the O-ring prior to installation and sufficient care was exercised in not twisting the O-ring during installation. Views of the piston through the optical access port, at four crank angle positions are shown in figures I14, I15, I16 and I17 of Appendix I.

Chapter 6

Experimental Setup

6.1 Kubota Engine Setup

The Kubota diesel engine was bolted to a cast iron support block which was anchored to the laboratory floor. The fuel tank and engine radiator were independently mounted above the engine on support brackets which were bolted to the cast iron support block. An electrically driven blower provided the forced convection required to cool the radiator fins. The coolant was pumped upwards via a pump, to the radiator, where it was cooled and returned to the engine via a return line. Fuel was gravity fed to the engine via the fuel strainer.

The engine was started using the Kubota starter motor with the aid of an industrial 12 volt power supply unit. A small bolt, screwed into a threaded hole on the rim of the flywheel provided a TDC pulse everytime it crossed the magnetic field of a magnetic pickup bolted to the cast iron support block. This TDC signal was used in triggering a CCD camera and a Xenon flashlamp. The CCD camera was independently supported at 24 inches above the optical access port on the engine. The camera was anchored to the floor and not the engine block due to vibration considerations. A plate type beamsplitter was positioned over the optical access port. The beamsplitter was clamped in a Melles Griot optical bracket which was in turn supported by a short column screwed into the manifold plate. See figure L1 of Appendix L for a sketch of the engine setup.

6.2 Window Installation

The trapezoidal fused silica window was installed in a mating groove machined in the cylinder liner. High temperature RTV epoxy was used as the adhesive. A thin uniform layer of this epoxy was applied on the four (4) sloping faces of the window before insertion into the matching liner groove. Excess glue was then scraped away from the edges of the window. Care was taken not to smear the window during this process. The window was then held in place at its ends by two oil control rails. These oil control rails were slid to their supporting locations with the top of the piston. This ensured that the axes of the rails and the cylinder liner coincided. Care should be taken not to scratch the liner surface with the ends of the oil control rails. Tape was wrapped around the ends of the rails to ensure that scratching did not occur.

The ends of these oil control rails were then wedged to prevent relative end movement which would otherwise occur as the window was cured into position at 82°C. See figure L2 of Appendix L. The oil control rails were selected since they provided the greatest circumferential support area.

The first attempt at the installation process resulted in the window protruding slightly into the bore. After the curing process the cylinder liner was honed for 1 hour, using the finest grit honing stones and subsequently polished using a lint free rag and diamond paste. Care should be taken not to chip the edges of the window during the honing process. It is important that the window be at least a few microns recessed after the curing process in order to facilitate honing to an appropriate window liner flushness.

It is recommended that three (3) end-wedged oil control rails with axes coincident with the liner axis, and positioned at the ends and center of the window be used instead of two rails. This will result in better load distribution during curing and better window-liner flushness.

6.3 Cylinder Liner Installation

An orientation mark was drawn down the length of the cylinder liner, bisecting the window. This centerline was projected over the end faces of the cylinder liner and was aligned with a center mark on the engine block. The cylinder liner was then carefully inserted. Care should be exercised in maintaining alignment, since liner rotation is not possible once the end of the liner is gripped by the O-rings in the engine block. Correct window orientation was then checked by inserting the optical access collar. If the flat on the cylinder liner was not parallel to the base of the manifold plate, the process would have to be repeated.

6.4 Data Acquisition and Supporting Equipment

The data acquisition equipment used in this experiment consisted of a Pulnix Charge Coupled Device (CCD) Camera and a Macintosh Personal Computer with the necessary graphics card and software installed. The supporting equipment included a Stroboslave Flashlamp capable of up to 25,000 flashes per minute, an Argon ion laser, with 4W output and tunable to three wavelengths including, 514.5 nm, 488 nm, and 364 nm a plate type beamsplitter and a Melles Griot orange filter, used to filter the fluorescence of the Rhodamine 6G dye used. The following is a description of the major components and an outline of their theory of operation.

6.5 Principles of CCD operation

A CCD array may be used to collect and read out optically generated signals. The basic structure is illustrated schematically below in figure 6.1 for an *n*-channel array.

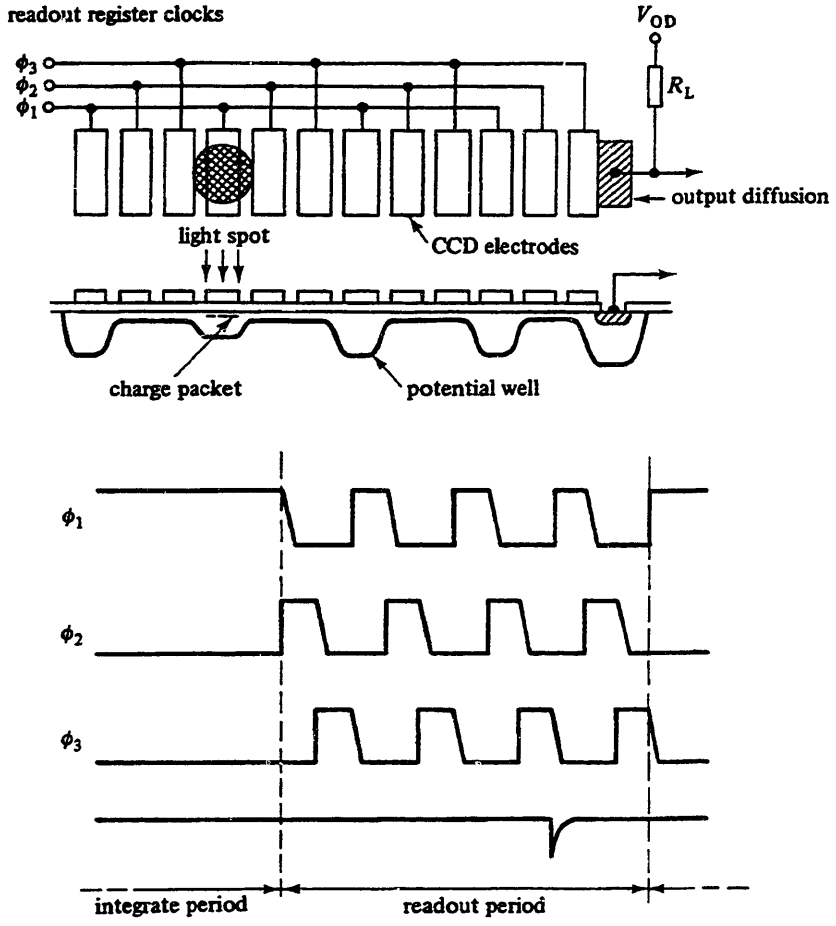

Fig. 6.1 Basic Principle of CCD Operation.

An optical system is used to focus an image (depicted as a single light spot in this case) on the front face of the CCD. Initially any one set of electrodes, for example ϕ_1 is held at a positive clock voltage thus creating a potential well under each of these electrodes, the other electrodes are held at zero volts or a small resting potential. Photons entering the silicon substrate, either through or between the electrodes (depending on the electrode material), generate electron-hole pairs by virtue of the photoelectric effect. The minority carriers or electrons generated within the depletion regions or within a minority carrier diffusion length of the depletion regions, are collected under each ϕ_1 electrode[35].

The number of electrons collected under a given electrode within a given period of time, generally called the integration period, is proportional to the local light intensity. Thus the pattern of charge that collects under the electrodes is an analogue replica of the light intensity across the original image. At the end of the integration period the charge pattern is read out by clocking the array in a conventional manner, care being taken to ensure that the clocks run long enough to allow each potential well to empty. The single output pulse that would ideally result from imaging a single source of light is shown above in figure 6.1. At the end of the readout period the device is again switched to the integration mode and the cycle is repeated.

We will now examine CCD image sensor characteristics to determine factors that limit its performance. Resolution, sensitivity and dynamic range are the major performance criteria applicable to this research.

6.5.1 Resolution

The image sensor resolution constitutes a very important parameter of CCD image arrays. Spatial resolution is defined as the ability to discriminate between closely spaced points in the image. Spatial frequency of an image focused on to the imaging device and modulation transfer function (MFT) constitute a convenient means of assessing resolution. Any image can be Fourier analyzed into periodic intensity variations. The spatial frequency of these Fourier components is normally expressed in line pairs per mm, where one line pair is the spacing between maxima of intensity. The spacing of electrodes is also expressed as a spatial frequency f_0 (i.e. elements per mm) and the spatial frequency f of the image focused on the device may be normalized as the ratio f/f_0. The resolution is limited ultimately by the spacing of the resolution elements to a normalized spatial frequency $f/f_0 = 0.5$, known as the Nyquist limit, therefore at least two resolution elements are necessary to image one line pair.

6.5.2 Dark Current

Dark current affects all silicon imaging devices. Dark current is rooted in the thermal generation of minority carriers which takes place in any semiconductor. Dark current generation tends to be non uniform over a whole array and resulting fixed pattern noise is a major factor in determining CCD sensitivity and dynamic range. Dark current also causes potential wells to be slowly filled with dark generated charges, with the result that there is a maximum useful light integration time.

Dark current is highly temperature dependent, increasing by a factor of approximately 2 for every 10°C rise in temperature. Therefore an effective means of cooling the CCD array is required to keep the dark current generation to a minimum and maintain sensitivity.

6.5.3 Channel Options

Surface channel CCD (SCCD) and buried channel CCD (BCCD) constitute the two main types of CCD channel options available. The main aim as far as CCD data acquisition is concerned is high image readout rates at high efficiency. BCCD's are very attractive as far as high speed data acquisition is concerned for the following reasons:

a) They possess the highest possible readout rates

b) Higher transfer efficiency

c) Less temporal noise due to trapping states.

BCCD's however have higher theoretical dark current. SCCD's have only one advantage and that is that the array electrodes can be biased into accumulation to prevent charge spreading as a result of an optical overload. SCCD's must be operated with a bias charge to ensure an adequate transfer efficiency at low signal levels.

6.5.4 CCD Sensitivity and Dynamic range

CCD image sensors for high speed data acquisition should be capable of operation at low levels of illumination. In other words the image sensor should possess high sensitivity which is especially required for the current Kubota experimental setup in which light must be focused down a narrow optical access port. The CCD image sensor should also have a wide dynamic range, in other words a sufficient range to accommodate large variations in levels of illumination encountered. Dynamic range is determined at the upper end by the maximum charge handling capability and at the lower end by the various noise sources present. Device sensitivity, i.e., the lowest signal level at which the device can operate is clearly a function of both the noise performance and responsivity.

6.5.5 Responsivity

This is defined as the generation of signal charge from light energy and is usually expressed in amperes per watt.

6.6 The Pulnix TM-9700 CCD Camera

The Pulnix TM-9700 CCD camera was utilized in obtaining the first fluorescent photographs of the Kubota piston ring pack. The camera can be locked by an external horizontal sync and can be reset asynchronously by applying a input voltage pulse. Shutter speed is controlled by either an external double pulse or internal speed control with a 10-position dial on the back panel. The TM-9700 has a built-in frame memory in order to convert progressive scanning images to RS-170 interlace scanning images. This feature provides the following advantages:

a) Asyncronously captured images are output as standard continuous video signals so that a normal monitor or frame grabber can display or process without a special asynchronous video grabber.

b) Integration video is continuously output until the next capture. Normally, the camera cannot output the video signal during the integration, and the periodic integration causes a blinking video signal. The TM-9700 memory keeps the stored image until the next image is completed, so that there is no blank interval during the integration.

c) Digital format of the video output can be used as a direct interface with a computer. The format is interlace or progressive.

The TM-9700 utilizes a state of the art CCD called a Progressive scanning interline transfer CCD which scans all lines sequentially from top to bottom at one frame rate (30Hz). Like a non-interlaced computer screen, it generates a stable crisp image without alternating lines and provides full vertical TV resolution of 484 instead of 350. The interline transfer architecture is also important to generate simultaneous shuttering. This is different from full frame transfer architecture which requires a mechanical shutter or strobe light in order to freeze the object in motion[36]. For further information on the Pulnix TM-9700 CCD camera used, refer to Appendix M.

6.7 The Stroboscope and its Application

The stroboscope is an instrument that utilizes intermittent light to allow the visual observation of periodic motion whether rotating or reciprocating. Two general methods are used to control the light. The first method involves the use of a rotating disk with an appropriate slit or set of slits to interrupt the light, thereby acting as a mechanical shutter. The second method involves the use of an electronic flashlamp driven by an oscillator to provide the pulsing light.

The stroboscope is generally pulsed at an integral multiple of the subject frequency under consideration[37]. That is if the consecutive pulses come at the same phase as the periodic motion being observed, the object appears to be at rest. It should be noted that this phenomenon occurs only at a strictly defined ratio between the flash frequency and the motion frequencies[38]. This technique is applied in freezing the motion of the piston, which can be observed at a particular point in every revolution if the strobe flash rate is identical to the frequency of rotation of the crankshaft. If piston observation at the same point in every cycle is required then the strobe flash frequency is half the frequency of rotation of the crankshaft. If the strobe flash frequency is slightly different from the fundamental frequency of object motion, then the object appears to move in slow motion either forwards or backwards depending on whether the flash frequency is less than or greater than the fundamental frequency respectively. Images obtained in these circumstances are called 'drifting' or unstable images. Small irregularities in the speed of the oscillating object are very evident since they are directly observable instead of being superimposed upon the actual speed of rotation[39].

6.7.1 Synchronous and Non-Synchronous Images

If steady state engine operation is assumed, i.e. no change in engine rpm occurs, and the strobe frequency is set equal to an integral multiple of the piston reciprocating frequency, then the stroboscopic piston images observed are non-synchronous. The strobe frequency in this case is adjusted externally to match the object reciprocating frequency and not through any relation between the stroboscope and the observed motion. Nevertheless in this case, the initially motionless image of the object begins to drift. Because of this a method was sought to trigger a flashlamp via periodic pulses from the reciprocating piston under consideration. Therefore the images obtained would be stable even though the engine operation may not. Such images are called synchronous. The time-occurrence of the synchronous stroboscopic image is dependent soley on the investigated phenomenon, and may be non-periodic. The instant when the synchronous image is created is in this case linked to the passage of a particular feature on the piston through a certain crank angle degree either before or after top center (TC). As previously described a magnetic pickup triggers a flashlamp and a CCD camera simultaneously. The triggering circuit should have an optional time delay built in, such that sequential pictures of the piston motion can be captured. The triggering circuit should also have the capability of skipping every other trigger signal, such that a picture of the piston in every cycle can be obtained. One cycle of a four stroke engine is two revolutions of the crankshaft.

6.8 Stroboscopic Blur *f{(pulse width (w), velocity (v)}*

Like a photographed image of a fast motion, a subjectively perceived stroboscopic image also displays some unsharpness known as blur. The cause of blur in the stroboscopic effect is due to the finite image duration in which interval the position of the observed object changes. Blur depends on the stroboscope design (image duration) and object velocity[40]. Blur due to image duration can be eliminated by varying the flash pulse width. Pulse width decrease of a few mircoseconds can significantly sharpen an image. Typical pulse widths are on the order of microseconds to nanoseconds at best. In the case of reciprocating sinusoidal motion, the blur depends on the phase of the motion. It is smallest for extreme positions at which the velocity of the oscillating object passes through the zero value, i.e. the top center (TC) and bottom center (BC) locations, and greatest in the central position at which the velocity reaches its maximum, i.e. the piston midstroke location.

6.9 Stroboslave Type 1539-A

The type 1539 Stroboslave is a small, inexpensive stroboscope. This stroboscope has no internal oscillator for flashing-rate control. Therefore, it must be triggered by an external device. The stroboslave is typically used for high-speed photography and observation of objects moving at high speeds in this case the piston. For these applications, the instrument is triggered by an electrical pulse generated by a magnetic pickup assembly as previously described. A time delay can be built into the triggering circuit, such that sequential points in the same revolution or cycle can be observed. The external trigger automatically synchronizes the flash with the reciprocating movement of the piston. If the flashing rate of the stroboslave differs slightly from the fundamental speed of the reciprocating object, the object will appear to move slowly through a complete cycle.

The 1539 model stroboslave produces a peak light intensity of up to 11 million beam candles when used on the HIGH-intensity range, and up to 18 million beam candles when used for single-flash applications. The Stroboslave operates over the basic ranges, 0 to 25,000 flashes per minute[41].

(This Page Intentionally Left Blank)

Chapter 7

Fundamental Dye Chemistry

7.1 Introduction

This chapter has been included to give the reader an overview of the important facets of dye chemistry as they apply to this research. The information included here summarizes detailed literature research conducted in this area and shows the initial development of the dye selection process as it applies to the 2D-LIF diagnostic technology being developed on the Kubota, single cylinder diesel engine. The chemistry relevant to organic dye lasers is applicable in this study, as far as efficient pumping of lasing media, fluorescent lifetimes, solvents and fluorescent quenching are concerned. The major groups of dyes that will be considered here are the Xanthene dyes, notably the Rhodamine family of dyes and the Coumarin dyes.

Lasing as used in this chapter means the emission or fluorescence wavelength. The absorption wavelength is the same as the excitation wavelength, i.e. the wavelength at which the dye is excited at.

7.2 The Chemistry of Organic Dyes

The term dye as used in this chapter will encompass all substances containing conjugated double bonds. If two double bonds are separated by a single bond, as in the molecule butadiene, the two double bonds are called conjugated. Dye in the proper sense of the word, means all compounds having a high absorption in the visible part of the spectrum and characterized by several conjugated double bonds. The basic mechanism responsible for light absorption by compounds containing conjugated double bonds is the same, in whatever part of the spectrum these compounds have their longest wavelength absorption band, whether near-infrared, visible, or near-ultraviolet.

The thermal and photochemical stability of dyes is of utmost importance for laser applications. That is, applications in which laser energy is used to excite media containing a fluorescent dye. There are many commonalties between dyes used as laser mediums and the same dyes which may be optically pumped by either a laser or a flashlamp as we will see. Now thermal and photochemical properties vary widely, with almost infinite variety of chemical

structure, that practically no generally valid rules can be formulated. Thermal stability is closely related to the long-wavelength of absorption. A dye absorbing in the near-infrared has a low-lying excited singlet state and, even slightly lower than that, a metastable triplet state. The triplet state has two unpaired electrons and thus, chemically speaking, biradical character. There is good reason to assume that most of the dye molecules that reach this highly reactive state by thermal excitation will react with solvent molecules, dissolved oxygen, impurities, or other dye molecules to yield decomposition products. At this point we should be mindful of the engine operating conditions under which we intend to use any particular fluorescent dye, i.e. high temperature, impurity mixing due to oil decomposition products etc[42].

7.3 Initial Dye Selection Criteria

7.3.1 Introduction

A laser dye solvent combination must satisfy five criteria in order to provide adequate lasing performance. The first is that the laser dye must have a reasonable quantum yield of fluorescence in the chosen solvent, because this characteristic is intimately related to the probability of stimulated emission. The second is that the lasing medium must have high photochemical stability, because the majority of the dye laser configurations require that the dye be capable of undergoing multiple excitation cycles for continued operation, whether these cycles are in a laser dye cell cavity or an internal combustion engine lubricant film layer. The third is a minimal overlap between the dye fluorescent spectrum and its absorption spectrum, because lasing rarely occurs within the region of overlap due to self absorption by the lasing dye. The fourth is the requirement that the laser dye absorb radiation in a region of the spectrum accessed by the pump source and maintain a population inversion required for stimulated emission. The fifth is adequate solubility and thermal stability of the dye in the chosen solvent. The following paragraphs provide a brief perspective on the experimental variables over which researchers have control with respect to optimizing laser dye performance[43].

7.3.2 Dye Maximum Absorbing Wavelength

Organic dyes are characterized by a strong absorption band in the visible region of the electromagnetic spectrum. Such a property is found only in organic compounds which contain an extended system of conjugated bonds, i.e. alternating single and double bonds[42]. The laser

dye should have an absorption spectrum which matches the spectral distribution of the pump source. Since a substantial part of the light energy emitted by flashlamps is in the ultraviolet region, only dyes with moderate to strong absorption throughout this region can take full advantage of the pump light. If, on the other hand, the pump source is a laser with monochromatic emission, the dye should have a strong absorption at this wavelength.

The higher the maximum absorbing wavelength the more thermally stable the dye. Obviously it becomes more and more difficult to find stable dyes having the maximum of their long-wavelength band of absorption in the infrared beyond 1.0μm, and there is little hope of ever preparing a dye absorbing beyond 1.7μm that will be stable in solution at room temperature. This enters as another of our selection criteria. The short-wavelength limit of dye-laser operation, already mentioned implicitly, is given by the absorption of dyes containing only two conjugated double bonds and having their long-wavelength absorption band at wavelengths of about 220nm. It should be noted that the fluorescence stoke shift is always red shifted. That is the emission wavelength is always longer than the excitation or absorbed wavelength. The emission wavelength should be consistent with inexpensive detectors and removed from that of adventitious fluorescent impurities in the media to be monitored.

7.3.3 Solvent Effects

Assuming complete absorption of the pump radiation for a specific dye (and at constant temperature), the energy conversion efficiency is strongly dependent on the solvent[42]. Some common solvents used in dissolving organic dyes include, alcohols with hydrogen acceptor and donor sites : Ethanol (C_2H_5OH), n-propanol (PrOH), n-butanol (BuOH), and ethylene glycol (EG); non-alcohols with only hydrogen acceptor capacity : Dimethyl sulfoxide (DMSO), Dimethylformamide (DMF). Other solvents include Hexafluoroisopropanol (HFIP), Trifluoroethanol (TFE), Dichloromethane (DCM), Methanol (CH_3OH), and N, N-dipropylacetamide. It should be noted that appropriate solvent selection is critical for the following reasons:

a) *Solvent, dye and oil rheology*

The solvent should not change the physical properties of the lubricating oil. Based on this consideration alone, the alcohols were eliminated as possible solvents due to significant dye precipitation effects observed with these solvents. In general oil rheology can be preserved by preparing molar dye/oil solutions with the least amount of solvent. The dye samples were

therefore prepared with the minimum amount of solvent required for dissolution. Dichloromethane was the solvent selected for use with the Kubota Engine.

b) *Solvent Type*

The type of solvent used will influence the absorption wavelength as well as the Stokes Shift of the dye/oil solution. This becomes important in selecting a matching optical pumping source, i.e. laser of the appropriate excitation wavelength, as well as an appropriate filter set for absorption and emission wavelengths in the case of flashlamp pumping.

c) *Solvent Polarity*

Most laser dyes are polar molecules, and excitation into their lowest-lying singlet state is accompanied by an increase in the dipole moment. Accordingly, solvent polarity plays an important role in shifting the lasing wavelength. In a majority of circumstances, increasing solvent polarity will shift the gain curve toward longer wavelengths, and in the case of the more polar dyes, the shift can be dramatic (20nm-60nm). Increasing solvent polarity has a secondary advantage of increasing the Stokes Shift of the absorption and the fluorescence curves, and the increased separation decreases self absorption. Thus, the total lasing energy and the bandwidth of the gain curve increase with increasing polarity. Virtually all dye gain curves are shifted to longer wavelengths by increasing the solvent refractive index because the polarizability of the excited state is greater than the polarizability of the ground state[43].

d) *Solvent pH*

Changing the pH can have a dramatic effect , but this effect is highly dependent on the chemical structure of the dye. The pH of the solvent also has an influence on the absorption and emission wavelengths of the dye/oil solution and should be considered. When the pH of a dilute solution of Rhodamine B (RB) is decreased, a progressive shift of the absorption and emission spectra to lower energies, i.e. longer wavelengths and an increase in absorptivity of around 15% is observed due to a change from the zwitterionic to the cationic form of the dye. The zwitterionic form of rhodamine B is ($RB^{\pm}$) and the cationic form is (RBH^{+}) [44].

7.3.4 Dye Concentration

Adjusting laser dye concentration is one of the most important components of the optimization process. The optimum concentration is highly dependent on the optical configuration of the dye laser and the nature of the pump source. There are some observations that apply to virtually all optical configurations and pumping sources. The first is related to the problem of self absorption. This phenomenon increases in importance as concentration is

increased, and hence, increasing concentration generally shifts the gain curve to longer wavelengths an thus a concomitant decrease in lasing energy. The second is associated with the requirement that the number of excited dye molecules per unit volume be sufficient in producing lasing. Increasing dye concentration increases the optical density of the dye solution at the pumping frequency, and thus increases the number of molecules in the excited state[43].

7.3.5 Dye Mixtures

Experimental Engineers should be aware that there are many situations in which binary mixtures of two different laser dyes can be used to improve performance.[45] Drullinger has discussed the advantage of using binary mixtures of "adjacent" dyes to minimize dye self-absorption problems by generating a new gain curve which lies in the regions between the gain maxima of the single dyes[43]. The term "adjacent" refers to dyes which, when pumped by themselves, generate gain curves which are close, but not identical, in terms of spectral region. In general, an appropriate choice of two dyes will generate a new gain curve which is roughly intermediate in wavelength to that observed for the two individual dyes and has a maximum lasing intensity close to the average of the intensities of the individual dye gain curves. Accordingly, the efficiency of the lasing process is not significantly diminished by using binary mixtures. The use of binary mixtures can be of considerable advantage[44].

A second advantage in using laser dye mixtures is associated with the ability of higher energy dye to transfer energy to a lower energy to a lower energy dye in order to maximize energy coupling into the lasing medium[47]. The efficiency of this process is proportional to the extent to which the fluorescence spectrum of the higher energy overlaps the absorption spectrum of the lasing dye. Rhodamine dyes, because of their high fluoresence quantum yields, can be used to transfer energy to longer wavelength dyes which are not pumped efficiently by themselves via nitrogen lasers. Thus, the use of an energy transfer dye can extend the range of wavelengths available to researchers with access to a single pump source[43].

7.3.6 Triplet Influence and Intersystem Crossing

In the case of flashlamp-pumped lasers, triplet effects become important because of the long risetime or duration of the pump light pulse. A dye laser may be pumped above the threshold by a fast-rising light source. On the other hand, the necessary population density in the excited singlet state may not be achieved with the slowly rising light source, even if the asymptotic pump level is the same for both situations. Even more important than the depletion

of the ground state are losses due to molecules accumulated in the triplet state. This gives rise to triplet-triplet absorption spectra, which may very often extend into the region of fluorescence emission. The triplet state can be regarded as a parallel energy state in which radiationless transitions can occur, see figure 7.1 of the energy level diagram of an organic dye molecule. Triplet losses are time-dependent, and hence affect the efficiency as well as the emission wavelength of the dye/oil solution[42]. Triplet lifetime is very important, the smaller the better. Cyclooctatetraene used as an acceptor molecule with dissolved rhodamine 6G resulted in reduced triplet lifetime[42].

Triplet quenchers represent a type of additive that can be used when the dye molecule displays a high probability of intersystem crossing. Triplet quenchers either enhance intersystem crossing of the dye's lowest-lying triplet state back into the ground state, or prevent formation of the triplet state. Both mechanisms improve lasing efficiency. Although oxygen is not usually considered to be an additive, its presence is detrimental to the performance of many dyes because it enhances triplet formation or forms epoxides with the dye molecule. Deoxygenating solvents by bubbling nitrogen through the solvent prior to addition of the dye decreases oxygen concentration and often will improve lasing efficiency of dyes dissolved in polar solvents[42].

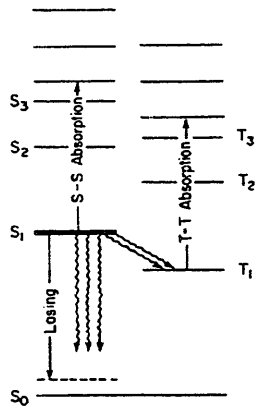

Fig. 7.1. Energy Level Diagram of a Typical Organic Dye Molecule

The radiationless transition from an excited singlet state to a triplet state can be induced by internal perturbations (spin-orbit coupling, substituents containing nuclei with high atomic number) as well as by external perturbations (paramagnetic collision partners, like O_2 molecules in the solution or solvent molecules containing nuclei of high atomic number. These

radiationless transitions are usually termed "intersystem crossing" and are characterized by the rate constant k_{ST} [42].

There is also a possibility of quenching a dye triplet by collision with a quencher molecule in the triplet state through the process of triplet-triplet annihilation, which leaves the dye in the excited singlet state and the quencher molecule in the ground state, with subsequent fluorescence emission radiationless deactivation of the excited singlet state. In this case, the quencher molecules must first be excited to the first excited singlet state and pass by intersystem crossing to the triplet state, before they can become effective. The first excited singlet state of quencher molecules must always lie higher than that of the dye, so that no pump radiation useful for pumping the dye is absorbed and no fluorescence quenching energy transfer can occur from the first excited singlet state of the dye to that of the quencher molecule. This means that, for efficient quencher molecule triplet production. the pump light source must have a high proportion of ultraviolet pump light. Because of these disadvantages and its generally lower effectiveness, this indirect method of triplet quenching seems less attractive[42].

Lasers equipped with commercial xenon flashlamps have slower risetimes. Consequently the number of dyes that will lase in these devices is restricted and triplet quenchers must be used if long pulse emission is wanted. Nevertheless, high average and peak powers and relatively high conversion efficiencies can be obtained in this way. Pappalardo et al. using a laser with 600μsec pump pulse obtained a 500μsec dye laser pulse from $5x10^{-5}$ molar rhodamine 6G solution containing $5x10^{-3}$ mole/l of cyclooctatetraene as triplet quencher. The fluorescence lifetime of rhodamine 6G, has been measured to be about $5x10^{-9}$ sec[42].

7.4 The Xanthene Family of Dyes

The xanthene dyes cover the wavelength region 500-700nm and are generally very efficient. Unlike most coumarin derivatives, the xanthene dyes are soluble in water, but tend to form aggregates in this solvent. Another important fact is that rhodamine 6G and rhodamine B have been on the market in good quality and give excellent lasing results even without further purification[42] . See figure N1 and N2 of Appendix N, for the absorption and emission spectra of rhodamine 6G in ethanol and rhodamine B in methanol respectively. The absorption and emission wavelengths of the common xanthene dyes are listed in table 7.1 for a given set of solvents.

Table 7.1 Rhodamine dyes. λ_{abs} maximum of main absorption band; λ_{las} approximate lasing wavelength (flashlamp-pumped, untuned).

Dye	Solvent	λ_{abs} (nm)	λ_{lase} (nm)
Rhodamine 110	HFIP	487	540
	TFE	490	550
	EtOH, basic	501	560
	EtOH, acidic	510	570
Rhodamine 19	DMSO	518	575
	EtOH, basic	518	575
	EtOH, acidic	528	585
Rhodamine 6G	HFIP	514	570
	TFE	516	575
	EtOH	530	590
	DPA	537	595
	DMSO	540	600
Rhodamine B	EtOH, basic	543	610
	EtOH, acidic	554	620
Rhodamine 3B	HFIP	550	610
	TFE	550	610
	EtOH	555	620
	DMSO	566	630
Rhodamine 101	HFIP	572	625
	TFE	570	625
	EtOH, basic	564	630
	EtOH, acidic	577	640
	DMSO	586	650
HFIP hexafluoroisopropanol, TFE trifluoroethanol, DMSO dimethyl sulfoxide, DPA N,N-dipropylacetamide			

Reproduced from: Topics in Applied Physics, Dye Lasers, Volume 2, 2nd edition F.P. Schafer

The absorption maximum of rhodamine is surprisingly dependent on the solvent, in particular with those dyes whose amino groups are not fully alkylated, eg. rhodamine 110 and rhodamine 6G. Rhodamine dyes that carry a free (nonesterified) COOH group can exist in several forms. In polar solvents like ethanol or methanol the carboxyl group participates in a typical acid-base equilibrium. The dissociation is enhanced by dilution or, most easily, by adding a small amount of base. It can be followed spectroscopically, since absorption and fluorescence of the zwitterionic form of the dye are shifted to shorter wavelengths. While this shift amounts to only 3 nm in water, it is about 10nm in ethanol. If a solution of such a dye is prepared in a

neutral solvent, it will usually contain both forms of the dye. However, on addition of a small amount of either acid or base, a solution containing essentially only one of the two forms is obtained. In nonpolar solvents e.g. acetone, the zwitterionic form is not stable[42]. See figure 7.2 below.

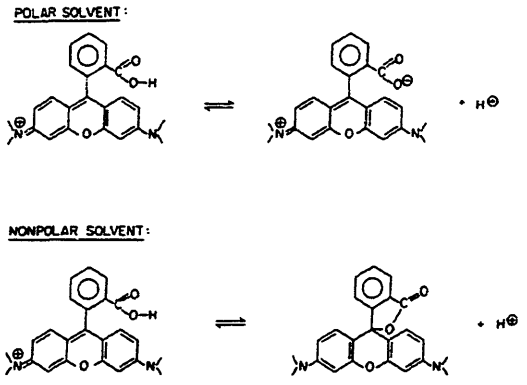

Fig. 7.2 The Polar and Non Polar forms of Rhodamine 6G

In xanthene dyes that contain mobile dialkylamino substituents the fluorescence efficiency is influenced by a variety of factors. The temperature and viscosity of the solvent affect this important property. It is particularly interesting also that certain low-viscosity solvents appreciably increase the fluorescence efficiency of these dyes above the value found in ethanol. It was found that the fluorescence quantum yield of rhodamine B has a value of 40% in acidic ethanol, but of 60% in basic ethanol, whereas the fluorescence efficiencies of rhodamine 110, rhodamine 19, and rhodamine 101 are independent of acidity [42].

7.4.1 Temperature Effects and Solvent Effects on dye efficiency

For the laser dye rhodamine B, the fluorescence efficiency in ethanol is dependent on the temperature. About 40% at 25°C, the quantum yield increases to nearly 100% if the temperature is lowered, but it drops to only a few percent in boiling ethanol. On the other hand rhodamine 6G and rhodamine 110, which in alcoholic solution have fluorescent quantum yields of 85% and 95% respectively, are independent of temperature. It is interesting that rhodamine B has a quantum efficiency of nearly 100% in viscous solvents like glycerol. This suggests that the chromophore is fully rigid in the ground state and loosens up only after excitation, provided the solvent is of low viscosity. In glycerol the viscosity is sufficiently high to prevent thermal equilibrium being reached during the radiative lifetime of a few nanoseconds[42].

7.4.2 Hydrogen Vibrations

This process involves the conversion of the lowest vibronic level of the excited state S_1 to a higher vibronic level of the ground state S_0 which then rapidly relaxes to the lowest vibronic level S_0. Replacement of the hydrogen by deuterium should reduce the rate of nonradiative decay by this mechanism, and thus increase the fluorescence efficiency. When rhodamine 110 was dissolved in monodeuterated methanol (CH_3OD) quantum yield of fluorescence increased 85 to 92% compared with the yields when methanol was the solvent[42].

7.4.3 Fluorescence Quenching by Charge Transfer Interactions

Certain anions can quench the fluorescence of dyes. The qenching efficiency is strongly dependent on the chemical nature of the anion. The quenching ability, which is very strong in the case of iodide (I^-), decreases in the order : Iodide (I^-), thiocyanate (SCN^-), bromide (Br^-), chloride (Cl^-), and perchlorate (ClO^-_4). This succession suggests that the excited state of the dye is quenched by a charge transfer interaction. Since this effect is undesirable for our purposes the use of the perchlorate as the anion is preferable to the common chloride. Because in many laser dyes the chromophore carries a positive charge, these dyes invariably have an anion, commonly chloride or iodide. Whether the fluorescence efficiency is affected by the anion accompanying the chromophore depends on the concentration and the polarity.

It was found that the fluorescence efficiencies of rhodamine 6G iodide and perchlorate in 10^{-4} molar solutions in ethanol were identical and very high, indicating no quenching by the anions in either case. However the fluorescence of rhodamine 6G iodide at the same concentration in the nonpolar solvent chloroform was almost completely quenched, whereas the perchlorate was as efficient as in ethanol. Apparently the dye salts are fully dissociated in the polar solvent ethanol, but practically undissociated in chloroform. Hence in ethanol the quenching anions do not have sufficient time to reach the excited dye molecules during their lifetime, whereas, in chloroform, they are immediately available for reaction. It is therefore advisable to use the perchlorate form of rhodamine in lasing solutions of low polarity and when high concentrations are required. In addition to the anions mentioned here, a number of other compounds quench the fluorescence by a similar mechanism[42].

7.4.4 Quenching by Energy Transfer

Another mechanism by which excited states, singlet as well as triplet, are quenched externally can operate if the quenching molecule has a level of energy equal to or greater than the state to be quenched. Under favorable conditions such energy transfer can occur over distances up to 10nm. Therefore in liquid solutions the reactants can approach each other very closely, energy transfer processes are very efficient, provided the diffusion time is shorter than the lifetime of the excited state. This type of process can therefore either quench the triplet state or the main fluorescent state. However the main interest in this kind of process in connection with laser dyes arises from its application to the quenching of undesired triplet states.

7.4.5 Excited State Reactions

For organic solvents, there is usually a strong interaction between excited molecules and those in the ground state, and this shows up at high concentrations, see figure 7.3 below. Note the drop in fluorescence efficiency with increasing concentration for rhodamine 6G in methanol.

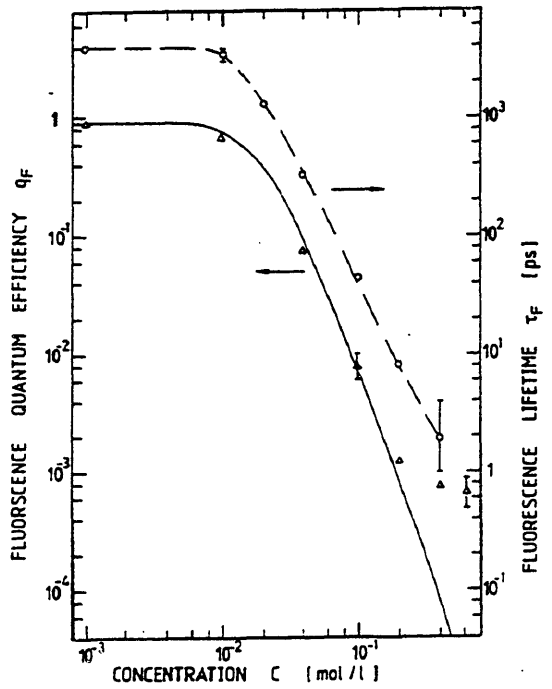

Fig. 7.3 Fluorescence Quantum Efficiency (q_f) vs. Concentration (C) for Rhodamine 6G in Methanol. The triangles are experimental values, the solid curve is calculated and the fluorescence lifetimes τ_f are represented by the open circles and the dashed line.

While the absorption spectrum of rhodamine 6G in ethanol is unchanged even at concentrations as high as 10^{-2} molar, the fluorescence at such concentrations is strongly quenched owing to collisions of the excited dye molecules with those in the ground state. It is not known if in cases like this dimeric dye molecules exist for a short time, however, if they do, they are nonfluorescent[42].

7.4.6 Effect of Oxygen on Flashlamp-Pumped Organic Dye Lasers (Rhodamine 6G as lasing medium)

Dissolved oxygen was found to dramatically influence the intensity of flashlamp-pumped organic-dyes. Snavely and Schafer have noticed that dissolved oxygen enhanced the lasing intensity of rhodamine 6G. Appropriate solutions of varying pH were prepared by adjusting the acidity/basicity with NaOH or HCL as required. The solutions were then filtered through 0.5μm filters. Oxygen can either help or hinder lasing potential of the organic dye, and for some dyes there is an optimum concentration. A possible explanation of these responses is that oxygen can enhance the transition from the triplet to the ground singlet state, which would increase the lasing energy. For those dyes whose performance is improved by oxygen, the principal effect is to lengthen the pulse. In a long-pulse system, the maximum pulse length for an oxygen-free dye solution is a few microseconds, indicating triplet-state quenching of the lasing medium. With dissolved oxygen, the output pulse length may be as long as the flashlamp pulse. Oxygen can also quench the excited singlet state by enhancing transitions between it and the triplet state. This would decrease the lasing intensity by reducing the quantum efficiency and increasing triplet-state absorption. Both processes are probably operative in all dyes and the one that dominates establishes whether oxygen helps or hinders lasing. In cases where there is an optimum oxygen concentration, the dominance probably switches from helping to hindering as the concentration of the oxygen is increased. Oxygen dissolved in the dye solution can also form peroxides, hyperoxides, cause oxidation of functional groups, and effect oxidative coupling[48].

7.4.7 Intersystem Crossing Rate and Triplet State Lifetime for a Lasing Dye (Rhodamine 6G)

To a very good approximation, the decay of the triplet concentration is due entirely to oxygen collisions. The triplet lifetime is thus inversely proportional to the concentration of dissolved oxygen, and to the collision quenching rate constant k_{coll}. [49]

7.4.8 Fluorescence enhancers for Rhodamine 6G

Two hydrocarbons, octatetraene C_8H_{18} (COT), and cycloheptatriene C_7H_8 (CHT), have been found to function effectively as quenchers of the triplet state of rhodamine 6G in ethanolic solution. Experiments have been performed with ethanolic solutions containing 5 x 10^{-5} M rhodamine 6G and 5 x 10^{-3}M COT. [50].

7.4.9 Photodecomposition and Dye Degradation

It should be emphasized that photodecomposition, as it applies to laser dyes, is actually the combination of two effects. One is true photodecomposition of a molecule because of absorbed radiation. The result is reduced concentration of the original compound. The second effect is the formation of photodecomposition products, which absorb the laser radiation. If this absorption is strong, minute amounts of the photodecomposition product will affect lasing efficiency as well as the experimental results, even though the original concentration of the dye itself has only been reduced by a small amount[51].

Photochemical stability is one of the most important considerations in selecting a dye and has been a major concern for years with flashlamp-pumped dyes. Photo-disintegration of the dye molecule and subsequent reactions of the photo-products with the solvent or with impurities is a very complex subject and is not fully understood. The as-received dye solvent purity and dye purity can play a major role. It has been estimated that most common solvents are saturated with air at concentrations of 10^{-3} to 10^{-4} M. In many cases this oxygen contaminant reacts with the solvent and the dye under intense UV pumping. The photochemistry may not always cause the lasing energy to decrease in a linear or exponential fashion[51].

As the dye degrades, its absorption increases. The rate at which this causes the output to drop depends on the operating conditions. This is illustrated in figures 7.4a and b, below for rhodamine 6G. The curves for fig 7.4a are for flashlamp pumping, with the pump intensity I_P =

20kW/cm^2. Those of fig 7.4b are for laser pumping at I_P = 1MW/cm^2. The efficiency falls up to ten times faster in the flashlamp case[52].

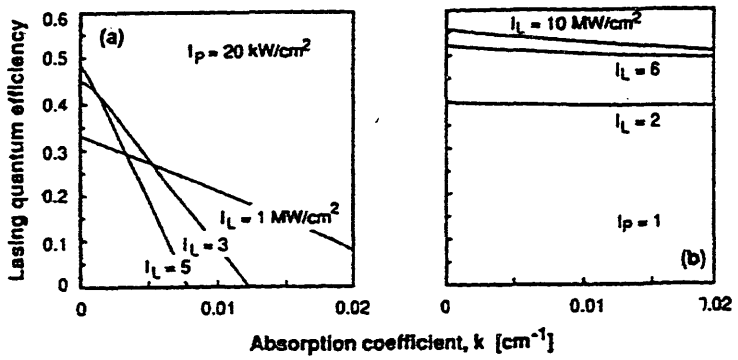

Fig. 7.4 Lasing Quantum Efficiency vs. Absorption, (a) Pump Intensity 20kW/cm^2 (flashlamp) and Lasing Intensities 1-5 MW/cm^2, (b) Pump Intensity 1MW/cm^2 (laser pump) and Lasing Intensities 2-10 MW/ cm^2

Among laser dyes, Rhodamine 6G holds a special position. It is one of the most efficient laser dyes presently known and also has good photochemical stability. Any new laser dye claiming superior performance must measure up to Rhodamine 6G[42]. The highest conversion efficiency for laser pumping and lamp pumping has been obtained in the 565-600nm region with solutions of the xanthene dyes, in particular, rhodamine 6G. The conversion efficiency refers here to the efficiency of conversion of pumping into stimulated emission[53].

The organic dyes used in these lasers tend to degrade when exposed to UV and near UV components of the flashlamp output, and create species that absorb at the lasing wavelength. Spectral filtering of the flashlamp light can reduce the degrading effect by removing the portion of the spectrum that causes the greatest damage to the dye but adds little to the useful pumping. The UV degradation problem was investigated by Knipe and Fletcher and by Jones et al. in a series of papers. This explains why rhodamine dyes are not good candidates for flashlamp pumping as opposed to coumarin dyes.

7.5 The Coumarin Family of Dyes and their Derivatives

This group consists of a widely used set of laser dyes emitting in the blue-green region of the spectrum. They are derived from coumarin by substitution with an amino or hydroxyl group in the 7-position. Some members of this dye rank among the most efficient laser dyes known today. There is a marked change in basicity that occurs on optical excitation, which

causes a shift of the fluorescence to longer wavelengths. The chromophore of such compounds can be described essentially by the mesomeric forms A and B as depicted in figure 7.5 below.

Fig. 7.5 **Mesomeric forms of Coumarin**

In the electronic ground state S_0 of the coumarins, the mesomeric structure A is predominant and structure B makes only a minor contribution to the actual π-electron distribution, the opposite is true for the first excited singlet state S_1, in which the polar form B is predominant. Therefore on optical excitation the (static) electric dipole moment increases, and a major rearrangement of the surrounding solvent molecules takes place immediately after excitation. Thus the energy of the excited state is markedly lowered before light emission occurs. This is the reason for the large energy difference between absorption and fluorescence (Stokes shift) in the coumarin derivatives. This is a major advantage in using coumarin dyes, since separation of absorption and emission peaks makes optical setup that much easier. Coumarin 6 in alcoholic solution lases untuned at 540nm and is unmatched in efficiency and photochemical stability by other dyes which lase at this wavelength[42].

An important advantage in flashlamp pumping is the relatively strong absorption of coumarin dyes below 300nm. Since a substantial part of the light energy emitted by flashlamps is in the ultraviolet region, only dyes with moderate to strong absorption throughout this region can take full advantage of the pump light. If, on the other hand, the pump source is a laser with monochromatic emission, the dye should have a strong absorption at this wavelength. It was found that under flashlamp pumping conditions, where most coumarin dyes lased very efficiently, other dyes having approximately the same long-wavelength absorption and fluorescence efficiency, but very little UV absorption, did not lase at all[42]. In specific cases of filtering of exciting radiation, the coumarin in ethanol solutions, absorbed 25% more light than did rhodamine 6G[54].

Coumarin 6 was the fluorescent dye applied by Toyota in their 2D-LIF research. At a concentration of 7 x 10^{-4} mol/l (M), they reported several advantages, among them being, high solubility, sufficient fluorescence intensity, and thermal stability[55].

7.6 Dye Safety

All laser dyes and solutions containing laser dyes should be handled in well-ventilated environments and all individuals handling the solutions should wear rubber gloves. Kues and Lutty screened 150 laser dyes, and found that 28 dyes were extremely toxic, and some had toxicities so severe that a lethal dosage of 5mg/kg was observed in mice[50]. The cyanines and carbocyanines were observed to be the most toxic. This situation is complicated by the common use of dimethyl sulfoxide (DMSO) to solvate these dyes. DMSO facilitates the transfer of the toxic dyes through the skin, and the hazards associated with the use of a toxic dye dissolved in a membrane-transferring solvent should not be underestimated[43]. All laser dyes should be treated as carcinogens and handled as such. It is strongly recommended that all researchers working with laser dyes read the safety reports provided by the MIT safety office.

7.7 Conclusions

Based on the information compiled from this literature research the following conclusions were made.

Coumarin - Advantages

1. One of the most attractive advantages of the coumarin dyes is the large energy difference between the absorption and the emission peaks. The Stokes Shift is on the order of 93nm for coumarin 307(503) and 39nm for coumarin 6(540).
2. Coumarin 6 in alcoholic solution lases untuned at 540nm and is unmatched in efficiency and photochemical stability by other dyes which lase at this wavelength.
3. An important advantage in flashlamp pumping is the relatively strong absorption of coumarin dyes below 300nm. See figure N3 and N4 of Appendix N for the absorption and emission spectra of two representative coumarin dyes.

Coumarin - Disadvantages

1. Coumarin 6 absorbes at 458nm and hence does not match any of the major output

wavelengths of the Argon ion laser. See figure N5 of Appendix N for the absorption and emission spectra of Coumarin 6 in methanol.

2. At a price of $62 per gram, Coumarin 6 (540) is expensive.

Rhodamine 6G - Advantages

1. Rhodamine 6G in alcoholic solution has a temperature independent fluorescent quantum yield of 85-95%.
2. Rhodamine 6G has been on the market in good quality and gives excellent lasing results without further purification.
3. The highest conversion efficiency for laser pumping and lamp pumping has been obtained in the 565-600nm range with Rh6G.
4. Rhodamine 6G absorbes at 528nm in methanol, and 514nm in hexafluoroisopropanol. This closely matches one of the Argon ion output wavelengths.
5. Priced at $19 per gram, rhodamine 6G perchlorate and chloride are attractive candidates.

Rhodamine 6G - Disadvantages

1. While the absorption of rhodamine 6G in ethanol is unchanged even at concentrations as high as 10^{-2} M, the fluorescence at such concentrations is strongly quenched. (see figure 7.3)
2. Rhodamine dyes are not good candidates for flashlamp pumping due to degradation when exposed to UV and near UV components of the flashlamp output.
3. A narrow Stokes shift makes filtering the fluorescence difficult.

(This Page Intentionally Left Blank)

Chapter 8

System Calibration

8.1 Introduction

Calibration is defined as the determination of the relation between the indicated value on a measuring instrument and the true value of the quantity to be measured. The true value is the value that would be obtained if all sources of error were eliminated[57]. There are two main types of calibration systems. The first and the simplest is called the bench calibration system in which an attempt is made to duplicate as closely as possible the conditions under which the experiment is performed, i.e. temperature, pressure, lubricant type, dye concentration etc, on an auxillary device. Dynamic calibration on the other hand involves the faithful reproduction of actual experimental conditions under which data is collected on the experimental rig itself, in this case a single cylinder diesel engine.

8.2 Bench Calibration Device

8.2.1 Material Constraints

For the purposes of calibrating initial data sets, a bench calibration setup similar to that indicated in figure O1 of Appendix O was employed. It was decided to use the Kubota piston as the basis for the calibration device. The material constraints were therefore automatically met. A groove was then formed on the surface, with a depth profile varying from 0μm to 190μm. This depth range includes the range of clearances representative of diesel engine micro geometry[58].

8.2.2 Temperature Constraints

A 12 inch by 0.5 inch Omega heating tape was wrapped around the piston, leaving the calibration groove on the piston exposed. The heating tape was in turn connected to an Omega 6000 temperature controller, with a range from 0 to 500°F. The engine operating temperature is 397°F. It is especially important that the temperature

constraint be observed, due to the sensitivity of the dye quantum efficiency to thermal load.

8.2.3 Dye Type and Concentration Constraint

The same dye utilized in the engine at the same concentration is used in the bench calibration device. For preliminary testing rhodamine 6G perchlorate at $7x10^{-4}$ mol/L was used. The dye filled the calibration groove. The dye/oil solution was carefully applied with a micro syringe.

8.3 Special Considerations

8.3.1 Window-Piston Contact

If the window does indeed contact the skirt of the piston, the bench calibration device should incorporate a window that is also in contact with the piston skirt. This leads to the following considerations:

1. Because the piston is barrel shaped in the region of the skirt, the inside surface of the window will not fit flush against the surface of the piston and will therefore retain a wedged shape film of oil of unknown thickness variation.
2. Machining the surface of the piston skirt to an external radius matching the internal radius of the window is possible but costly, due to the requirement that a special tool be built for this purpose. The piston cannot be machined using a conventional turning or grinding operation due to the presence of a surface interruption in the region of the wrist pin. Also material removal via these methods results in a smaller final external radius, contrary to what is required.
3. The additional requirement that the surface of the piston be polished to a sub-micron finish to reduce the error in film thickness incurred when these surface irregularities become filled with dyed lubricant. Polishing the surface also changes its reflectivity. Therefore for simplicity it was assumed that the window protrusion into the cylinder liner can be ignored and the window does not contact the side of the piston. A duplicate window therefore did not constitute a part of the calibration device.

8.3.2 Groove Projected Area

Groove projected area is important from the point of view of photobleaching effects associated with fluorescent dyes and continuous excitation sources. Generally fluorescent dyes are kept under continuous circulation to avoid photobleaching which becomes significant under prolonged exposure to an excitation energy source. Dye circulation modifications would complicate the calibration device and was not included in the initial design.

8.3.3 Thermal Expansion

Since this calibration device must be heated to engine operating temperature, thermal expansion of the groove became a concern. There was no way of measuring the change in groove depth at the target temperature. An assumption about the thermal expansion would therefore have to be factored into the calibration results.

8.4 Groove Type and Associated Machining Processes

A groove representative of the typical clearances encountered in production diesel engines was required. A groove depth ranging from 150 to 200μm would be satisfactory. Several groove types were considered, including a terraced groove, constant gradient inclined groove, semicircular groove and a hemispherical or diamond type indentation groove. The following methods were considered in achieving the appropriate groove type.

8.4.1 Chemical Etching

An etching method was attempted in establishing regularly spaced terraces in the surface of the piston skirt by applying an aluminum etchant (P.A.N.). Perchlorate acid (77%), Acetic acid (20%) and Nitric acid (7%) combination. This method failed for the following reasons:

1. The reaction was self terminating and produced a precipitate on the surface of the material being etched. This occurred because the etchant works for pure aluminum only and not on aluminum alloys. Attempts to obtain the exact piston material composition were foiled by the manufacturers.
2. The reaction produced unsatisfactory surface roughness.

3. The maskant could not be applied accurately without a precision tool.
4. It was difficult to control the rate of chemical reaction at the metal-liquid interface. Samples to be etched can be pulled from a bath of the etchant at a given rate, with the zone last removed exhibiting the greatest surface metal removal. Takiguchi showed that etching depth is linearly proportional to the time the chemical is left undisturbed on the surface of the metal[59]. Because terraced grooves are difficult to procure in practice it was decided to abandon this grooving technique in favor of one of the other three options. Bliven et al., experienced similar difficulty in obtaining perfectly etched grooves on the surface of a piston. The resulting surfaces were irregular due to the inability in controlling the rate of chemical etching at the microscopic scale. The size and number of irregularities on the etched surface also increases with etching time[12].

8.4.2 Rotary Wheel Abrasive Machining

A semicircular groove type geometry can be machined into the surface of the piston skirt via a rotating disk and application of a fine abrasive grit of silicon garnet or aluminum oxide. See figure 8.1 below. Silicon garnet should be used instead of the aluminum oxide ceramic powder due to the tendency of the aluminum oxide to bury itself in the softer piston material. Excellent surface finish can be obtained using this technique with groove width easily controlled by varying the width of the rotating disk. Groove depth can be controlled by lowering the wheel axis as required. Typical grit sizes are on the order of 0.5μm to 0.05μm. The geometry of the groove can be easily calculated or measured using a Talysurf Profilometer.

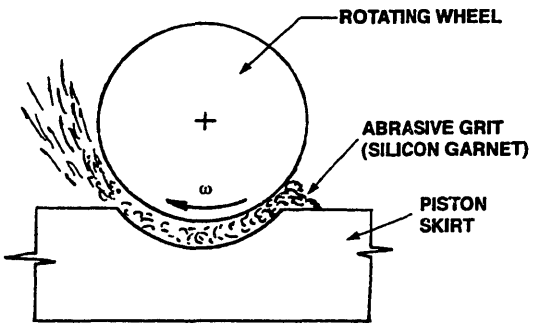

Figure 8.1 Semicircular Groove Method

8.4.3 CNC Machining

A CNC machine equipped with an appropriate set of cutters can be programmed to machine a groove of any shape in the x-z plane. Intricate geometries can be obtained using this method. The groove can then be mapped with the aid of a profilometer as a comparative check of the accuracy of the CNC machine. This method may be prohibitively expensive however.

8.4.4 Broaching

A fine broaching tool can be employed in carving an incline type groove with excellent surface finish. The inclined groove can in turn be mapped with a profilometer.

8.4.5 Scribing with a sharp tool

Kiesel[31] employed a method similar to the one above in scribing a groove on the surface of a piston with a sharp needle like tool. The depth could not be controlled however and resulted in discontinuities on the floor of the groove and on the edges. See figure 8.2 a, b and c below.

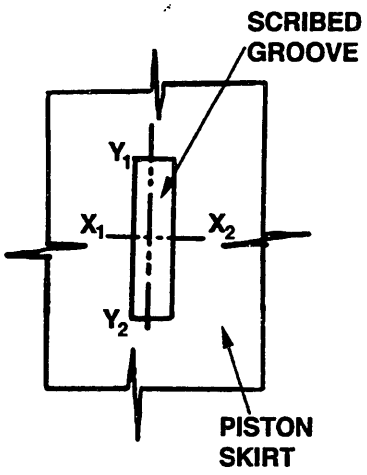

Figure 8.2a Plan view of scribed groove

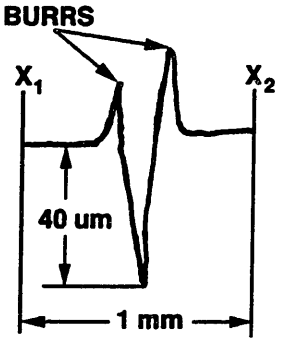

Figure 8.2b Section X_1-X_2

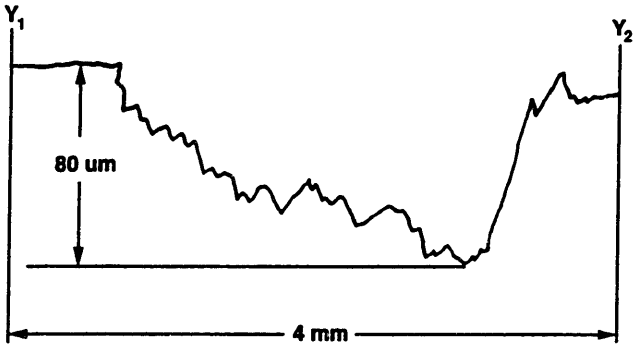

Figure 8.2c Section Y_1-Y_2

8.4.6 Electro-Discharge Machining (EDM)

This method can be employed in producing any type of intricate surface pattern on a metal surface. The appropriate pattern, which is the reverse of the surface profile desired, can be lowered into a bath of electrolyte solution. The pattern forms one of the electrodes i.e. the anode. The cathode, i.e. the part to machined, is eroded away as the gap between the anode and cathode is reduced. This is a very precise and costly machining process for low volume production runs.

8.4.7 Alternative Methods

The methods described above were either difficult to apply in practice, produced unsatisfactory surface finish or were very expensive. An impact method used in creating

a hemispherical groove with a ball bearing and a hammer proved to be very successful. A stainless steel ball bearing was held on the appropriate area of the piston skirt and struck from above with sufficient force to create an indentation of the appropriate depth. See figure 8.3a and 8.3b below.

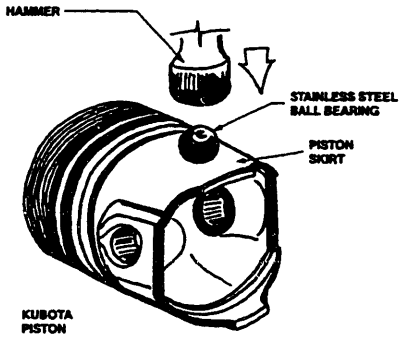

Figure 8.3a Impact Method

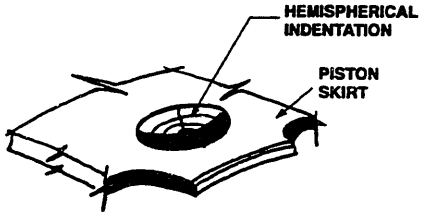

Figure 8.3b Hemispherical Groove

This resulted in a smooth, symmetric and repeatable surface profile. As indicated in figure O2 of Appendix O, the variation in depth is gradual. The depth profile can then be easily matched against a fluorescence profile along dimension X_1-X_2 resulting in the appropriate calibration curve. This dimension X_1-X_2 was clearly marked on the piston surface and aligned with the CCD camera. Figures O3 a-d of Appendix O represent fluorescence photographs at the various temperatures ranging from 100°F to 400°F. The decay in fluorescent intensity with increasing temperature is clearly evident in the photographs. The above procedure has been outlined to illustrate that a successful initial bench calibration can be performed by matching the appropriate fluorescence output to the measured engine operating temperature and the particular fluorescent dye in this case rhodamine 6G.

8.5 Conclusion

Fluorescence data is particularly difficult to calibrate. A bench calibration device is primarily useful in determining which dye has the best quantum yield at the engine operating temperature and an approximate relationship between oil film thickness and fluorescence intensity. An in situ calibration is recommended for continuous data acquisition. Any changes in dye fluorescent yield induced by temperature change or contamination can immediately be accounted for. A band of parallel grooves varying

linearly in depth can be established on the surface of the piston skirt to facilitate the in situ calibration. Care must be exercised in not deforming the piston while creating the grooves.

Piston tilt and fluorescence from oil films circumferentially displaced from the vertical line of sight of the camera must also be accommodated for. A schedule for changing the engine oil must be established for the Kubota diesel engine. Lubricating oils used in diesel engines become contaminated with particulates and other carbon deposits very easily, thereby limiting the fluorescent yield of the dissolved dye and hence the time duration over which accurate data can be collected.

(This Page Intentionally Left Blank)

References

1. HOT ROD, June 1995, pg. 93.
2. Environmental Protection Agency, National Air Quality and Emission Trends Report, 1995.
3. Field, G.J., Austin, R.M., Reynolds, J. A., Jagger, E.T., and Flitney, R.K., Second Review and Bibliography on Aspects of Fluid Sealing.
4. Shaw II, B., "Direct Observation of Oil Consumption Mechanism of Production Single-Cylinder Diesel Engine," S.M. Thesis, Department of Mechanical Engineering, MIT, 1992.
5. Shin, K., Tateishi, Y. and Furuhama, S., Measurement of Oil Film Thickness Between Piston Ring and Cylinder, SAE Paper #830068, 1983.
6. Wing, R. D. and Saunders, O., "Oil Film Temperature and Thickness Measurements on the Piston Rings of a Diesel Engine", *Proceedings of the Institution of Mechanical Engineers*, Vol. 186/172, pp. 1-9, 1972.
7. Smart, A. E., Ford, R. A. J., "Measurement of Thin liquid Films by a Fluorescence Technique", *Wear*, Vol. 29, pp. 41-47, 1974.
8. Ting, L.L., "Development of a Laser Fluorescence Technique for Measuring Piston Ring Oil Film Thickness", *Journal of Lubrication Technology*, Vol. 102, pp. 165-171, 1980.
9. Hoult, D. P., Rifai, M. "Measurement of Oil Film Thickness on Piston Lands," Third Symposium on energy Engineering Sciences, October 8-10, 1985, Pennsylvania State University.
10. Hoult, D., Billian, S., Lux, J. and Wong, V., "Calibration of Laser Fluorescence Measurements of Lubricant Film Thickness in Engines," SAE Paper #881587, 1988, SAE Transactions, Vol. 97.
11. McElwee, M., "Comparison of Single-grade and Multi-grade Lubricants in a Production Diesel Engine," S.M. Thesis, Department of Mechanical Engineering, MIT, June 1990.
12. Bliven, M., "Oil Film Measurements for Various Piston Ring Configurations in a Production Diesel Engine," S.M. Thesis, Department of Ocean Engineering, MIT, June 1990.
13. Lux, J., Hoult, D. and Olechowski, M., "Lubricant Film Thickness Measurements in a Diesel Engine Piston Ring Zone," STLE Preprint No. 90-AM-1H-1, STLE 45th Annual Meeting, Denver, CO, May 7-10, 1990, *Lubrication Engineering*, Vol. 47, No. 5, pp. 353-364.
14. Wong, V. and Hoult, D., "Experimental Survey of Lubricant-Film Characteristics and Oil Consumption in a Small Diesel Engine," SAE Paper #910741, SAE International Congress and Exposition, Detroit, MI, Feb 25 - Mar 1, 1991.
15. Ingles, E. N., "Instrumentation of a Diesel Engine for Oil Film Thickness Measurements Using Fiber Optics and Laser Fluorescence, " S.M. Thesis, Department of Mechanical Engineering, MIT, June 1991.
16. Tamai, G., "Experimental Study of Engine Oil Film Thickness Dependence on Liner Location, Oil Properties and Operating Conditions," S.M. Thesis, Department of Mechanical Engineering, MIT, August 1995.
17. Noordzij, B., "Measurement and Analysis of Piston Inter-Ring Pressures and Oil Film Thickness and their Effects on Engine Oil Consumption," S.M. Thesis,

Department of Mechanical Engineering, MIT, June 1996.
18. Shaw II, Byron. T., Hoult, D., and Wong, V., "Development of Engine Lubricant Film Thickness Diagnostics Using Fiber Optics and Laser Fluorescence," SAE Paper #920651, SAE International Congress and Exposition, Detroit Michigan, February 24-28, 1992.
19. Lee, M. J., "Film Thickness Measurements in a Production Spark Ignition Engine," B.S. Thesis, Department of Mechanical Engineering, MIT, May 1993.
20. Jackson, Mark A., "Assessment of a Sulfur Dioxide Based Diagnostic System in Characterizing Real Time Oil Consumption in a Diesel Engine," S.M. Thesis, Departments of Mechanical Engineering and Ocean Engineering, MIT, May 1996.
21. Miller, T. C., "Characterization of Lube Oil Derived Diesel Engine Particulate Emission Rate Versus Lube Oil Consumption," Masters Thesis, Departments of Ocean and Mechanical Engineering, Massachusetts Institute of Technology, 1996.
22. Artzner, Denis., "Investigation of Oil Consumption Mechanisms in a Spark-Ignition Engine," S.M. Thesis, Department of Mechanical Engineering, MIT, May 1996.
23. Schofield, D. M., "Diesel Engine Instantaneous Oil Consumption Measurements Using the sulfur Dioxide Tracer Technique, S.M. Thesis, Departments of Ocean and Mechanical Engineering, MIT, 1995.
24. Lusted, Roderick, M., "Direct Observation of Oil Consumption Mechanisms in a Production Spark Ignition Engine Using Fluorescence Techniques," S.M. Thesis, Department of Mechanical Engineering, MIT, May 1994.
25. Hartman, M. R., "Tritium Method Oil Consumption and Its Relation to Oil Film Thickness In a Production Diesel Engine," S.M. Thesis, Departments of Ocean and Mechanical Engineering, Massachusetts Institute of Technology, 1990.
26. Hill, S. et. Al., "A Systems Approach to Oil Consumption" SAE Paper 910743.
27. Deutsch, Eric, "Piston Ring Friction Analysis from Oil Film Thickness Measurements," MIT Masters Thesis, Department of Mechanical Engineering, February, 1994.
28. Versteegh, Richard., I.C. Engine Data Set, Sloan Automotive Laboratory, MIT
29. Furuhama, S, Hyuga, T. and Tateishi, Y, : "A Study of Oil Consumption Reduction Methods for Two-Ring Package with NSOR", Lubrication Engineering, Volume 44, 11, 922-930, November 1988.
30. Furuhama, S, Hiruma, M, : "Unusual Phenomena in Engine Oil Consumption", Lubrication Engineering, Volume 36, 10, 599-606, October 1980.
31. Kiesel, M, Caterpillar Visiting Engineer, Massachusetts Institute of Technology, Sloan Automotive Laboratory.
32. Kubota Engine Maintenance Manual.
33. Melles Griot 1995/96 Optics, Opto-Mechanics, Lasers and Instruments Catalogue.
34. Dahlheimer, John C., Mechanical Face Seal Handbook, Chilton Book Company.
35. Beynon, J.D.E., and Lamb, D.R., Charge-Coupled Devices and their Applications McGraw Hill Book Company, 1980.
36. Pulnix Operations and Maintenance Manual, Pulnix America, Inc 1330 Orleans Drive, Sunnyvale, CA 94089.
37. Miller, Charles E. Proceedings of the Ninth International Congress on High-

Speed Photography *Some Modern Application Techniques of Stroboscopic High-Speed Photography*, , General Radio Company, Concord Massachusetts, 01742 USA.
38. Stroboscopes for Industry and Research, by J. Rutkowski, Associate Professor, Warsaw Institute of Technology.
39. Electronic Flash, Strobe; Harold E. Edgerton, Massachusetts Institute of Technology, Cambridge, Massachusetts.
40. Stroboscopes for Industry and Research, by J. Rutkowski, Associate Professor, Warsaw Institute of Technology.
41. Stroboslave Instruction Manual, General Radio Company, West Concord, Massachusetts 01781.
42. Schafer, F.P., Topics in Applied Physics, Volume 1, Dye Lasers, 2nd Edition. pp. 2-170.
43. Laser Dye Technical Information, provided by *Eastman Kodak Company.*
44. Arbeloa, I. L, and Rohatgi-Mukherjee, K.K., Chemical Solvent Effect on Photophysics of the Molecular forms of Rhodamine B Solvation models and spectroscopic parameters. *Chemical Physics Letters*, August 8, 1996, Vol. 128, no. 5, 6.
45. Maeda M., Laser Dyes, Academic Press, New York, 1984.
46. Drullinger, R.E., Increased Gain Through Identification and Alleviation of Dye Self Absorption in Laser Pumped Dye Lasers, *Optics Communications,* 4, 2634(1981).
47. Pierce, B.M. and Birge, R.R., Lasing Properties oaf Several Near-IR Dyes for a Nitrogen Laser-Pumped Dye Laser with an Optical Amplifier, *IEEE Journal of Quantum Electronics* QE-18, 1164(1982).
48. *IEEE Journal of Quantum Electronics*, September 1970 pp. 570-572.
49. Journal of Chemical Physics, Vol. 53(11) pp. 4227-4229, Dec. 4th, 1970
50. *IEEE Journal of Quantum Electronics*, Vol. QE - 16(11), pp. 716-725
51. Duarte, Francisco J. High-Power Dye Lasers, pp. 99-100, and pp. 217.
52. Journal Applied Physics, Vol 64, No. 2, 15 July 1988, Triplet Extinction coefficients of some laser dyes I.
53. Optical Society of America,1989, pp. 419-421.
54. *Optical Spectroscopy* (USSR) 65(3), September 1988, © 1989, The Optical Society of America pp. 419-421. Lasing Studies of new Coumarin derivatives under laser and lamp excitation.
55. SAE Technical Paper Series 952346, *Development of Two-Dimensional Oil Film Thickness Distribution Measuring System*, By Hideto Inagaki and Akinori Saito - Toyota Central R&D Laboratories, Inc. and Motoichi Murakami and Toshiaki Konomi, Toyota Motor Corp.
56. Kues, H. A. and Lutty, G. A., Dyes Can Be Deadly, Laser Focus, Technology Update 1,May 1985.
57. Young, E.C., The Penguin Dictionary of Electronics, 2nd Edition.
58. Hoult, D. P., and Wong, V., Characteristics of Thin films of Liquid in High Temperature Engines, Proceedings of the coatings for Advanced Heat Engines Workshop, U.S. Dept of Energy, Maine Maritime Academy, Castine, Maine, August 6-9, 1990, Session III-Applied Tribology.
59. Takaguchi, M., and Hoult, D., Parametric Effects on Laser-Fluorescence Diagnostic Calibration, presented at the Consortium on Lubrication in Internal Combustion Engines, Massachusetts Institute of Technology, February 21, 1989.

(This Page Intentionally Left Blank)

APPENDICES

for

The Chrysler and Kubota Engine Research

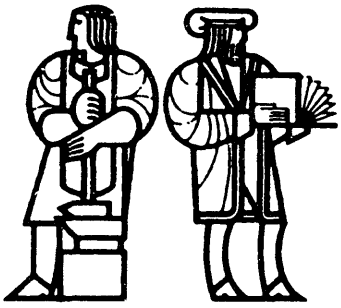

Massachusetts Institute of Technology

(This Page Intentionally Left Blank)

APPENDIX A

Chrysler Engine Specifications and Operating Characteristics

Table A1 Chrysler 2.2L Inline 4 Spark Ignition Engine

(Source: Chrysler Engine Service Manual)

Manufacturer	**Chrysler**
Type	Spark Ignition Throttle-Body Injection
Number of Cylinders	Inline 4
Displacement	2213 cc
Cylinder Displacement	553 cc
Bore	87.5 mm
Stroke	92.0 mm
Maximum Power	74 kW (100 hp) @ 5200 RPM
Maximum Power per Cylinder	18.5 kW (25 hp)
Maximum Power / Displacement	33.4 kW/l
Maximum Torque	149 N.m @ 3200 RPM
Cooling	Forced Circulation
Engine Block Material	Cast Iron
Piston Material	Aluminum Alloy
LIF Probe Location	40 mm from TDC of Cylinder no. 4
Oil Drain Design on Piston	Through Holes at back of OC Rail Groove
Oil Control Ring	3-Piece
Machining Marks (location)	Top, 2nd and 3rd lands

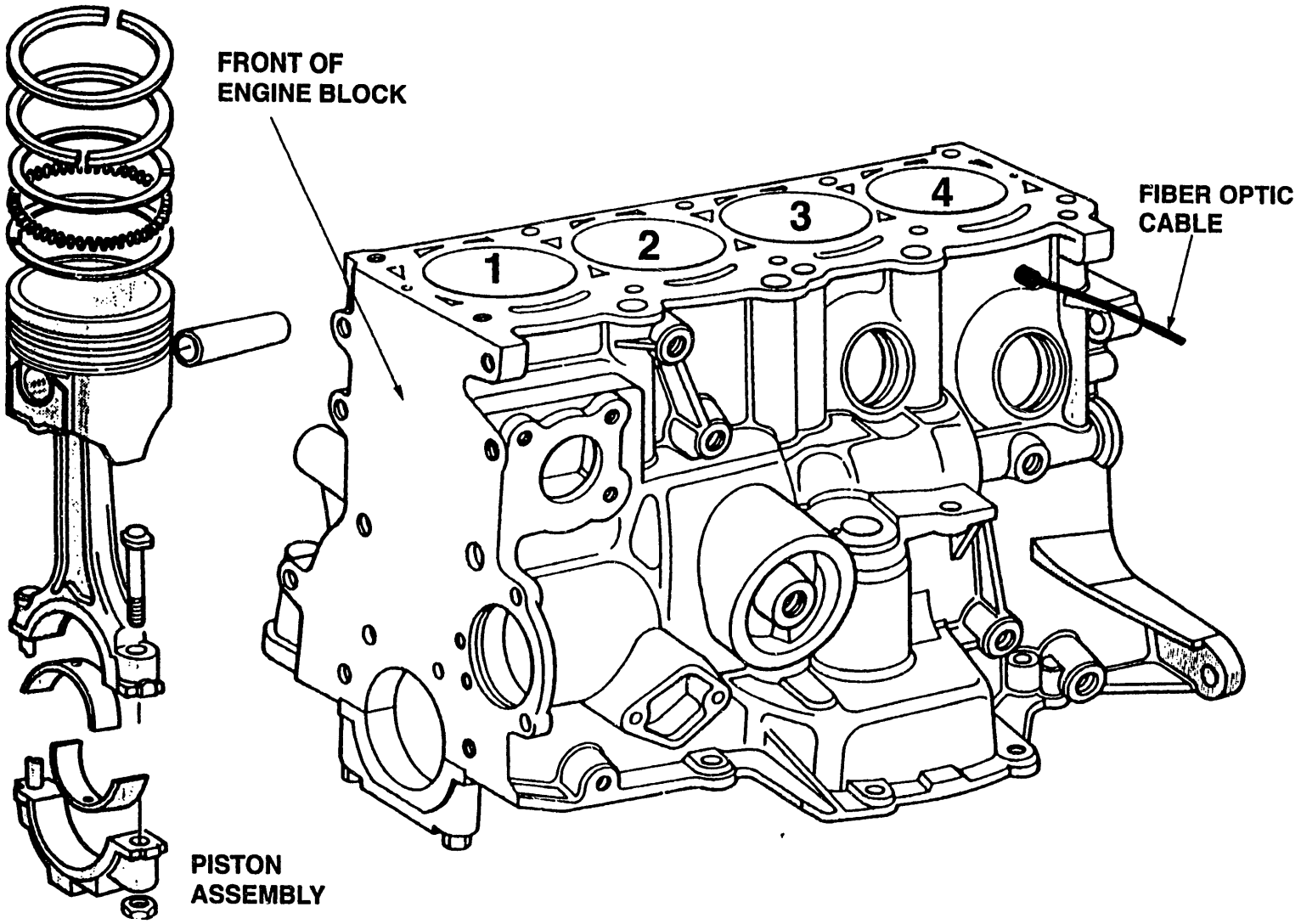

FIGURE A1 CHRYSLER ENGINE BLOCK AND PISTON ASSEMBLY

(This Page Intentionally Left Blank)

APPENDIX B

Fiber Optic Eccentric Coupler

The main purpose of the eccentric coupler, is to focus laser light directly into the fiber optic cable. The main parts of this coupler are shown below in figure B1.

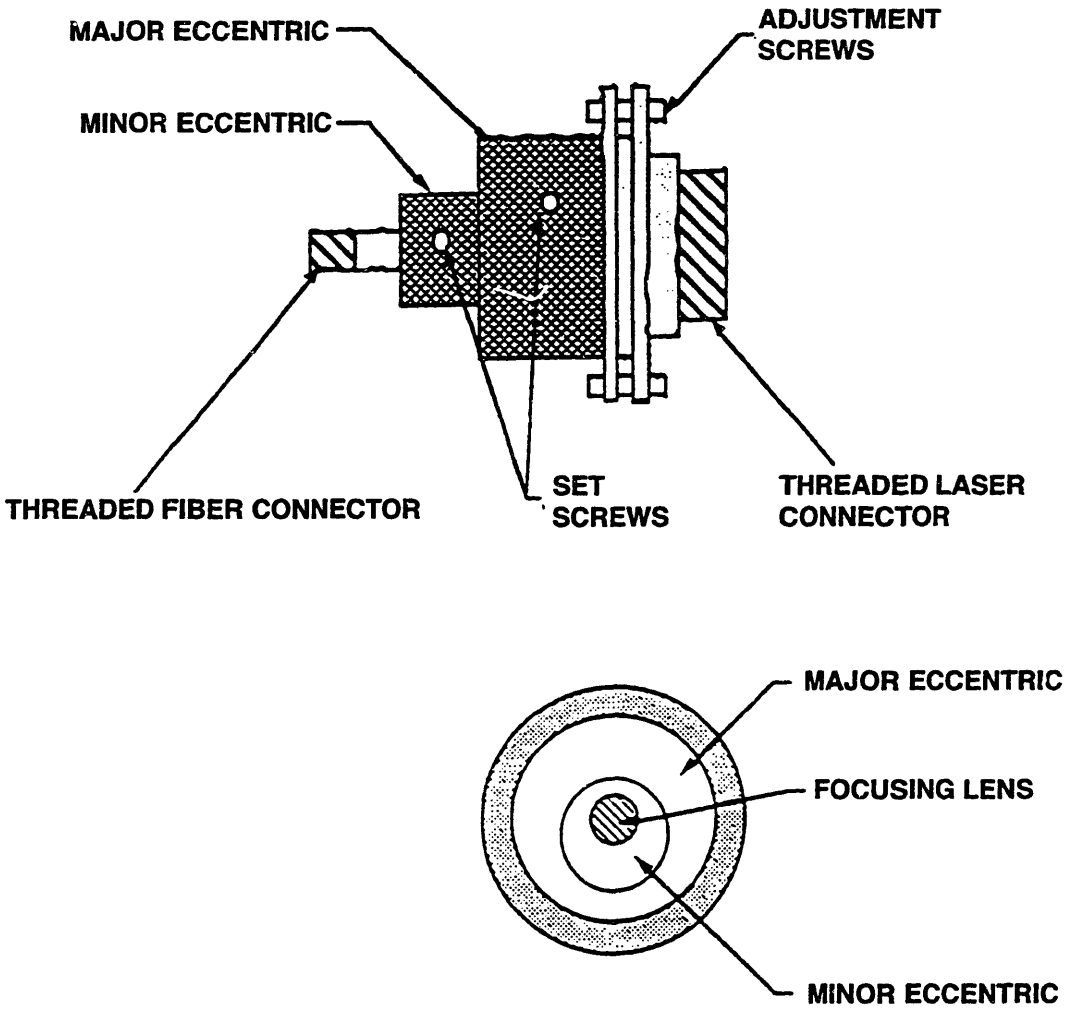

Figure B1 Schematic of Eccentric Coupler

APPENDIX C

Photo Multiplier Performance Data

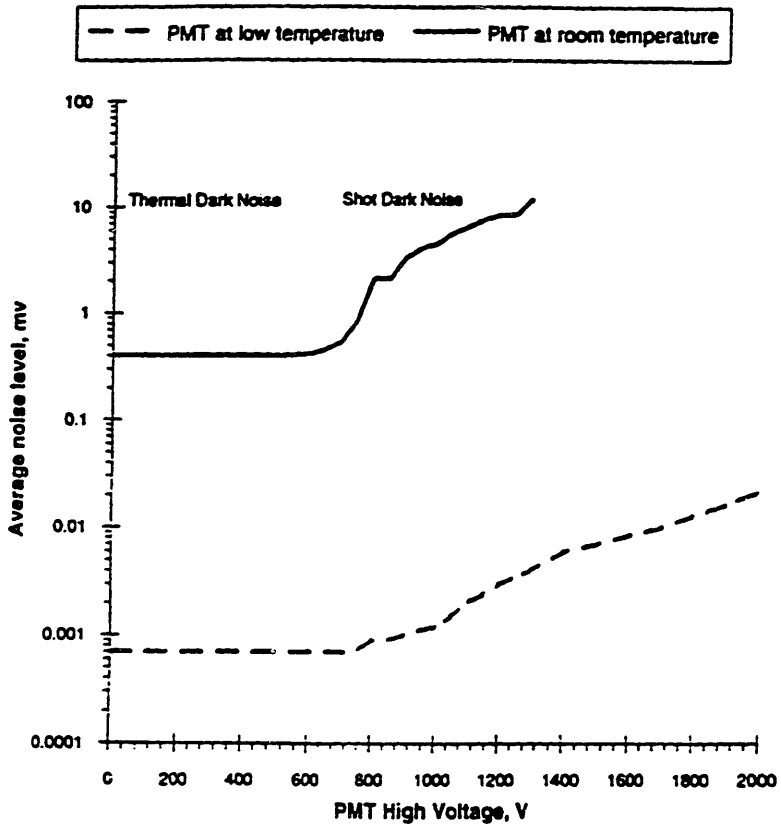

Figure C1 PMT Signal Noise vs. PMT Voltage
(Tamai's Experimental Data)

APPENDIX D

LIF System Components

Component	Manufacturer	Part Number
14 mW He-Cd laser, 442 nm Power Supply	Liconix	4214N
Optical filter (442 nm) 2 req'd	Oriel	52086, 1 in OD
Filter Holder	Oriel	51594
Eccentric Coupler	General Fiber-Optic	8612-12501
Bifurcated Fiber Optic Cables	General Fiber-Optic	B16-0200-HAS-C22-G-0066-2.5-SMA/3
LIF Focusing Probe	F.H. Peterson Machine Corp.	Custom made see fig. 2.6
Laser-to-Engine LIF Focusing	Melles Griot	01LPX007
Probe Lenses (2 per probe)	Gould Precision Optics	Custom made for application
LIF Windows (fused silica)	Gould Precision Optics	Custom made for application
-Start of PMT Focusing Assembly-		
Oriel Fiber Input Flange	Oriel	77850
Flange Collar	Oriel	77829
Collar Coupler (male/male)	Oriel	78122
Optic Holder w/ lens holding collar. (1 of 3)	Oriel	7123
Lens (Laser to PMT #1, focal length = 38mm, convex toward PMT.)	Oriel	41330
Optic Holder w/ lens holding collar. (2 of 3)	Oriel	7123
495 nm Optical Filter (2 req'd)	Omega Optical	495DF20
Optic Holder w/ lens holding collar. (3 of 3)	Oriel	7123
Lens (Laser to PMT#2 focal length = 150 mm convex away from PMT.)	Oriel	41370
4 inch Spacer	Oriel	7132
Collar Coupler (female/female)	Oriel	77829
PMT Housing	Products Research	Custom made for application
-End of PMT focusing Assembly-		
Photo Multiplier Tube (PMT)	Hamamatsu	R4220
PMT Socket and Amplifier	Hamamatsu	C1053-01
High Voltage PMT Power Supply	Bertan	230-03R
+/- 15 Volt PMT Power Supply Amplifier	Newark Electronics	SLD-12-1010-12
100 kHz Low Pass Filter with BNC input and output	Sloan Electronics	Custom made for application
Coumarin fluorescent dye (5g)	Exciton Inc.	Coumarin 523
Data Acquisition System	Keithley Metrabyte	DAS-58

TABLE D1 LIF SYSTEM COMPONENTS

APPENDIX E

Chrysler Engine Operating Procedures

Table E1 Start-up Procedure for the Chrysler 2.2L S.I. Engine

Step #	Component	Position or Action
———	**Pre-Startup Checks**	———
1	Engine Oil Dipstick	In operating range
2	Engine Coolant	In sight glass
3	Dyno Oil Sump	In sight glass
4	Dyno Foundation	Clear of fluid puddles, Drip pan in place
5	Engine Foundation	Clear of oil puddles
6	Fuel Can	Half Full Minimum
———	Valve Line-up	———
7	Circulating (Circ) Water supply Valve (on South wall)	
8	Circ Water Supply Manifold	a. Oil Cooler Supply: Check OPEN b. Coolant HX Supply: Check OPEN c. Fuel Cooler Supply: Check OPEN (These are the red handled valves on the circ water supply manifold)
9	Circ Water Drain Manifold	Coolant Head Tank Vent Isolation: Check OPEN
10	Steam Supply Manifold	Check all valves SHUT
11	Coolant Head, Tank Drain Valve	Check SHUT
12	Coolant Head, Tank Isolation Quick-throw valves	Check OPEN (in-line position)
13	At Fuel Manifold	a. Pump Discharge Control Valve: Check TO ENGINE POSITION. b. Fuel Return Isolation: Check OPEN (Both valves should be pointing at the 9 o' clock position)
13a	Oil Cooler Recirculating Pump	Check: a. Coupling is fully mated. b. Three-way discharge valve is positioned to discharge to the sump.
14	Power Strips on back of Control Panel	Switch ON, light ON
15	Ignition/Fuel Power Strip	Switch ON, light OFF
16	Heat Exchanger Oil Out Setpoint	190 degrees Fahrenheit
———	**DYNO STARTUP**	———
17	"Sloan-Lab Dyno breaker in RM 037C"	ON Position Check indication on Dyno Control Panel (Blue Light)
18	Trench Fan Controller	ON, Light ON.
19	MG-SET switch on Dyno control Panel	ON
20	DYNO REV SWITCH at Dyno Control Panel	REV (starts dyno oil pump) allow 5 minutes for warm up before proceeding
21	Power Switch for Stepper Motor (rocker switch at bottom of Dyno control cabinet)	ON, light ON
22	At Engine Control Panel	a. RPM Display: ON, Light ON b. Temp Display: ON, Light On c. Oil Recirc Pump: ON, Light OFF d. Load Cell Readout: ON (reading zero)

23	Dyno MANUAL RHEO	Check at "0" position by using the DYNO rocker switch in the "lower" direction until you hear the rheostat click.
24	Dyno Start Switch	——Critical Step—— START; MANUAL RHEO to increase speed to 1200 RPM as indicated by the manual rheo indication of approximately "10".
25	Engine Oil Pressure	——Critical Step—— 70 to 80 psi, cold, Idiot light off. **IF EITHER LOW PRESSURE OR IDIOT LIGHT CONDUCT IMMEDIATE DYNO SHUTDOWN** (see step 7 of the normal shutdown procedure)
26	Load Cell Readout	Positive (+) number [indicates motoring condition].
27	Dyno	a. Oil Pressure: approx. 10 psi. b. Drip-o-lators: min. 1 drip/5 sec. c. Fan: Positive Air Flow.
28	Wall Fan	ON Fan should be direct toward exhaust manifold.
29	Thermocouple Readouts	Check for proper operation; "EEE" readout means an inoperative thermocouple.
———	**ENGINE STARTUP**	———
30	Throttle Manometer	——Critical Step—— 10 inches of mercury or 35Kpa
31	Ignition Switch	ON, Verify 12 to 14 VDC indicated.
32	Load Cell	Check negative (-) number; indicating that the engine is firing.

Table E2 Normal Shutdown Procedure for the Chrysler 2.2L S.I. Engine

1	Throttle Rocker	35KPa
2	MANUAL RHEO	1200 RPM
3	Throttle Rocker	35KPa
4	OIL OUT Temp	Maintain Light Load until less than 95°C
5	IGNITION SWITCH	OFF
6	Load Cell Readout	Check Load (+)
7	OIL OUT Temp	70-80°C for proper cooldown
———	**SECURE DYNO**	———
8	MANUAL RHEO	——Critical Step—— Slow to "0" **immediately**
9	Dyno START Switch	STOP, **(Counter Clockwise)**
10	Dyno REV SWITCH	OFF **(Counter Clockwise)**
11	MG-SET SWITCH	STOP **(Counter Clockwise)**
12	At Engine Control Panel	Set all remaining switches OFF.
13	Power Strips of back of Engine Control Panel	OFF, light OFF
14	Circ Water Supply Valve	Shut
15	Dyno Oil Sump	In sight glass
16	"Sloan-Lab, GE Dyno" Breaker	OFF
17	Vent Fan Controller	After Visually verifying that no other lab engines are in operation, OFF

Table E3 Emergency Shutdown Procedure for the Chrysler 2.2L S.I. Engine

Step #	Component	Position or Action
1	IGNITION SWITCH	OFF
2	MANUAL RHEO	Rapidly to "0"
3	Dyno START SWITCH	STOP
----------	Continue normal shutdown procedure	----------

APPENDIX F

Chrysler Engine and System Operating Data for Simultaneous LIF and SO_2 Testing

SIMULTANEOUS LIF AND SO_2 DIAGNOSTIC DATA SHEET																	
CHRYSLER 2.2L S.I. ENGINE																	
	ENGINE DATA										SO_2 DATA						
SPEED	T1	T2	T3	T4	T5	T6	T7	T8	T9	Load Cell (lb)	Torque (ft-lb)	Intake Press. (Kpa)	BYPASS (LPM)	T1	T2	T3	T4
3000RPM	100	112	146	125	/	33	40	114	135	21.2	47.7	78	0.6	994	958	177	232
2500RPM	96	108	127	156	/	37	41	109	128	22.6	50.85	86	0.6	978	958	169	228
2000RPM	97	104	127	156	/	38	43	100	123	21.2	47.7	108	0.6	969	949	194	235
ENGINE TEMPERATURES											SO_2 DIAGNOSTIC SYSTEM TEMPERATURES						
T1 COOLANT INLET TEMP.											T1 SAMPLE LINE TEMP. PRIOR TO SOLENOIDS						
T2 COOLANT OUTLET TEMP.											T2 SAMPLE LINE TEMP. PRIOR TO FURNACE						
T3 EXHAUST GAS											T3 FLEXIBLE HEATED LINE TEMP						
T4 OIL SUMP											T4 TEMP. PRIOR TO BYPASS VALVE						
T5 NOT APPLICABLE											LONG LINE MAINTAINED AT 375F						
T6 FUEL IN											SHORT LINE MAINTAINED AT 575F						
T7 INTAKE AIR																	
T8 COOLANT CYLINDER no. 2																	
T9 COOLANT CYLINDER no. 4																	
					ALL TEMPERATURES ARE IN DEGREES FAHRENHEIT (F)													

TABLE F1 CHRYSLER ENGINE AND SYSTEM OPERATING DATA

APPENDIX G

Simultaneous LIF and SO_2 Data for the Chrysler 2.2L S.I. Engine at the Mid Load Condition

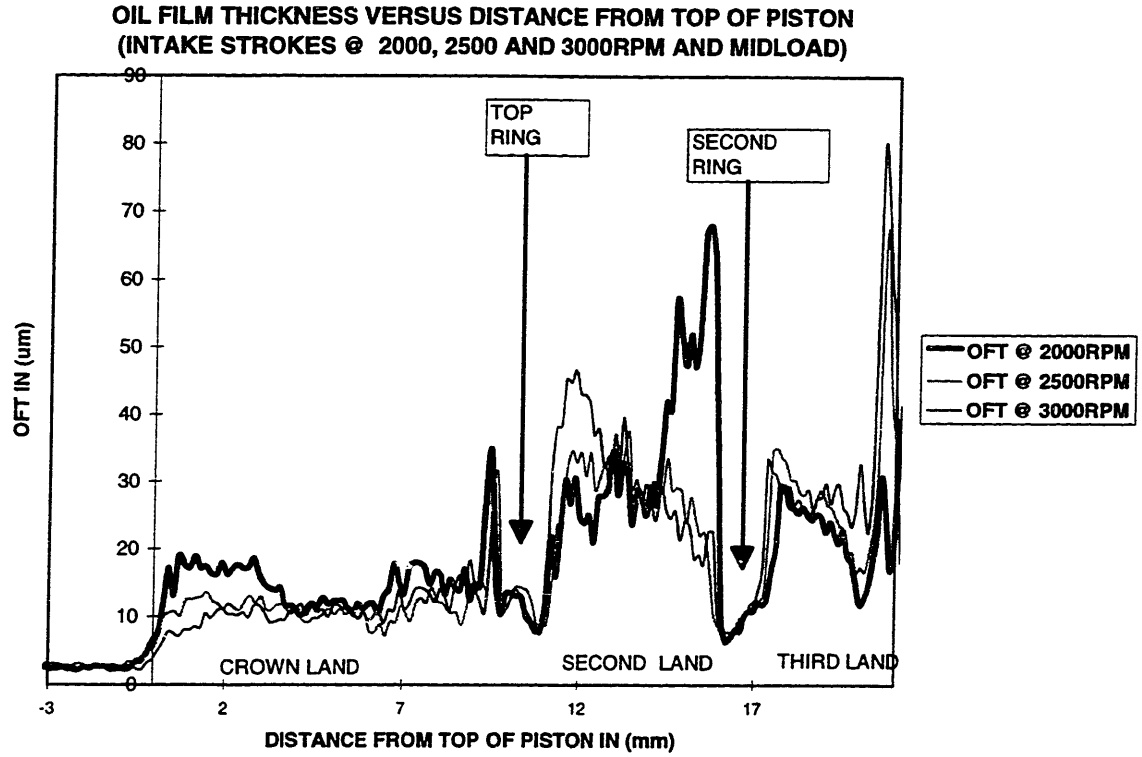

Figure G1 Oil Film Thickness Traces for the Intake Stroke at the above 3 speeds

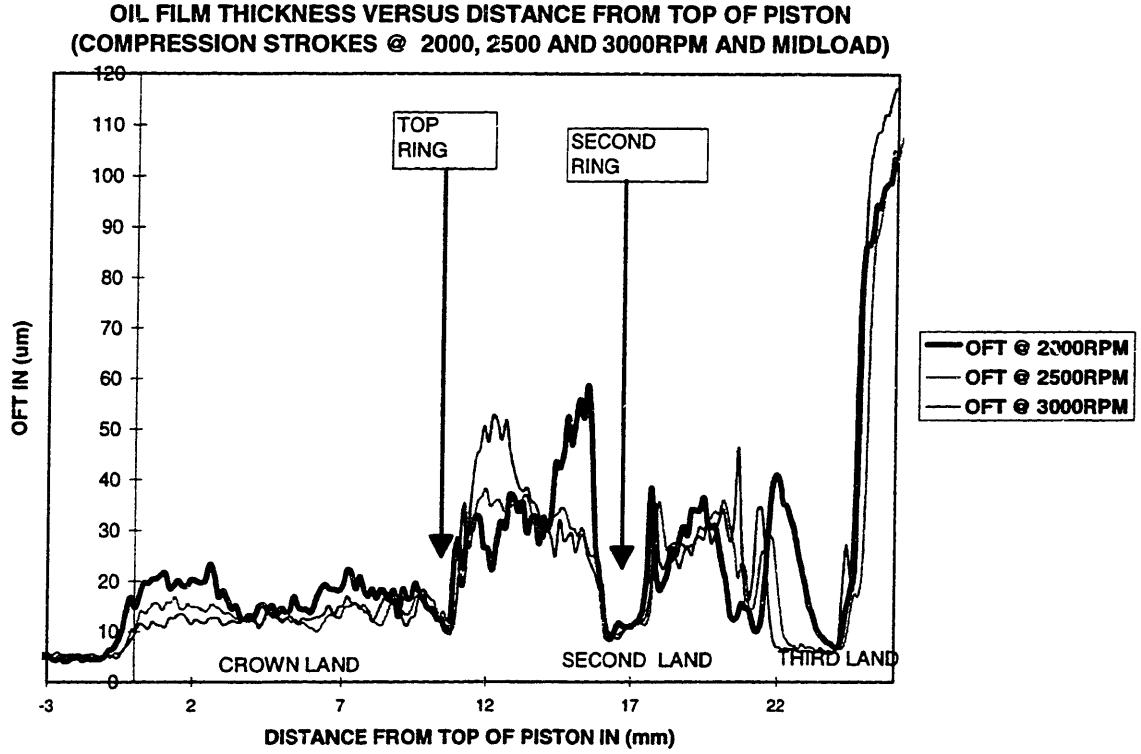

Figure G2 Oil Film Thickness Traces for the Compression Stroke at the above 3 speeds

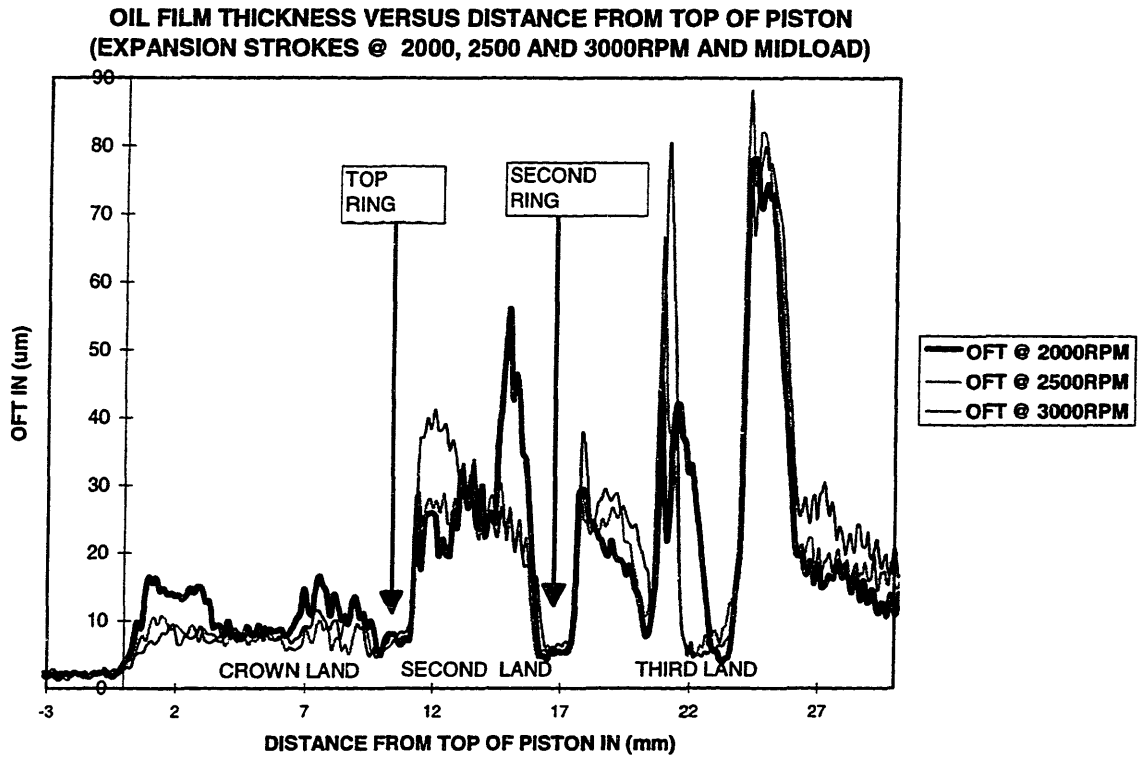

Figure G3 Oil Film Thickness Traces for the Expansion Stroke at the above 3 speeds

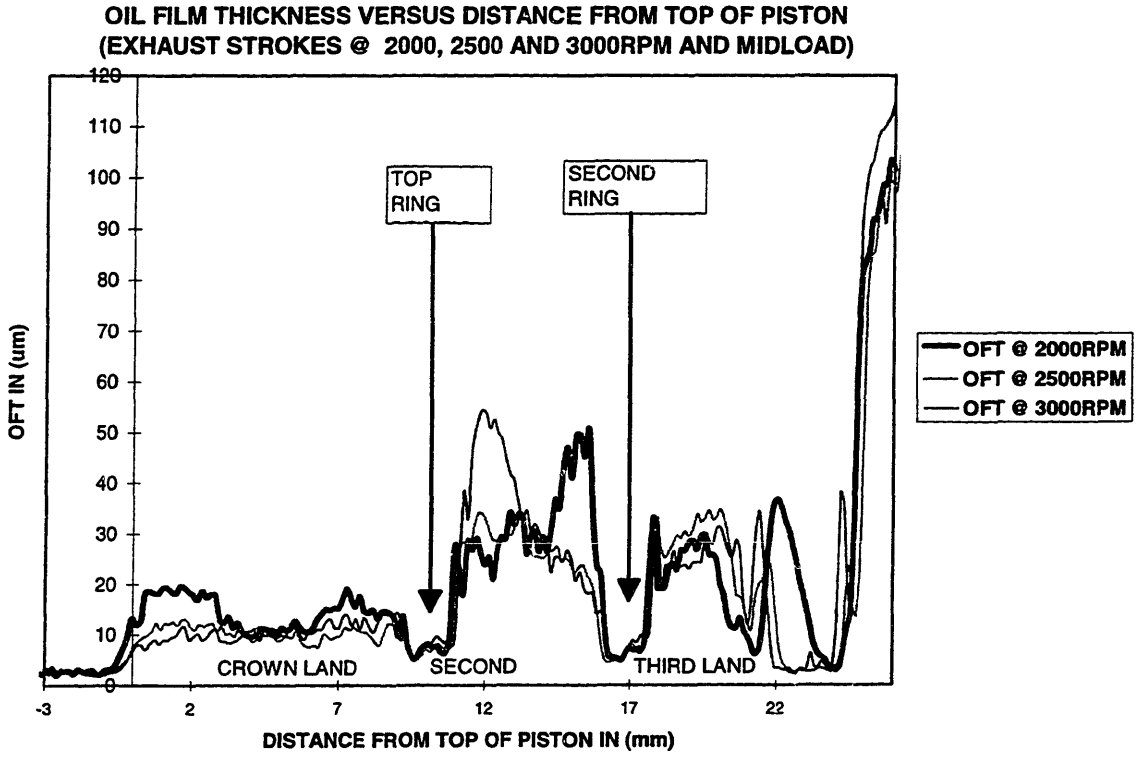

Figure G4 Oil Film Thickness Traces for the Exhaust Stroke at the above 3 speeds

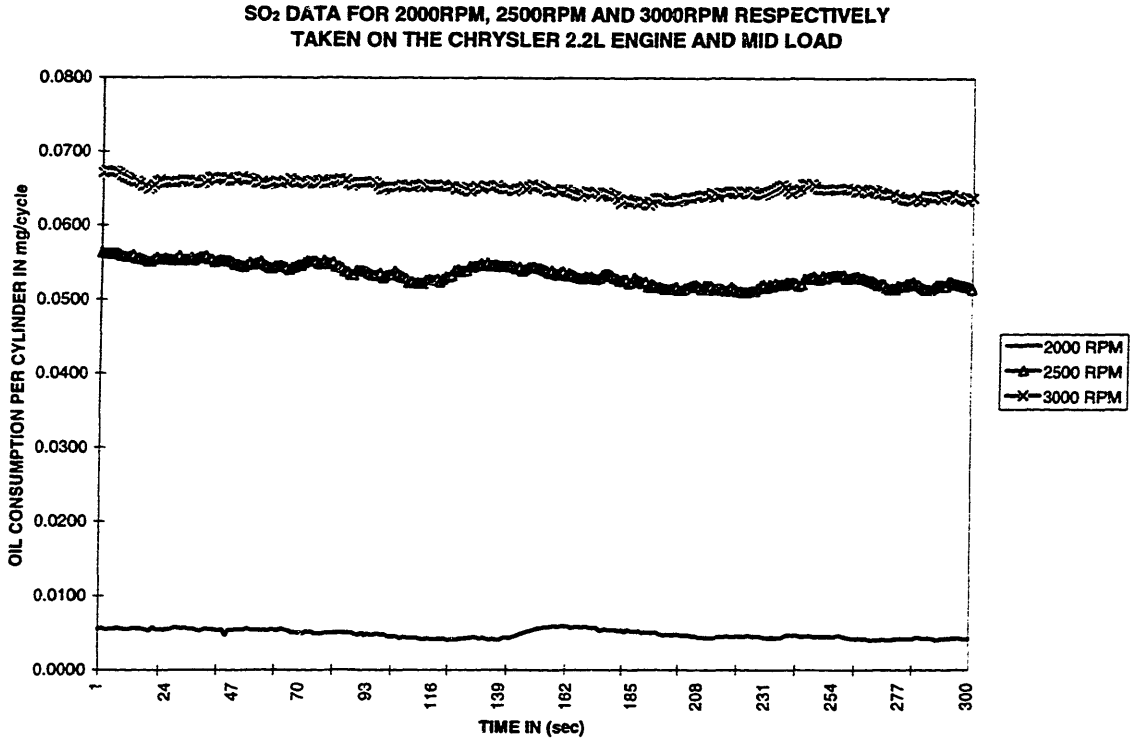

Figure G5 SO_2 Traces for the Chrysler 2.2L Engine at the above 3 speeds

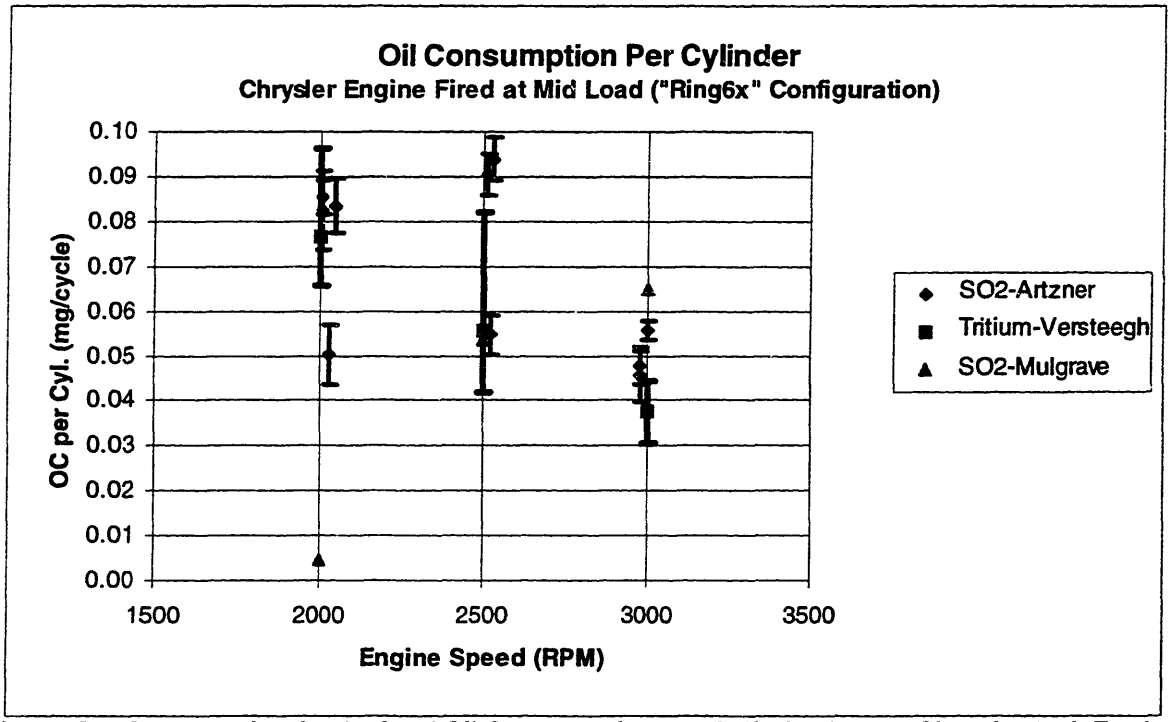

Figure G6 Comparative Analysis of Oil Consumption per Cylinder for the Chrysler 2.2L Engine

Table G1 Average Oil Film Thickness in Microns on the Top Land during the Compression Stroke

(Data taken with C1 ring pack, unpinned rings and modified second ring gap 6x)

	Engine Speeds		
Experimenters	**2000RPM**	**2500RPM**	**3000RPM**
Versteegh	8.0μm	8.6μm	6.0μm
Mulgrave	14.4μm	10.9μm	10.3μm

Table G2 Data for the C1 Ring Pack

Top Ring Height	**1.42 mm**
Second Ring Height	**1.42 mm**
Oil Control ring Height	**4.0 mm**
Top ring Gap	**0.25 mm to 0.51 mm**
Second Ring Gap	**0.23 mm to 0.48 mm**
Oil Control Ring Gap	**0.38 mm to 1.40 mm**
Top Ring Tension	**22.24 N (Diametral)**
Second Ring Tension	**20.90 N (Diametral)**
Oil Control Ring Tension	**40.47 N (Diametral)**

(This Page Intentionally Left Blank)

APPENDIX H

Kubota Engine Specifications and Operating Characteristics

Model		EA300	EA300-N	EA300-NB1	EA400-N	EA400-NB
Type		Horizontal, water-cooled, 4-cycle diesel engine				
Number of Cylinder		1				
Bore x Stroke		75 mm x 70 mm 2.95 in. x 2.76 in.			78 mm x 84 mm 3.07 in. x 3.31 in.	
Displacement		309 cc 18.86 cu.in.			401 cc 24.47 cu.in.	
Brake H.P.	SAE Gross	6.3 kW/3000 r.p.m 8.4 HP/3000 r.p.m			6.7 kW/2400 r.p.m 9 HP/2400 r.p.m	
	SAE Intermittent	5.2 kW/3000 r.p.m 7 HP/3000 r.p.m			5.8 kW/2400 r.p.m 7.8 HP/2400 r.p.m	
	SAE Cont.	4.5 kW/3000 r.p.m 6 HP/3000 r.p.m			5.1 kW/2400 r.p.m 6.8 HP/2400 r.p.m	
	DIN 6270-NA	4.5kW/3000 r.p.m 6 PS/3000 r.p.m			–	
	DIN 6270-NB	5.1 kW/3000 r.p.m 7 PS/3000 r.p.m			–	
	DIN 70020	5.7 kW/3000 r.p.m 7.7 PS/3000 r.p.m			–	
Cooling System		Radiator				
Combustion System		Precombustion Swirl Chamber (TVCS=Three Vortex Combustion System)				
Fuel		SAE No.2-D Light Diesel Oil				
Lubricating Oil		API service CB, CC-class (SAE #30, 20, 10W-30)				
Lubricating System		Forced Lubrication with Trochoid Pump				
Starting System		Hand Start		Electric Start	Hand Start	Electric Start
Direction of Revolution		Counterclockwise Facing Flywheel				
Cooling Water Capacity		1.2 ℓ 1.3 U.S.qts. 1.06 Imp.qts.			1.6 ℓ 1.7 U.S.qts. 1.41 Imp.qts.	
Fuel Tank Capacity		4.7 ℓ 1.24 U.S.gal. 1.03 Imp.gal.		4.8 ℓ 1.27 U.S.gal. 1.06 Imp.gal.	8.0 ℓ 2.11 U.S.gal. 1.76 Imp.gal.	
Engine Oil Capacity		1.3 ℓ 1.4 U.S.qts. 1.14 Imp.qts.			1.9 ℓ 2.0 U.S.qts. 1.67 Imp.qts.	
Dry Weight		50.0 kg 110.2 lbs.		54.0 kg 119.1 lbs.	86.0 kg 189.6 lbs.	93.0 kg 205.0 lbs.

TABLE H1 KUBOTA ENGINE SPECIFICATIONS

APPENDIX I

Kubota Engine Component Drawings

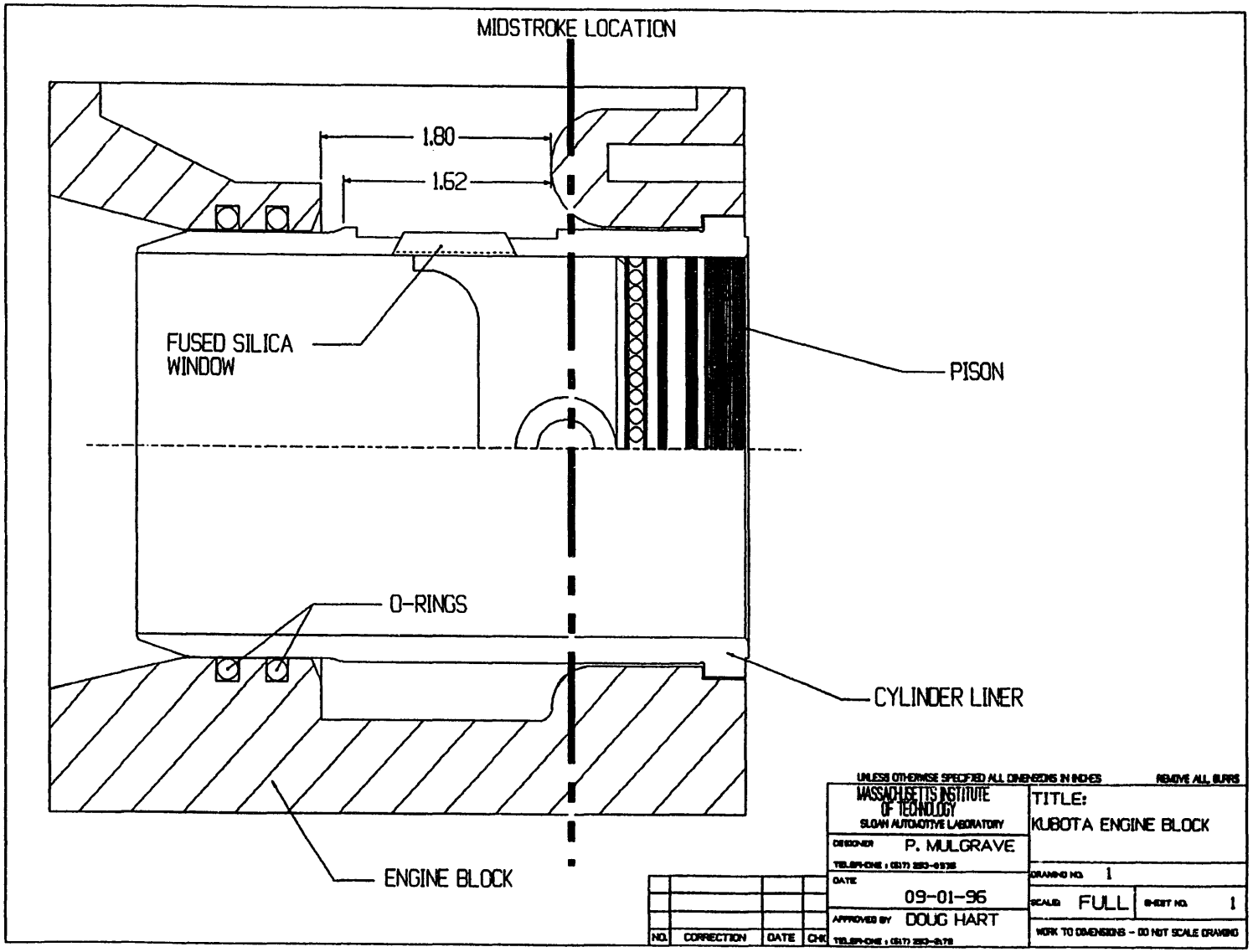
MIDSTROKE LOCATION
1.80
1.62
FUSED SILICA WINDOW
PISON
O-RINGS
CYLINDER LINER
ENGINE BLOCK
UNLESS OTHERWISE SPECIFIED ALL DIMENSIONS IN INCHES
REMOVE ALL BURRS
MASSACHUSETTS INSTITUTE OF TECHNOLOGY
SLOAN AUTOMOTIVE LABORATORY
TITLE:
KUBOTA ENGINE BLOCK
DESIGNER P. MULGRAVE
DRAWING NO. 1
DATE 09-01-96
SCALE: FULL
SHEET NO. 1
APPROVED BY DOUG HART
WORK TO DIMENSIONS - DO NOT SCALE DRAWING
NO. CORRECTION DATE CHK

FIGURE I1

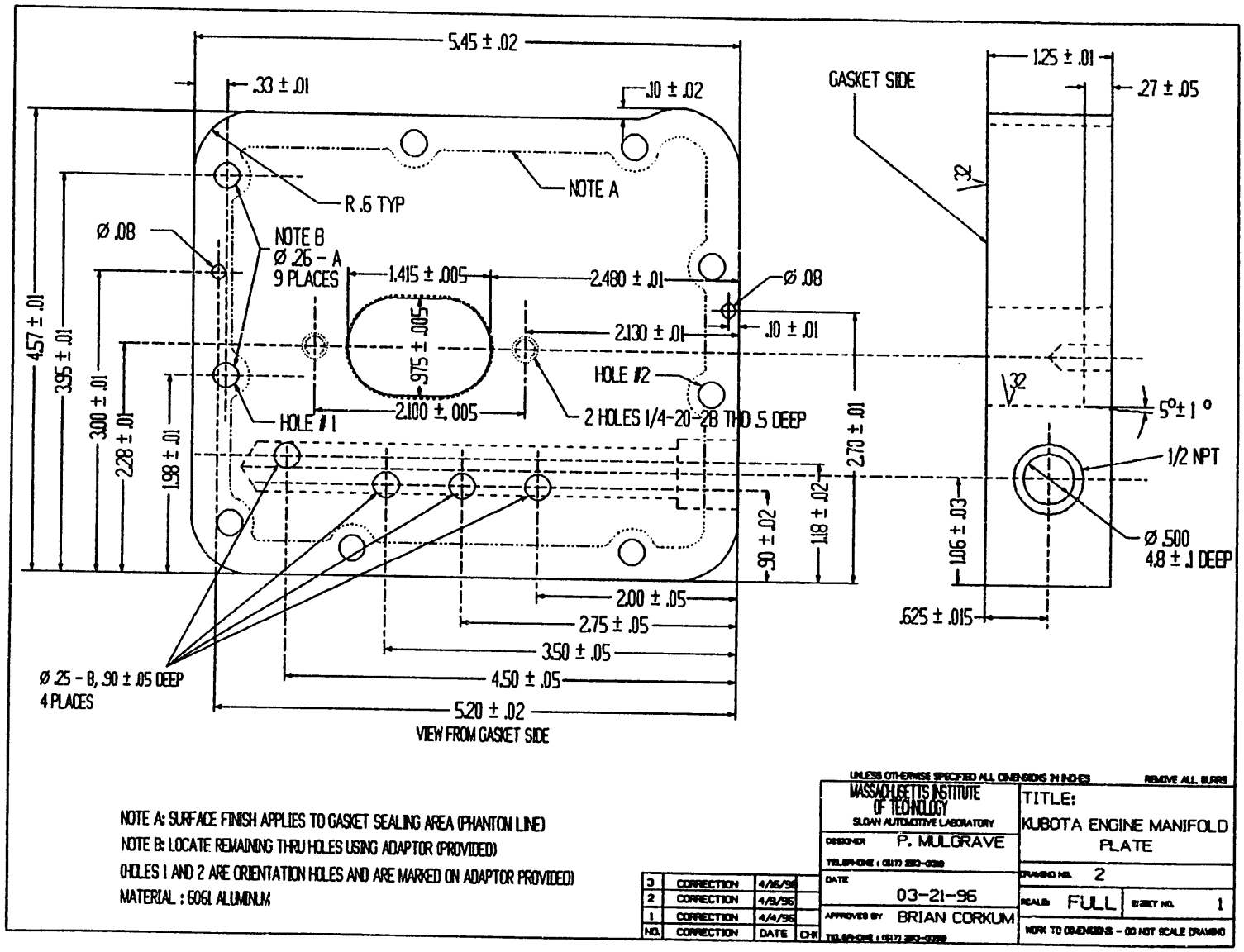
5.45 ± .02
.33 ± .01
.10 ± .02
R .6 TYP
NOTE A
Ø .08
NOTE B
Ø .26 - A
9 PLACES
1.415 ± .005
2.480 ± .01
Ø .08
.975 ± .005
2.130 ± .01
.10 ± .01
HOLE #2
HOLE #1
2.100 ± .005
2 HOLES 1/4-20-2B THD .5 DEEP
4.57 ± .01
3.95 ± .01
3.00 ± .01
2.28 ± .01
1.98 ± .01
2.70 ± .01
.90 ± .02
1.18 ± .02
2.00 ± .05
2.75 ± .05
3.50 ± .05
4.50 ± .05
5.20 ± .02
Ø .25 - B, .90 ± .05 DEEP
4 PLACES
VIEW FROM GASKET SIDE
GASKET SIDE
1.25 ± .01
.27 ± .05
32
32
5° ± 1°
1/2 NPT
Ø .500
4.8 ± .1 DEEP
1.06 ± .03
.625 ± .015
NOTE A: SURFACE FINISH APPLIES TO GASKET SEALING AREA (PHANTOM LINE)
NOTE B: LOCATE REMAINING THRU HOLES USING ADAPTOR (PROVIDED)
(HOLES 1 AND 2 ARE ORIENTATION HOLES AND ARE MARKED ON ADAPTOR PROVIDED)
MATERIAL : 6061 ALUMINUM
UNLESS OTHERWISE SPECIFIED ALL DIMENSIONS IN INCHES
REMOVE ALL BURRS
MASSACHUSETTS INSTITUTE OF TECHNOLOGY
SLOAN AUTOMOTIVE LABORATORY
DESIGNER P. MULGRAVE
DATE 03-21-96
APPROVED BY BRIAN CORKUM
TITLE: KUBOTA ENGINE MANIFOLD PLATE
DRAWING NO. 2
SCALE: FULL
SHEET NO. 1
WORK TO DIMENSIONS - DO NOT SCALE DRAWING
NO. CORRECTION DATE CHK
3 CORRECTION 4/16/96
2 CORRECTION 4/3/96
1 CORRECTION 4/4/96

FIGURE I2

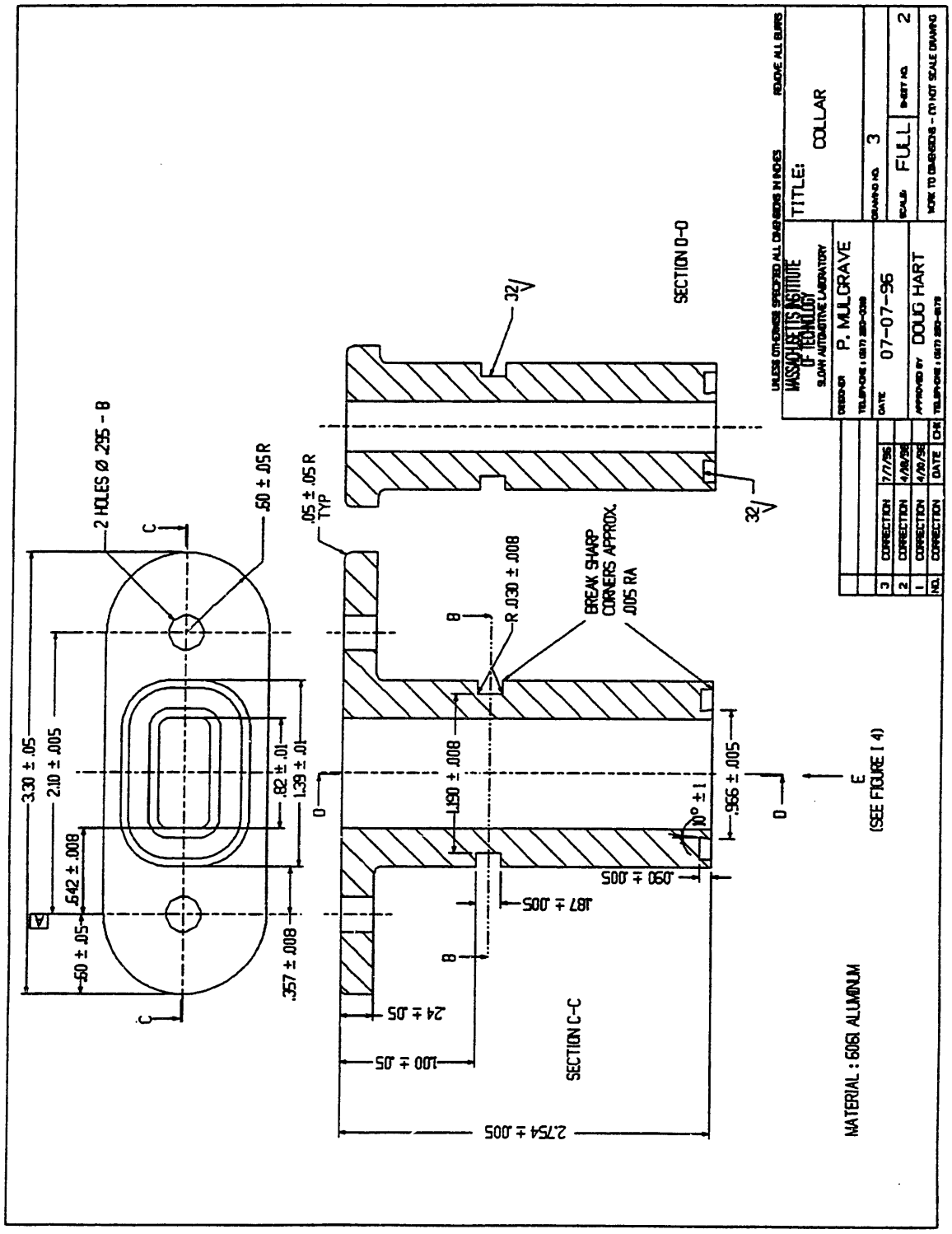
2 HOLES Ø .295 - B
.50 ± .05R
.05 ± .05R TYP
3.30 ± .05
2.10 ± .005
.82 ± .01
1.39 ± .01
.642 ± .008
.50 ± .05
.357 ± .008
SECTION D-D
32
32
R .030 ± .008
BREAK SHARP CORNERS APPROX. .005 RA
.150 ± .008
10° ± 1°
.966 ± .005
.090 ± .005
.187 ± .005
.24 ± .05
1.00 ± .05
2.754 ± .005
SECTION C-C
E
(SEE FIGURE I 4)
MATERIAL : 6061 ALUMINUM
UNLESS OTHERWISE SPECIFIED ALL DIMENSIONS IN INCHES
REMOVE ALL BURRS
MASSACHUSETTS INSTITUTE OF TECHNOLOGY
SLOAN AUTOMOTIVE LABORATORY
TITLE:
COLLAR
DESIGNED P. MULGRAVE
DATE 07-07-96
DRAWING NO. 3
SCALE FULL
SHEET NO. 2
APPROVED BY DOUG HART
WORK TO DIMENSIONS - DO NOT SCALE DRAWING
3 CORRECTION 7/7/95
2 CORRECTION 4/20/95
1 CORRECTION 4/20/95
NO. CORRECTION DATE CHK

FIGURE I3

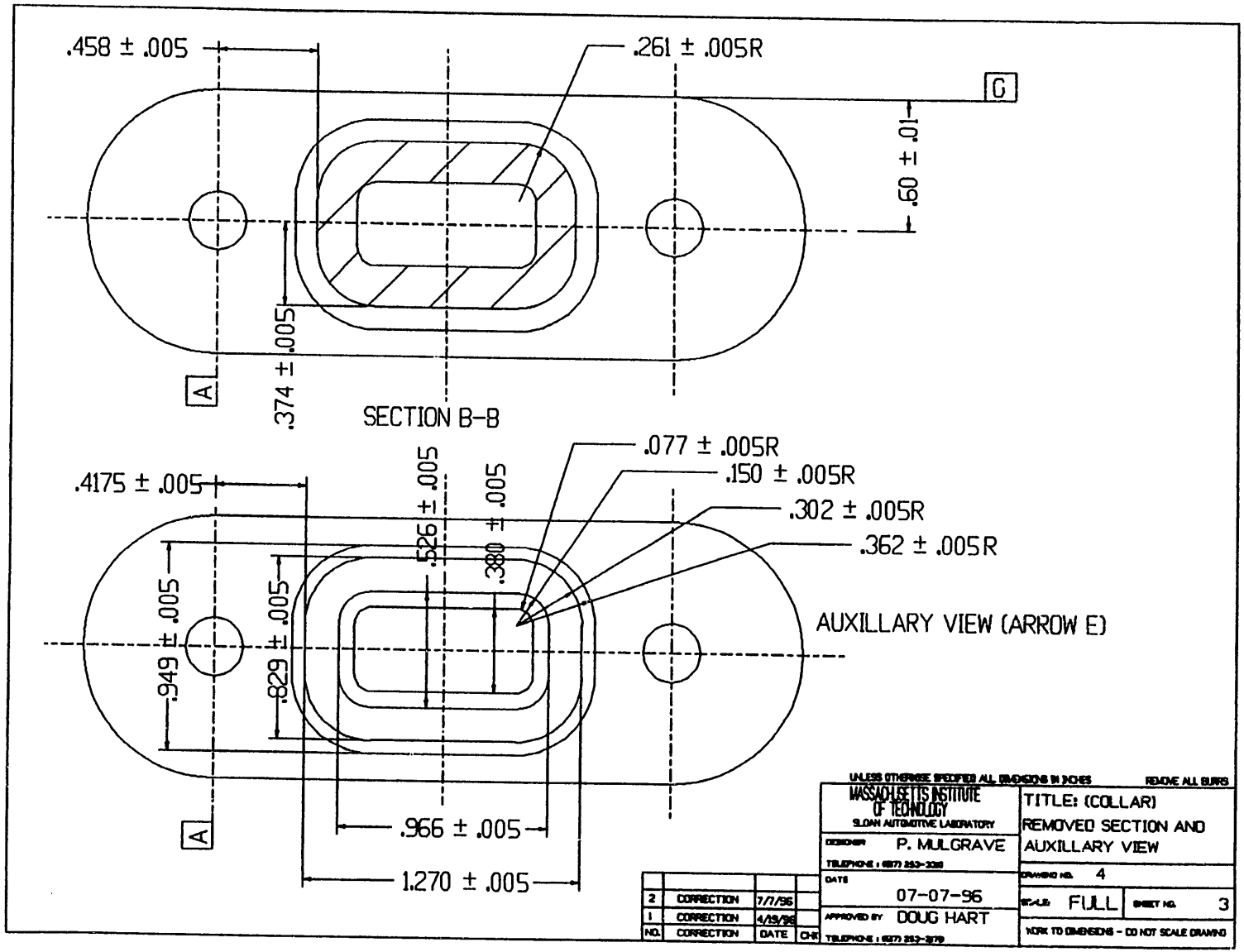
.458 ± .005
.261 ± .005R
C
.60 ± .01
.374 ± .005
A
SECTION B-B
.4175 ± .005
.526 ± .005
.380 ± .005
.077 ± .005R
.150 ± .005R
.302 ± .005R
.362 ± .005R
.949 ± .005
.829 ± .005
AUXILLARY VIEW (ARROW E)
.966 ± .005
1.270 ± .005
A
UNLESS OTHERWISE SPECIFIED ALL DIMENSIONS IN INCHES
REMOVE ALL BURRS
MASSACHUSETTS INSTITUTE OF TECHNOLOGY
SLOAN AUTOMOTIVE LABORATORY
DESIGNER P. MULGRAVE
TELEPHONE : (617) 253-3381
DATE 07-07-96
APPROVED BY DOUG HART
TELEPHONE : (617) 253-2179
TITLE: (COLLAR) REMOVED SECTION AND AUXILLARY VIEW
DRAWING NO. 4
SCALE: FULL
SHEET NO. 3
WORK TO DIMENSIONS - DO NOT SCALE DRAWING
NO. CORRECTION DATE CHK
2 CORRECTION 7/7/96
1 CORRECTION 4/19/96

FIGURE I4

FIGURE 15

FIGURE 16

FIGURE 17

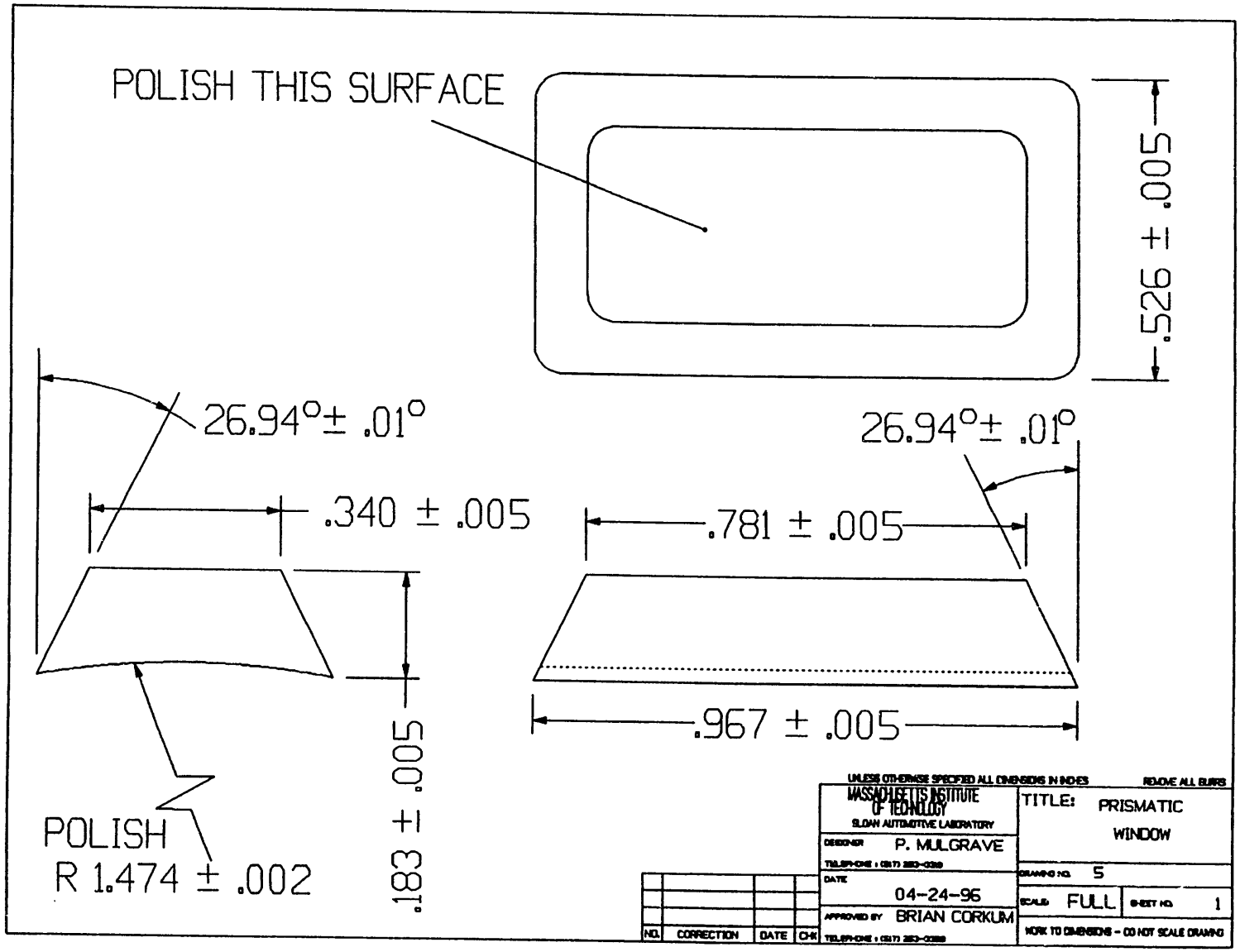
POLISH THIS SURFACE
.500 ± .005
.526
26.94° ± .01°
26.94° ± .01°
.340 ± .005
.781 ± .005
.967 ± .005
.183 ± .005
POLISH
R 1.474 ± .002
UNLESS OTHERWISE SPECIFIED ALL DIMENSIONS IN INCHES
REMOVE ALL BURRS
MASSACHUSETTS INSTITUTE OF TECHNOLOGY
SLOAN AUTOMOTIVE LABORATORY
DESIGNER P. MULGRAVE
DATE 04-24-96
APPROVED BY BRIAN CORKUM
TITLE: PRISMATIC WINDOW
DRAWING NO. 5
SCALE FULL
SHEET NO. 1
WORK TO DIMENSIONS – DO NOT SCALE DRAWING
NO. CORRECTION DATE CHK

FIGURE I8

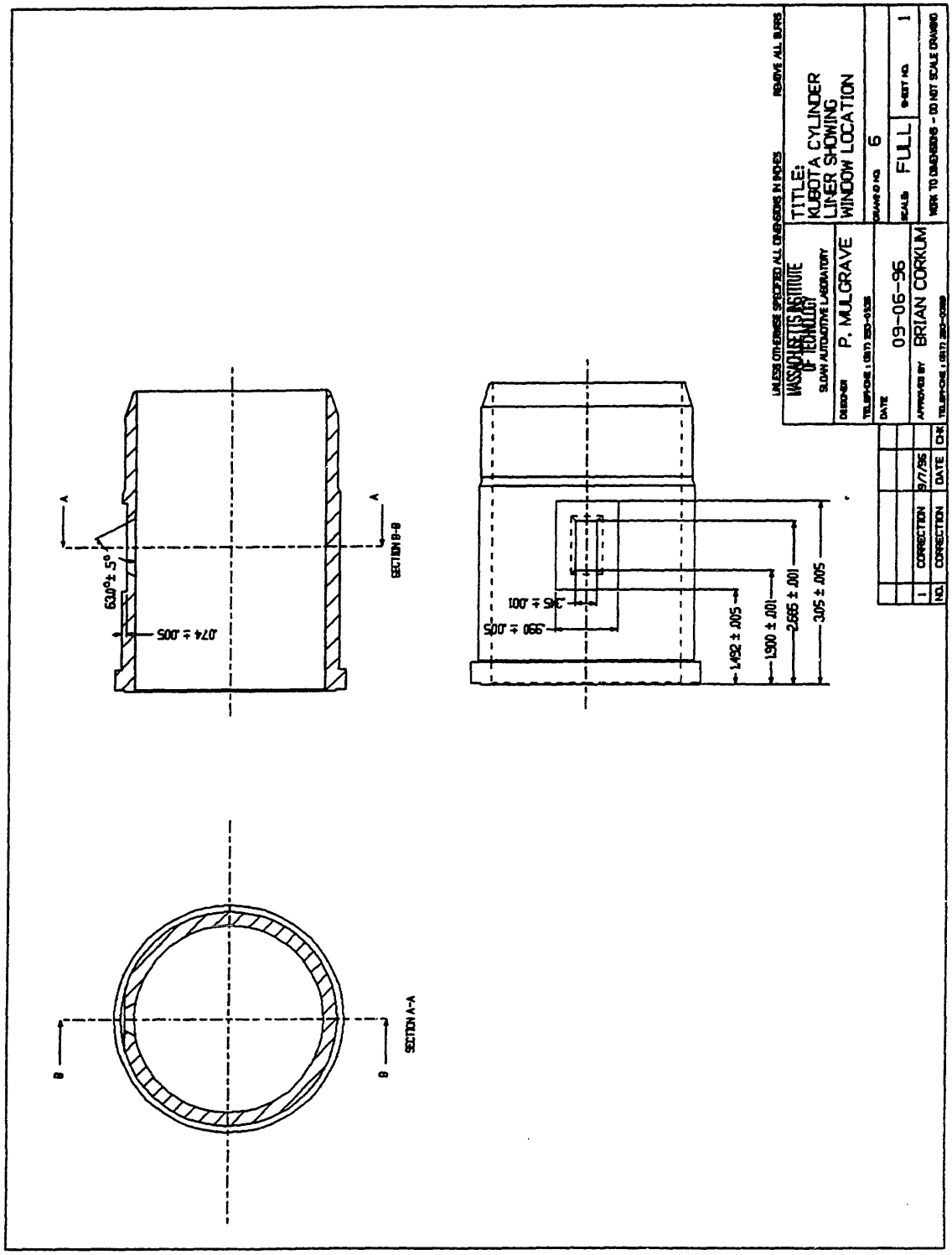
TITLE:
KUBOTA CYLINDER
LINER SHOWING
WINDOW LOCATION
MASSACHUSETTS INSTITUTE OF TECHNOLOGY
SLOAN AUTOMOTIVE LABORATORY
DESIGNER P. MULGRAVE
DATE 09-06-96
APPROVED BY BRIAN CORKUM
SCALE FULL
SHEET NO. 1
DRAWING NO. 6
UNLESS OTHERWISE SPECIFIED ALL DIMENSIONS IN INCHES
REMOVE ALL BURRS
REFER TO DRAWINGS - DO NOT SCALE DRAWING
NO. CORRECTION DATE CHK
1 CORRECTION 9/7/96
SECTION A-A
SECTION B-B
63.0° ± .5°
.074 ± .005
.990 ± .005
.345 ± .001
1.492 ± .005
1.900 ± .001
2.665 ± .001
3.05 ± .005

FIGURE I9

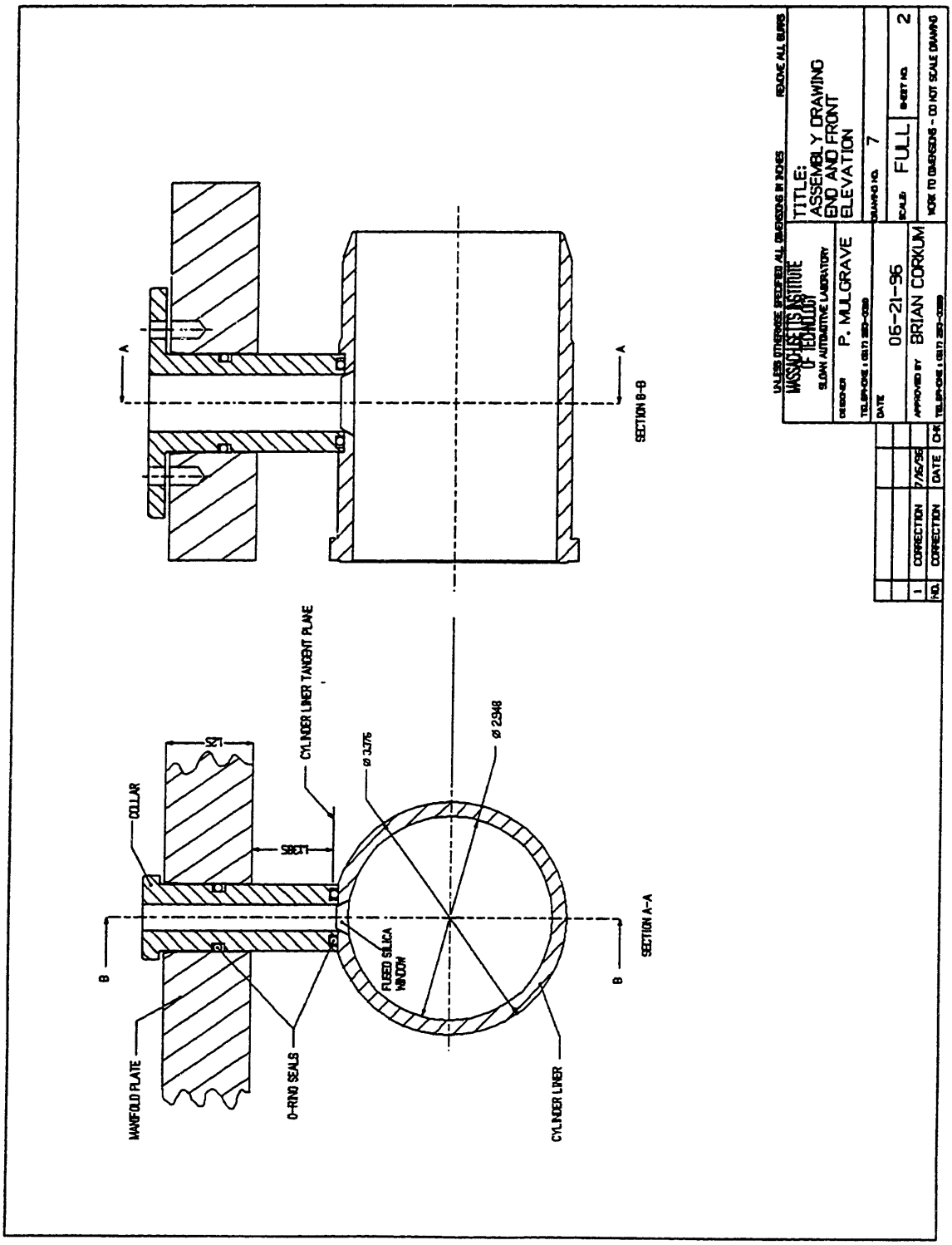
A
A
SECTION B-B
B
B
SECTION A-A
COLLAR
CYLINDER LINER TANGENT PLANE
Ø 3.375
Ø 2.948
1.385
.50
MANIFOLD PLATE
O-RING SEALS
FUSED SILICA WINDOW
CYLINDER LINER
UNLESS OTHERWISE SPECIFIED ALL DIMENSIONS IN INCHES
REMOVE ALL BURRS
MASSACHUSETTS INSTITUTE OF TECHNOLOGY
SLOAN AUTOMOTIVE LABORATORY
TITLE:
ASSEMBLY DRAWING
END AND FRONT
ELEVATION
DESIGNED P. MULGRAVE
DRAWING NO. 7
DATE 06-21-96
SCALE FULL
SHEET NO. 2
APPROVED BY BRIAN CORKUM
WORK TO DIMENSIONS - DO NOT SCALE DRAWING
NO. CORRECTION DATE CHK
1 CORRECTION 7/15/96

FIGURE I10

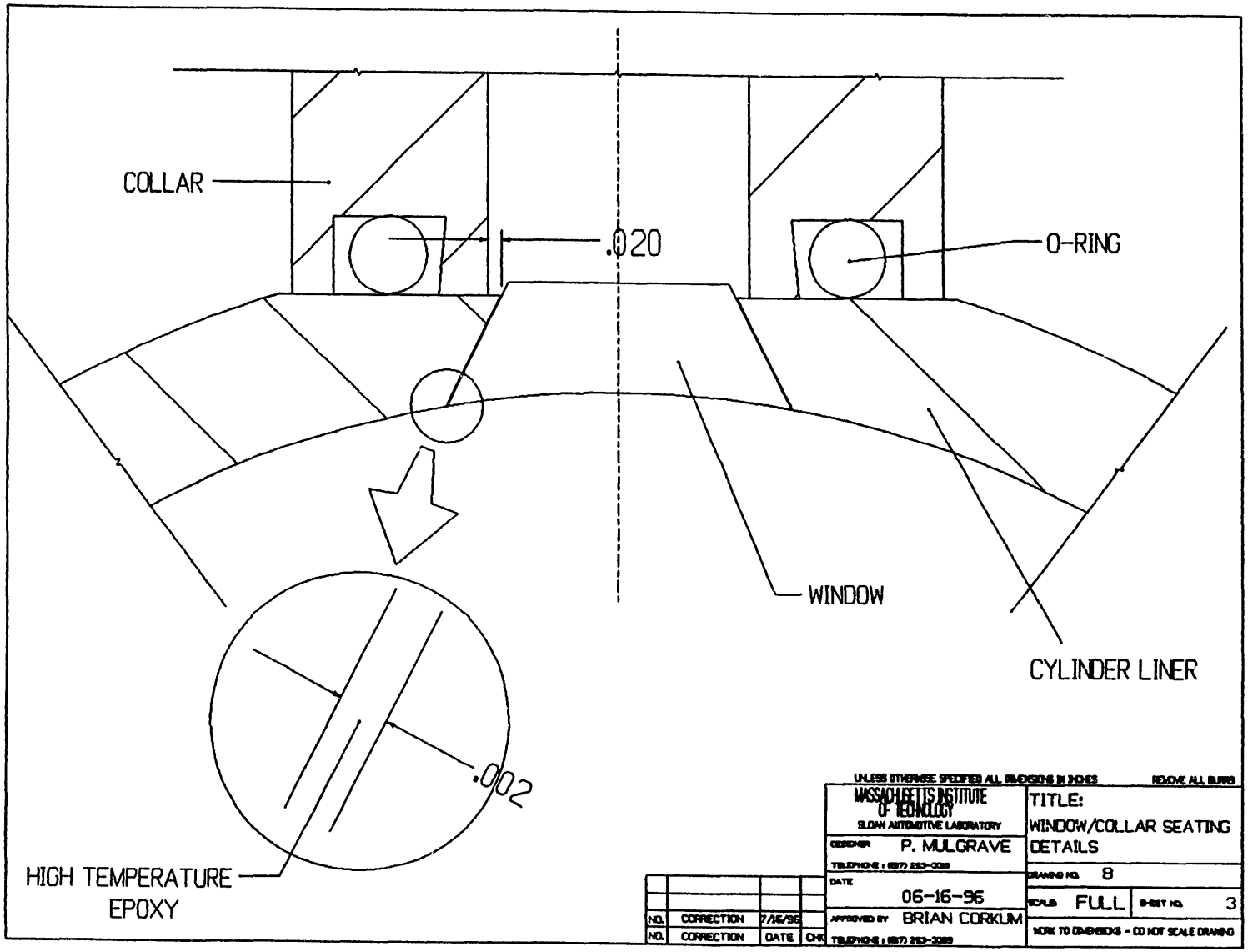
COLLAR
.020
O-RING
WINDOW
CYLINDER LINER
.002
HIGH TEMPERATURE
EPOXY
UNLESS OTHERWISE SPECIFIED ALL DIMENSIONS IN INCHES
REMOVE ALL BURS
MASSACHUSETTS INSTITUTE OF TECHNOLOGY
SLOAN AUTOMOTIVE LABORATORY
TITLE:
WINDOW/COLLAR SEATING DETAILS
DESIGNER P. MULGRAVE
DRAWING NO. 8
DATE 06-16-96
SCALE FULL
SHEET NO. 3
APPROVED BY BRIAN CORKUM
NO. CORRECTION 7/15/96
NO. CORRECTION DATE CHK
WORK TO DIMENSIONS - DO NOT SCALE DRAWING

FIGURE I11

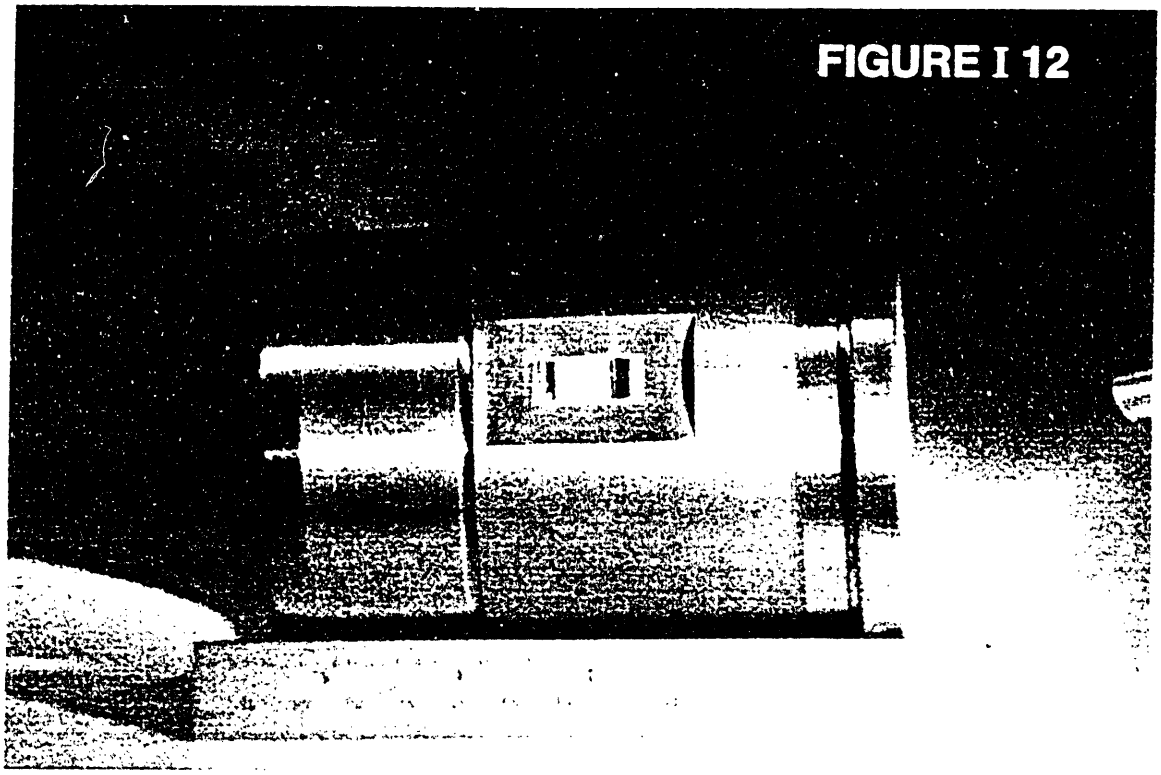
FIGURE I 12

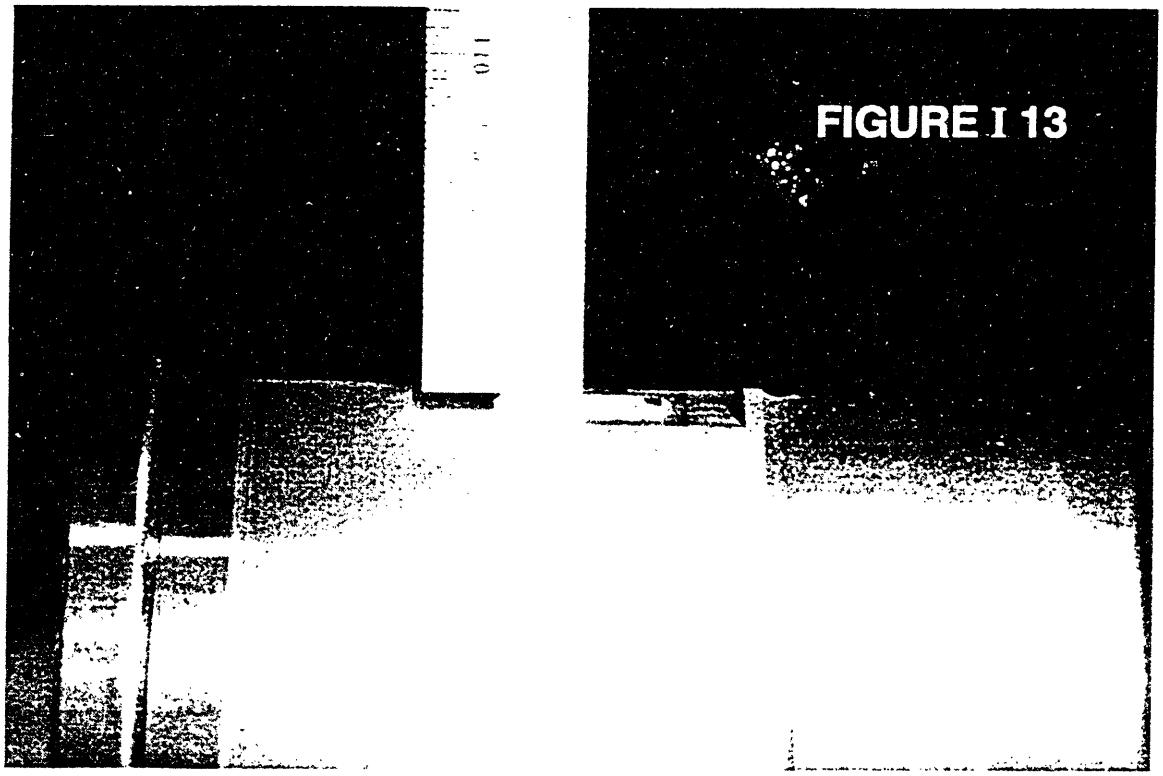
FIGURE I 13

VIEW THROUGH OPTICAL ACCESS PORT @ 140 CA BTC

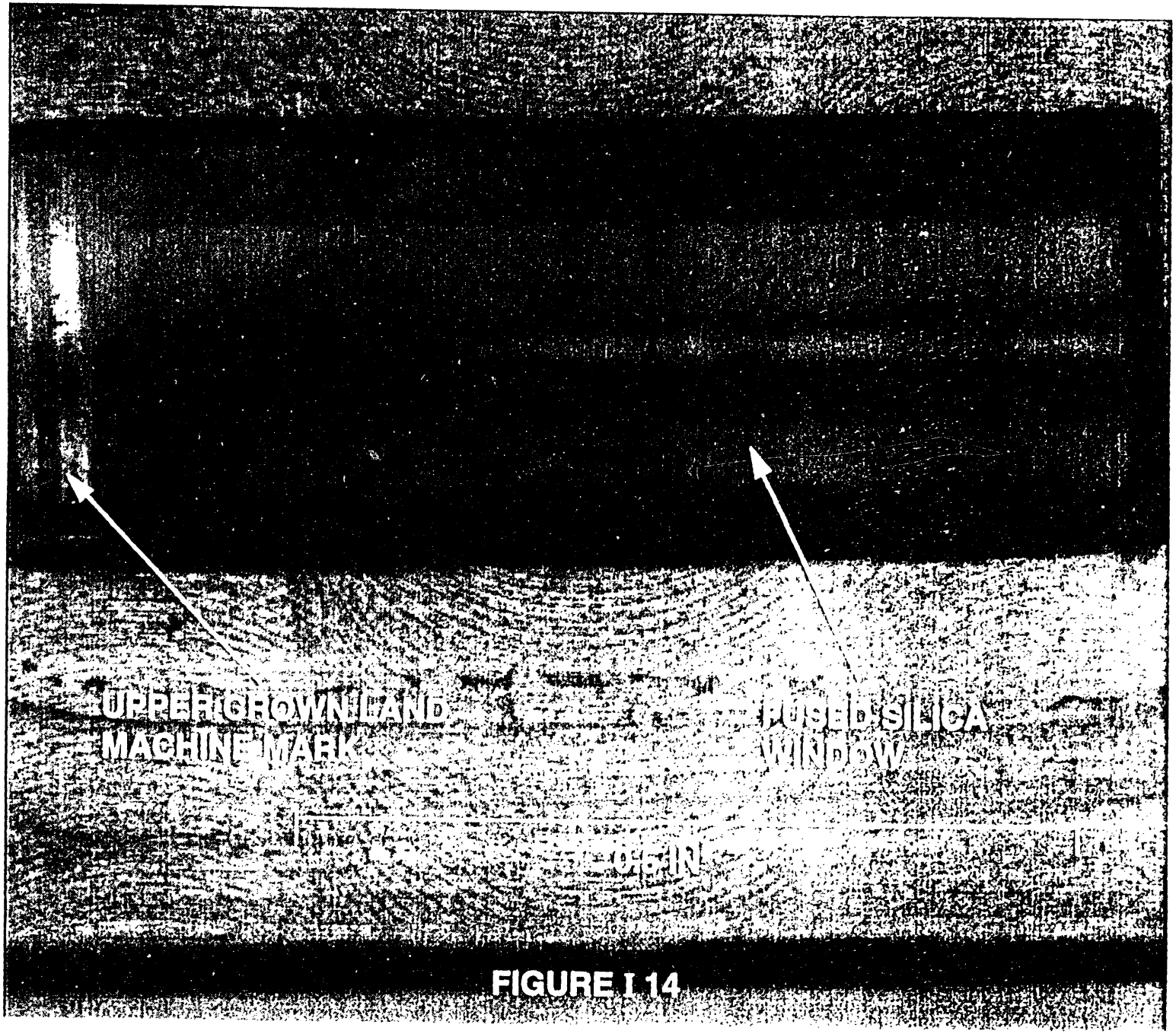

FIGURE I 14

VIEW THROUGH OPTICAL ACCESS PORT @ 114 CA BTC

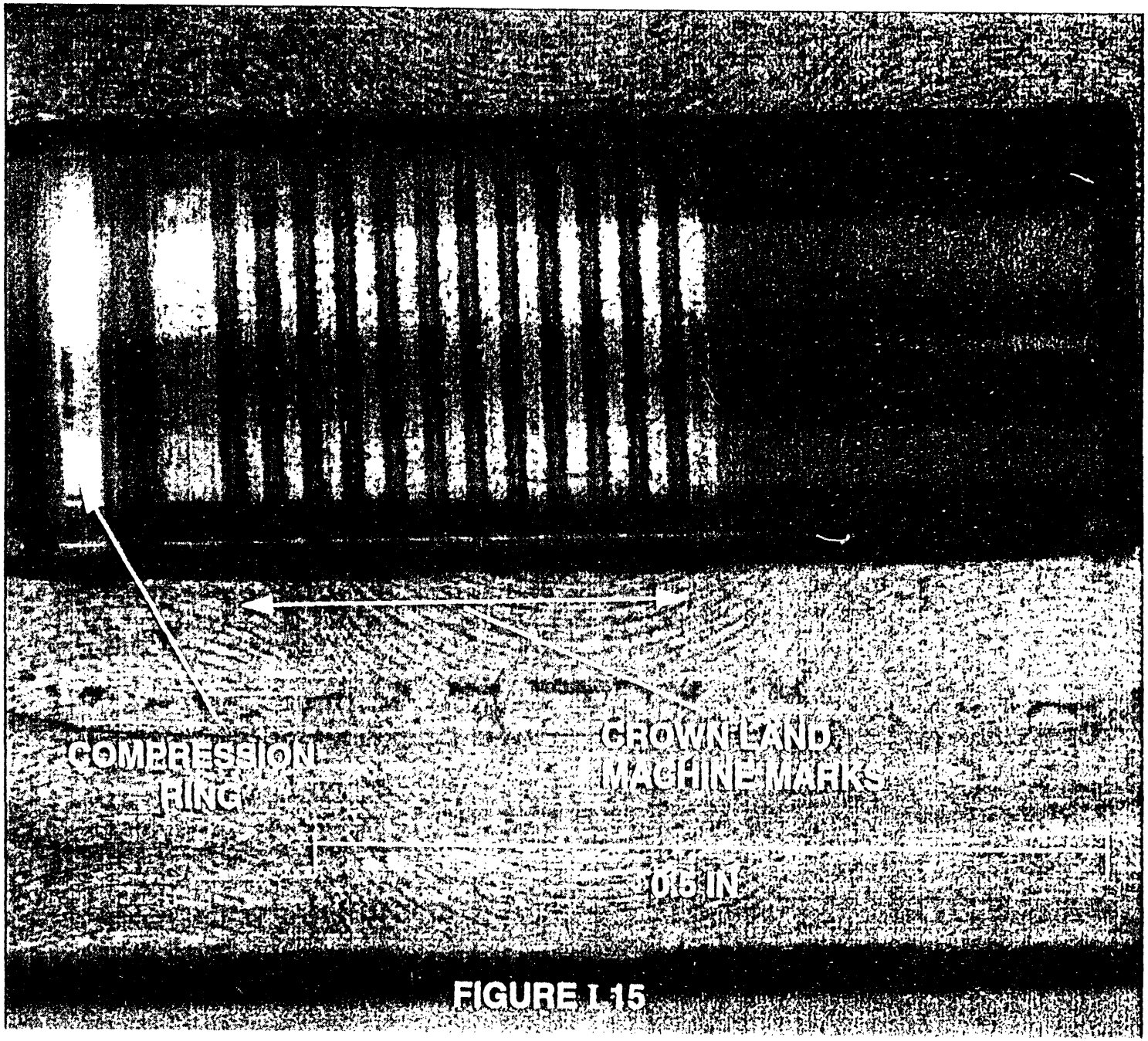

FIGURE I.15

VIEW THROUGH OPTICAL ACCESS PORT @ 100 CA BTC

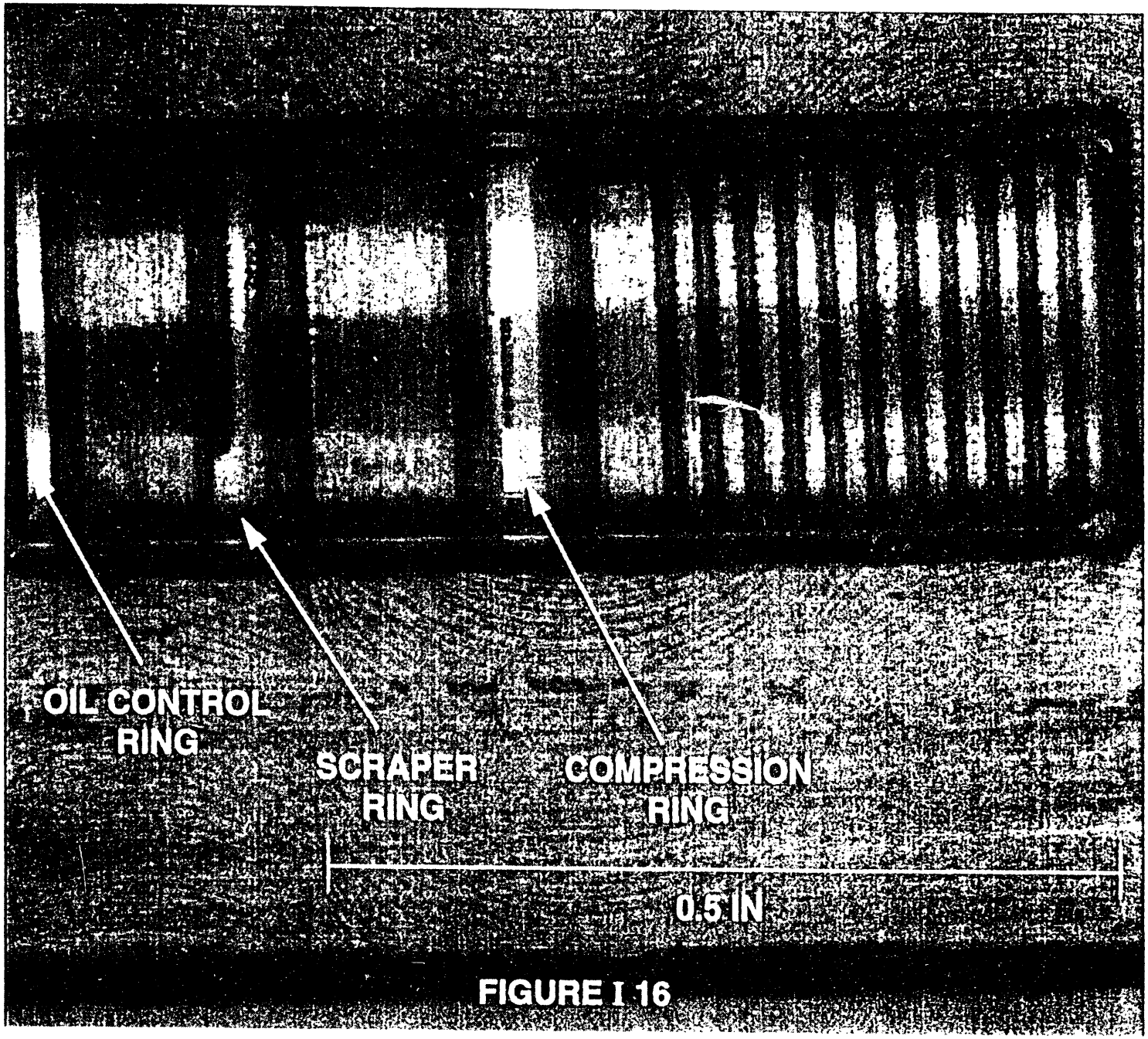

FIGURE I 16

VIEW THROUGH OPTICAL ACCESS PORT @ 88 CA BTC

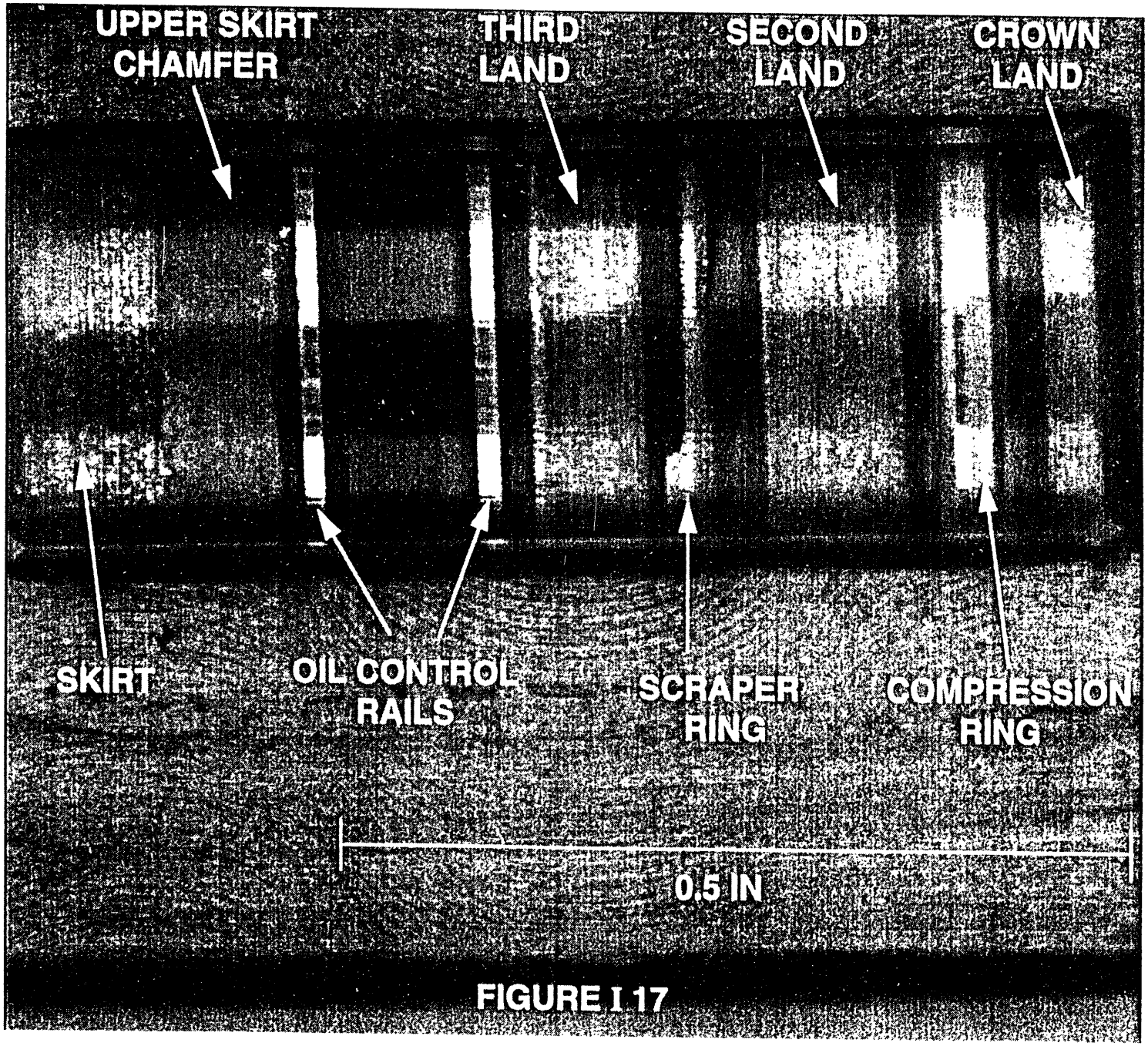

FIGURE I 17

(This Page Intentionally Left Blank)

APPENDIX J

1. External Transmittance For Sapphire of 1mm thickness.
2. Semilogarithmic Comparison of Internal Transmittances of UV grade synthetic fused silica and BK 7.
3. Transmittance curve for UV grade fused silica.
4. Table of Material optical properties.

Material Constants

Sapphire Constants

1. Density : 3.98 g cm^{-3} at 25°C.
2. Young's Modulus : 3.7 x 10^{10} dynes/mm^2.
3. Poisson's Ratio : -0.02.
4. Moh Hardness : 9 (by definition).
5. Softening Point : 1800°C
6. Specific Heat at 25°C : 0.18cal/g°C.
7. Coefficient of linear Expansion (0 to 500°C) : 7.7 x 10^{-6}/°C.

Synthetic Fused Silica Constants

1. Change of refractive index with temperature (0 to 700°C) : 1.28 x 10^{-5}/°C.
2. Homogeneity (Maximum index variation over 10cm aperture): 2 x 10^{-5}.
3. Continuous operating temperature : Maximum 900°C.
4. Coefficient of thermal expansion : 5.5 x 10^{-7}/°C.
5. Thermal conductivity (100°C) : 0.177 cal g^{-1} $°C^{-1}$.
6. Abbe constant : 67.8 ± 0.5.

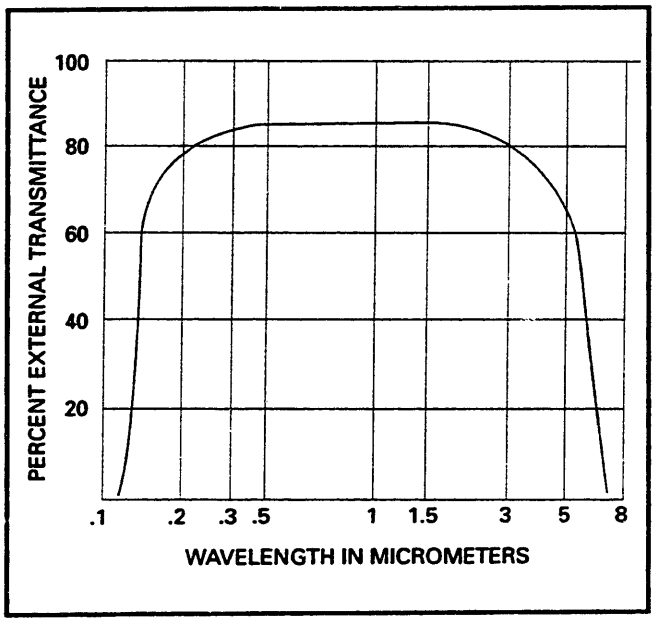

Figure J1 External Transmittance for Sapphire of 1 mm thickness

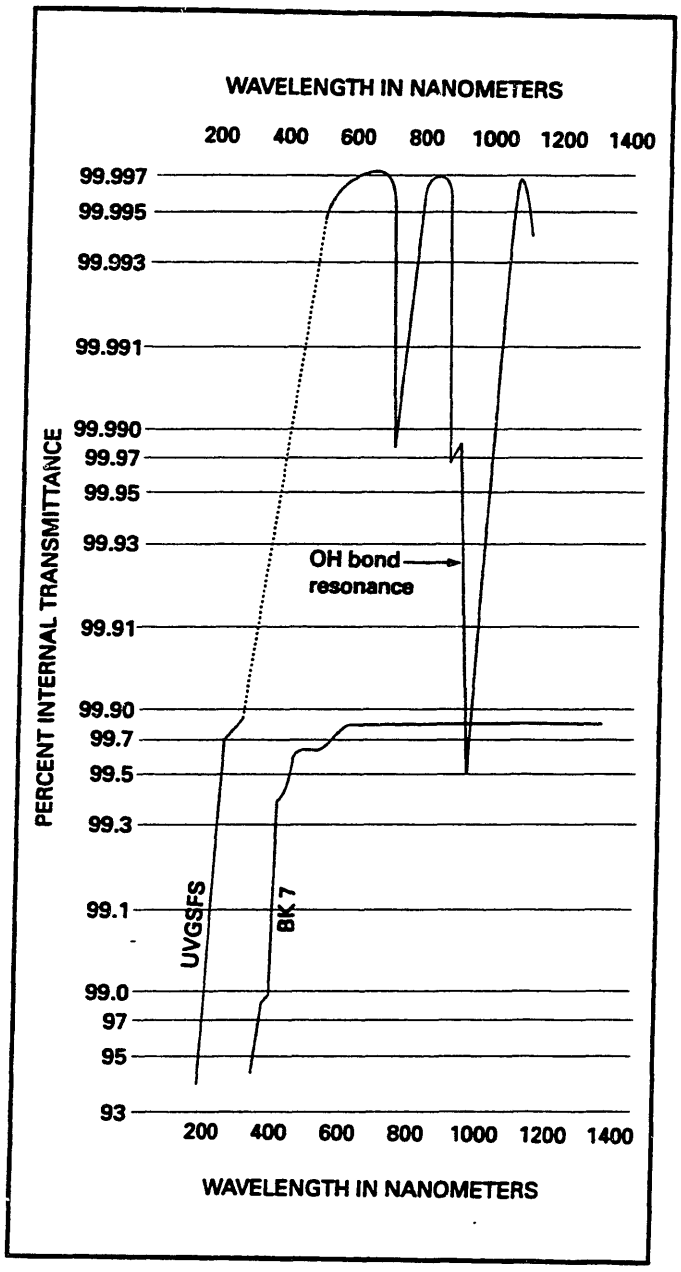

Figure J2 Semilogarithmic Comparison of Internal Transmittance of UV grade synthetic fused silica and BK7

The chart above has been provided by Melles Griot.

Material	Transmission Range	Index of Refraction	Thermal Expansion Coefficient /°C	Abrasion Resistance	Features
BK 7 *(page 4–8)*	BK 7	1.52 @ 0.55 μm		Good	Excellent all around lens material provides broad transmission with excellent mechanical characteristics
LaSF N9 *(page 4–8)*	LaSF N9	1.86 @ 0.55 μm		Good	Provides high refractive index at the expense of transmission and mechanical characteristics
SF 11 *(page 4–8)*	SF 11	1.79 @ 0.55 μm		Poor	Provides high refractive index at the expense of transmission and mechanical characteristics
F2 *(page 4–8)*	F 2	1.62 @ 0.55 μm		Poor	Represents a good compromise between higher index and acceptable mechanical characteristics
BaK 1 *(page 4–8)*	BaK 1	1.57 @ 0.55 μm		Good	Excellent all around lens material, but with slightly worse chemical characteristics than BK 7
Optical Quality Fused Silica *(page 4–11)*	OQSFS	1.46 @ 0.55 μm		Very Good	Provides good UV transmission and superior mechanical characteristics
UV Grade Fused Silica *(page 4–11)*	UVGFS	1.46 @ 0.55 μm		Very Good	Provides excellent UV transmission and superior mechanical characteristics
Optical Crown Glass *(page 4–15)*	OPTICAL CROWN	1.52 @ 0.55 μm		Good	Lower tolerance glass for use as a mirror substrate or in non-critical applications
LEBG Low expansion borosilicate glass *(page 4–16)*	LEBG	1.48 @ 0.55 μm		Good	Low thermal expansion and poor homogeneity make it useful for mirror substrates or condensers
Sapphire *(page 4–17)*	SAPPHIRE	1.77 @ 0.55 μm		Excellent	Excellent mechanical and thermal characteristics make it a superior window material
Zinc Selenide *(page 4–19)*	ZINC SELENIDE	2.40 @ 10.6 μm		Poor	Transmits in both IR and visible; poor mechanical characteristics

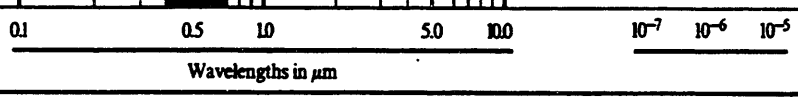

TABLE J1 MATERIAL OPTICAL PROPERTIES

(SOURCE : MELLES GRIOT)

APPENDIX K

Standard O-ring materials

NAME	DESCRIPTION:	**RECOMMENDED FOR
Buna N	(Nitrile) Widely used elastomer offering excellent resistance to most oils, silicone greases, hydraulic fluids, water and alcohols. Temperature range: -40° to +250°F.	COLD WATER GREASES OILS ALCOHOL PETROLEUM FLUIDS
Neoprene*	(Chloroprene) Exhibits moderate resistance to petroleum based fluids. Good resistance to weathering and ozone. Good resilience and low compression set. Temperature Range: -45° to +250°F.	AMMONIA MILD ACID FREON
Silicone	Used for wide temperature ranges and dry heat resistance. High resistance to sun and ozone injury. Poor tensile, tear, and abrasion resistance and high friction traits. Is fungus resistant, odorless, tasteless, and non-toxic. Temperature range: -75° to +450°F.	HIGH TEMP COLD TEMP OZONE FDA LOW OUTGASSING
Viton*	(Fluorocarbon) Excellent mechanical and physical properties. Used in high temp and chemical service. Fuels, greases, acids, solvents, sun and ozone resistance. Has low gas permeability. Temperature range: -20° to +400°F.	VACUUM FUELS ACIDS HIGH/LOW TEMP SOLVENTS LOW OUTGASSING
EPR	(EPDM - Ethylene Propylene) Used for hot water, steam, mild acids, alkalis, some solvents, and has excellent sun and ozone resistance. Temperature Range: -60° to -300°F.	GREASES ALCOHOL KETONES MILD ACID OZONE
Fluorosilicone	Used when high and low temperatures and harsh chemical and solvent resistance is required. Especially for aerospace industry. Temperature range: -75° to +400°F.	HIGH/LOW TEMP SOLVENTS FUELS OILS OZONE
Teflon*	Excellent resistance to high and low temperatures, solvents, acids, fuels, oils, and ozone. Teflon* is a chemically inert material. Problems with poor elastic memory, poor tear strength and tendency to cold flow with time. Teflon* coated and Teflon* encapsulated also available. Temperature range: -300° to +450°F.	HIGH/LOW TEMP ALL CHEMICALS FUELS OZONE
Chemraz*	Same temperature and chemical attributes as in Teflon* with the resilience and compression ability of other elastomers. Excellent resistance to steam and hot water. Temperature Range: -20° to +450°F.	HIGH TEMP ALL CHEMICALS STEAM/HOT WATER
EMI	Both solid and hollow rings are available in electrically conductive compounds. Offers superior shielding capability.	ELECTRICALLY CONDUCTIVE

*Trademarks of their respective companies.

**NOTE: For Reference: Exact usage dependent upon many conditions.

TABLE K1 STANDARD O-RING MATERIALS
(SOURCE: GREEN RUBBER COMPANY)

APPENDIX L

Kubota Engine Experimental Setup

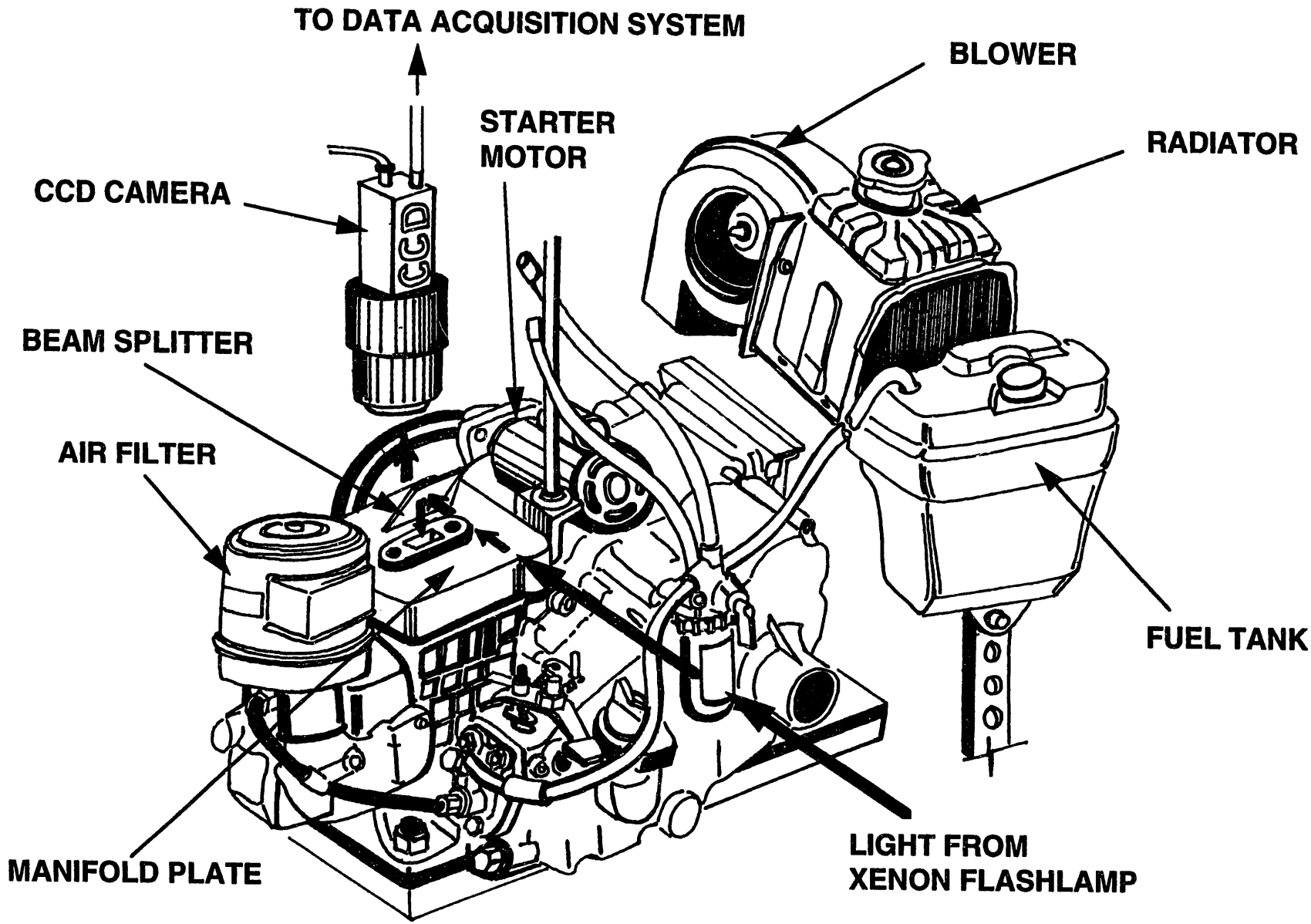

FIGURE L1 KUBOTA ENGINE SETUP

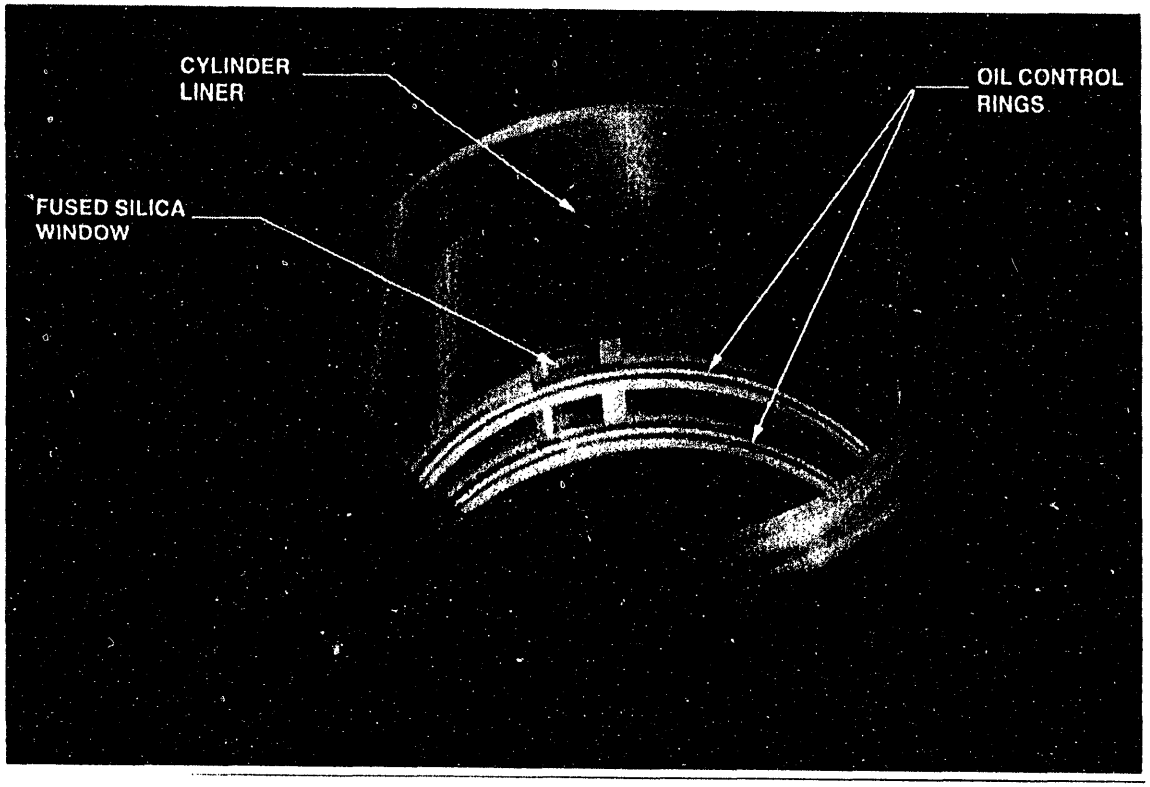

FIGURE L2 WINDOW INSTALLATION

(This Page Intentionally Left Blank)

APPENDIX M

Pulnix TM-9700 CCD Camera Specifications

Imager:	2/3" inch progressive scanning interline transfer CCD
Pixels	768 (H) x 484 (V)
Cell size	11.6 (H) x 13.6 (V) microns progressive scan
Imager size	8.9 (H) x 6.6 (V) mm
Chip size	9.9 (H) x 7.7 (V) mm
Dynamic range	60dB
Output sensitivity	10 µV/electron
Dark noise	40 electrons
Dark current	< 1 nA/cm^2
Quantum efficiency	25%, 20%, 12% (450, 550, 650 nm); TM-9700 only
Scanning:	525 lines, 30 Hz or 60 Hz 2:1 interlace
Clock	28.6363 MHz
Pixel clock	14.31818 MHz
Horizontal frequency	15.734 KHz
Vertical frequency	59.94 Hz
TV resolution:	570(H) x 484(V) lines
Video output:	1.0V p-p composite video, 75Ω and 8-bit RS 422 output
S/N ratio:	50 dB min. (AGC OFF)
Minimum illumination:	1.0 lux (F=1.4) without IR cut filter
AGC:	ON/OFF (OFF std.)
Gamma:	0.45 or 1.0 (1.0 std.)
Lens mount:	C-mount
Power requirement:	DC 12V, 500 mA
Weight:	330 grams (12oz.)
Operating temperature:	-10 °C to +50 °C
Storage temperature:	-30 °C to +60 °C
Operating humidity:	Max. 70%
Storage humidity:	Max. 90%
Vibration:	7 G (200Hz to 2000Hz)
Shock:	70 G
Dimensions:	44 mm x 48.5 mm x 136 mm (1.73" x 1.90" x 5.35")

Table M1 Pulnix 9700 Series CCD Camera Specifications

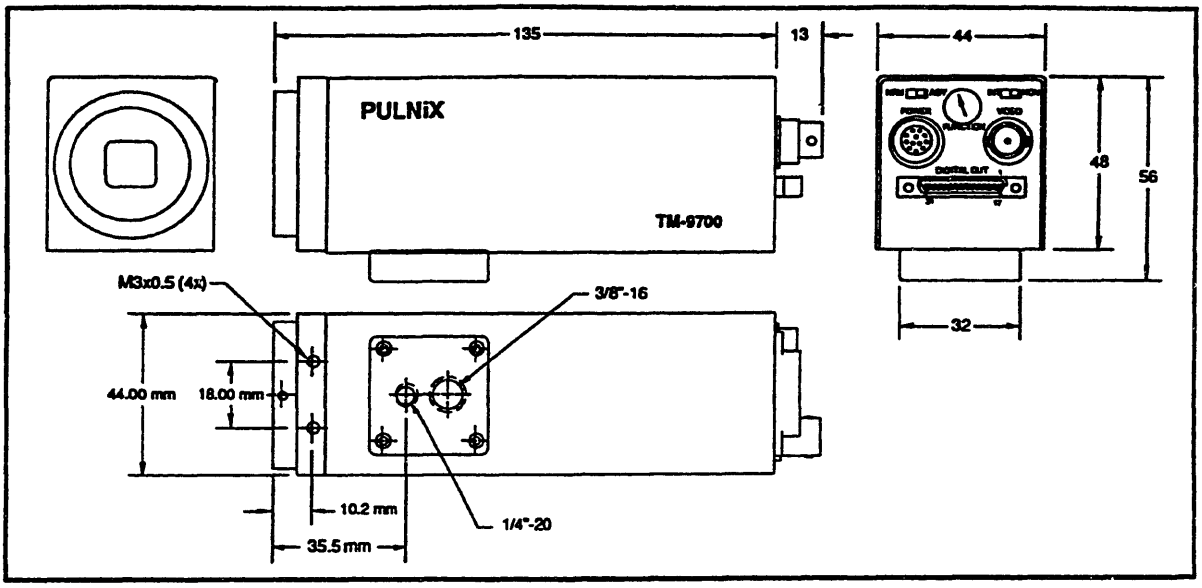

Figure M1 CCD Camera Physical Dimensions

(This Page Intentionally Left Blank)

APPENDIX N

Spectral Data for the major Xanthene and Coumarin dyes

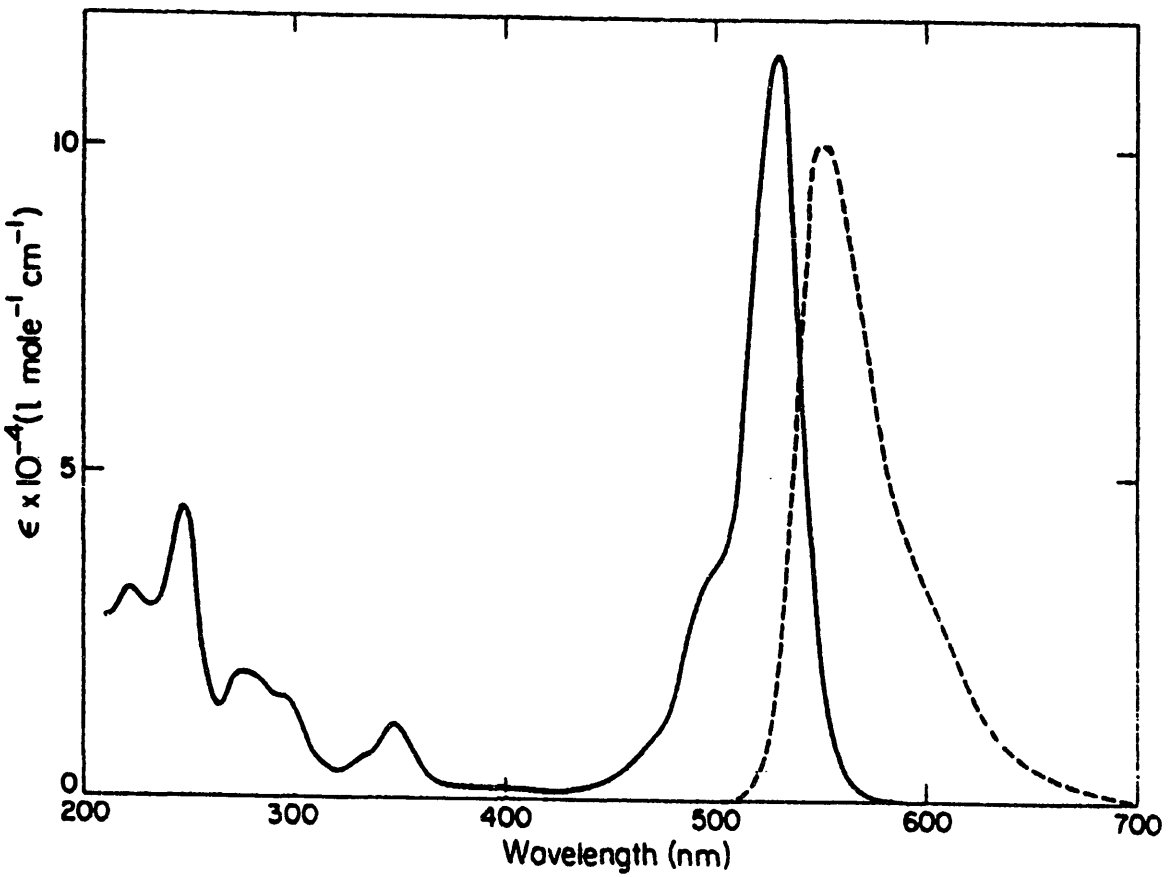

FIGURE N1 RHODAMINE 6G IN ETHANOL——ABSORPTION SPECTRUM (ϵ MOLAR DECADIC EXTINCTION COEFFICIENT), ---------- QUANTUM SPECTRUM OF FLUORESCENCE (ARBITRARY UNITS)

Rhodamine B

Lasing λ_{max} 609 (N_2)
588 (YAG)

MW 479.02

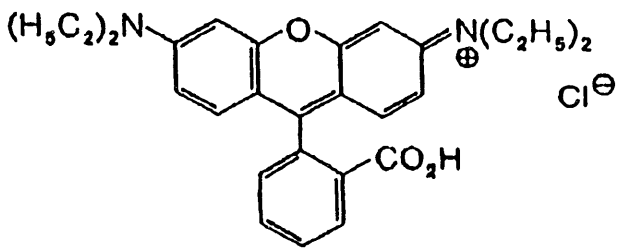

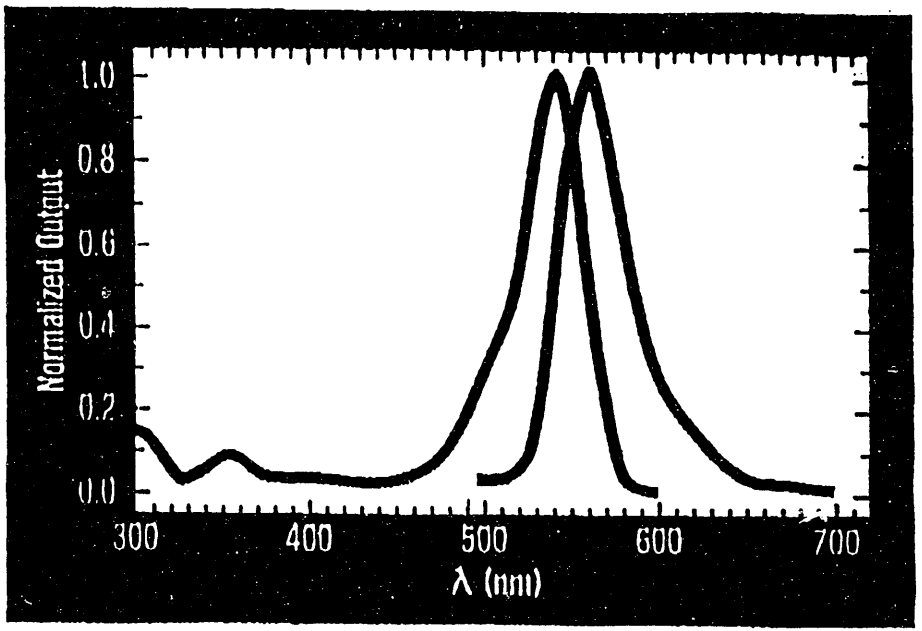

FIGURE N2

- **Absorption max: 545 nm**
  $\varepsilon_{max} = 1.06 \times 10^5$ L mole^{-1} cm^{-1}
  $\varepsilon_{532} = 7.2 \times 10^4$ L mole^{-1} cm^{-1}
  $\varepsilon_{337} = 4 \times 10^3$ L mole^{-1} cm^{-1}
- **Fluorescence max: 565 nm**
  Solvent: Methanol
  Uncorrected

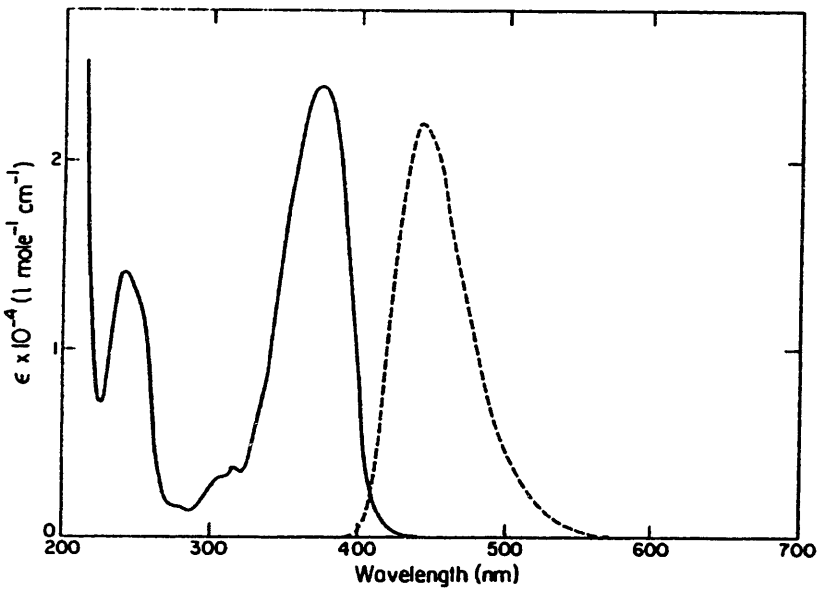

FIGURE N3 COUMARIN 1 IN ETHANOL——ABSORPTION SPECTRUM (ε MOLAR DECADIC EXTINCTION COEFFICIENT), ——— QUANTUM SPECTRUM OF FLUORESCENCE (ARBITRARY UNITS)

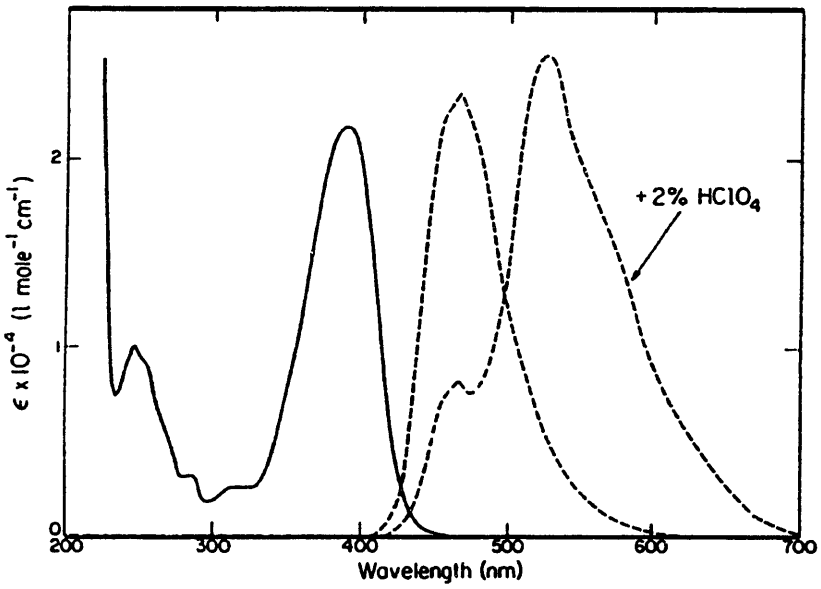

FIGURE N4 COUMARIN 102 IN ETHANOL——ABSORPTION SPECTRUM (ε MOLAR DECADIC EXTINCTION COEFFICIENT), ——— QUANTUM SPECTRUM OF FLUORESCENCE (ARBITRARY UNITS)

Coumarin 6

Lasing λ_{max} 523 (YAG)

MW 350.44

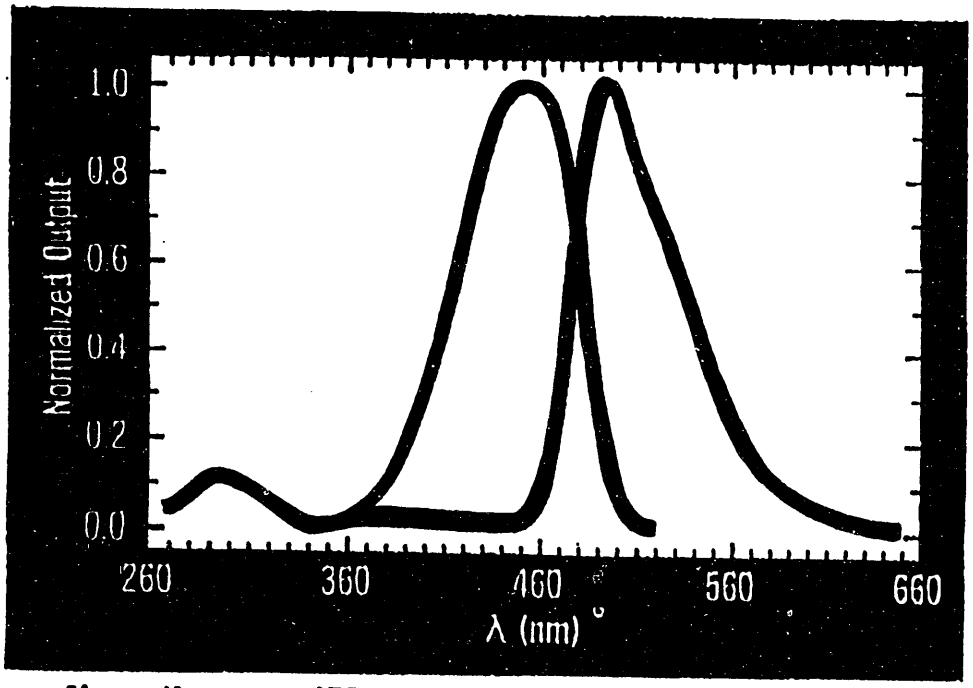

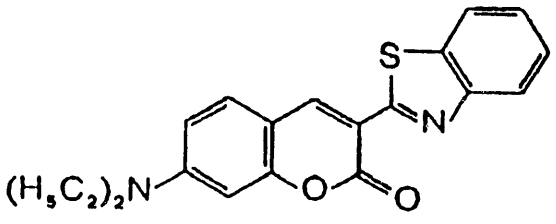

FIGURE N5

- **Absorption max: 458 nm**
  $\varepsilon_{max} = 4.08 \times 10^4$ L mole^{-1} cm^{-1}
  $\varepsilon_{337} = 1 \times 10^2$ L mole^{-1} cm^{-1}
- **Fluorescence max: 497 nm**
  Solvent: Methanol
  Uncorrected

(This Page Intentionally Left Blank)

APPENDIX O

Calibration Information

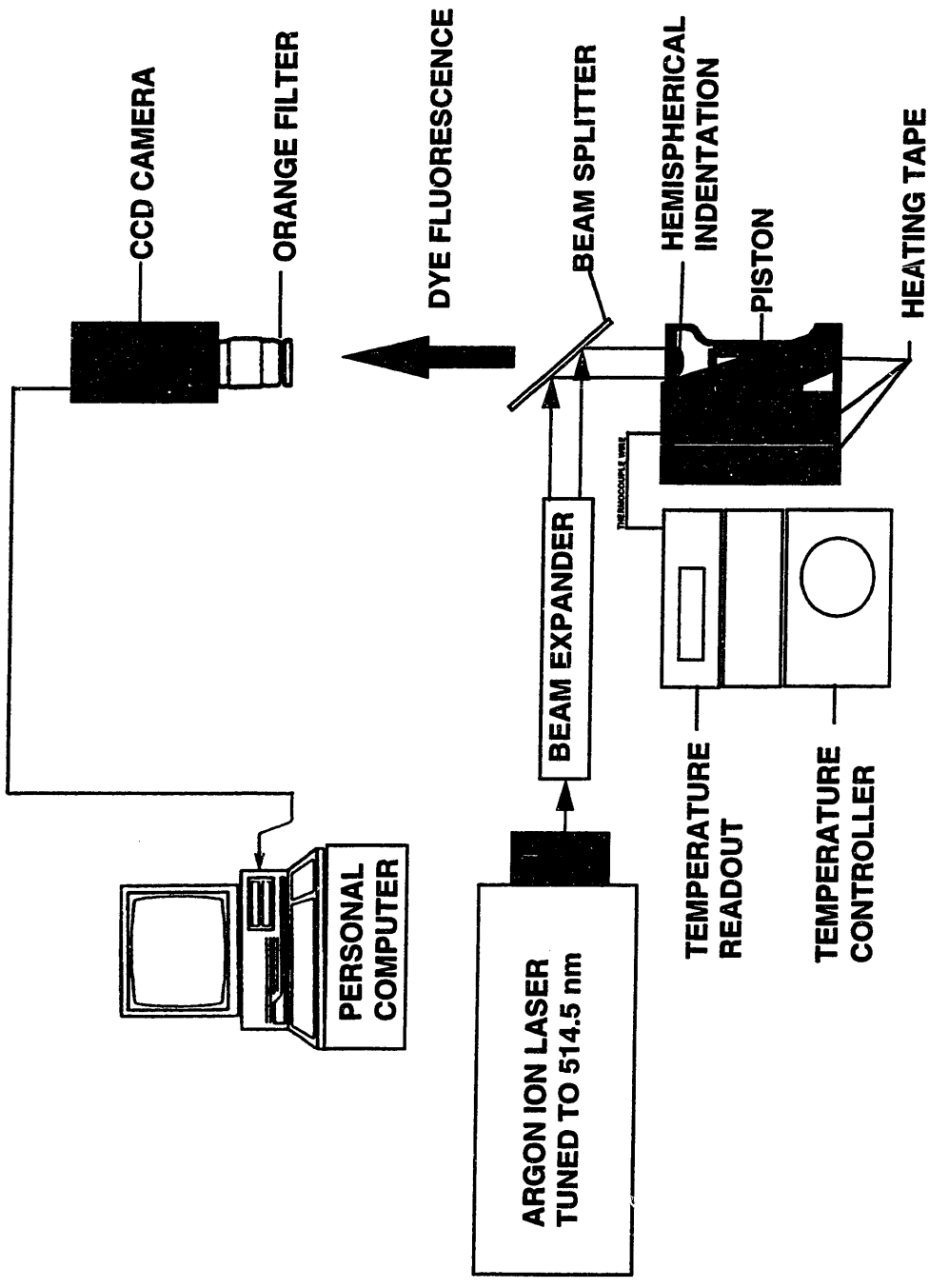

FIGURE 01 SCHEMATIC OF THE BENCH CALIBRATION SETUP

TALYSURF PROFILE OF THE HEMISPHERICAL INDENTATION GROOVE ALONG X_1-X_2

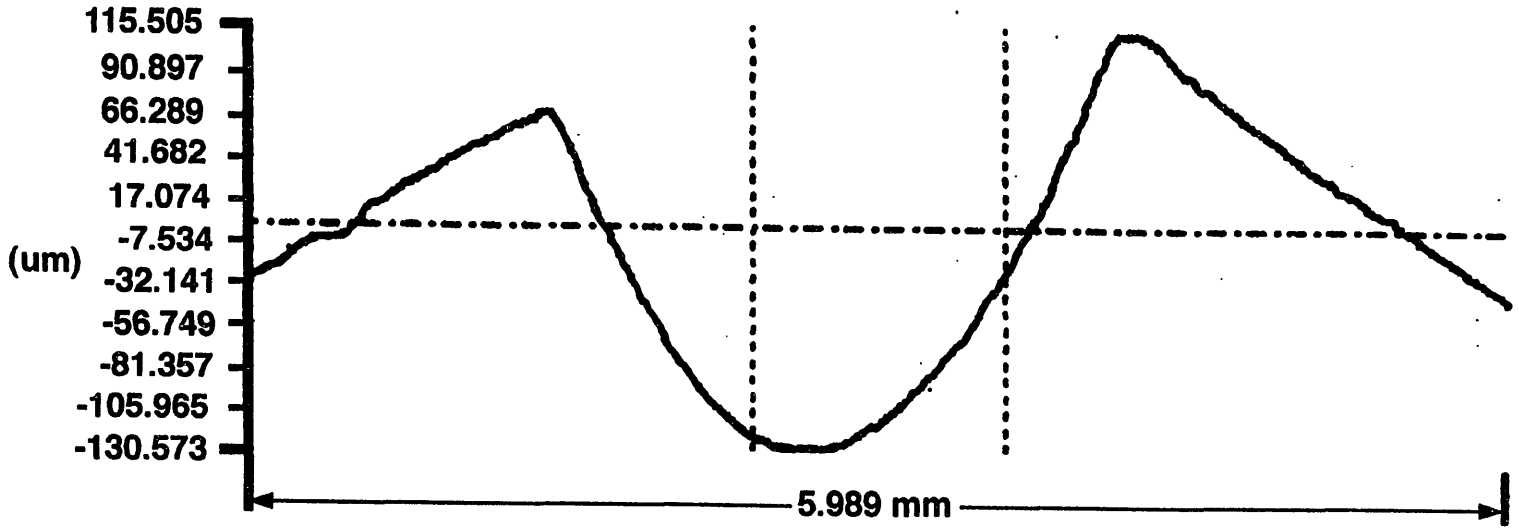

Peak To Valley = 246.078 um

FIGURE O2

Note that the groove profile is slightly assymetric which explains why the fluorescence intensity maximum is skewed to the left in the photographs overleaf.

Fluorescent Photographs of the Hemispherical Calibration Groove filled with a solution of Rhodamine 6G Perchlorate in SAE 15W40 oil at various temperatures

FIGURE O3a

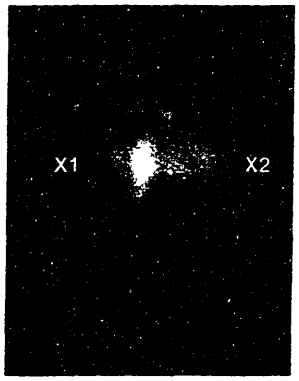

Dye/oil solution @ 100F

FIGURE O3b

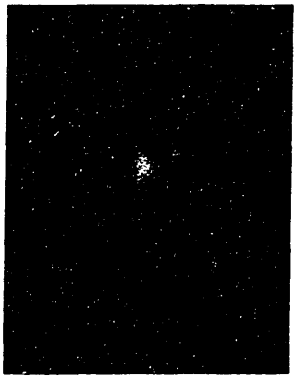

Dye/oil solution @ 200F

FIGURE O3c

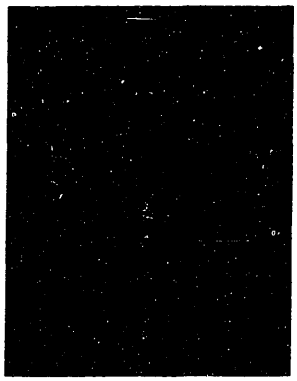

Dye/oil solution @ 300F

FIGURE O3d

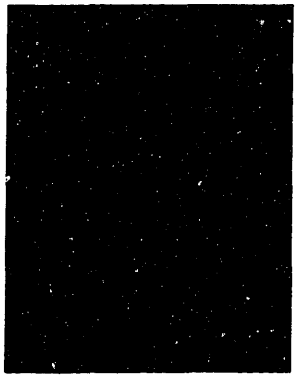

Dye/oil solution @ 400F